Bioinspired Underwater Adhesives by Using the Supramolecular Toolbox

Hofman, Anton H.; van Hees, Ilse A.; Yang, J.; Kamperman, Marleen

Published in:
Advanced materials

DOI:
10.1002/adma.201704640

Publication date:
2018

ADVANCED MATERIALS
www.advmat.de

Bioinspired Underwater Adhesives by Using the Supramolecular Toolbox

*Anton H. Hofman, Ilse A. van Hees, Juan Yang, and Marleen Kamperman**

Nature has developed protein-based adhesives whose underwater performance has attracted much research attention over the last few decades. The adhesive proteins are rich in catechols combined with amphiphilic and ionic features. This combination of features constitutes a supramolecular toolbox, to provide stimuli-responsive processing of the adhesive, to secure strong adhesion to a variety of surfaces, and to control the cohesive properties of the material. Here, the versatile interactions used in adhesives secreted by sandcastle worms and mussels are explored. These biological principles are then put in a broader perspective, and synthetic adhesive systems that are based on different types of supramolecular interactions are summarized. The variety and combinations of interactions that can be used in the design of new adhesive systems are highlighted.

1. Introduction

Adhesives developed by marine organisms have been the focus of a great number of studies over the last two decades. These organisms are able to bond materials underwater using protein-based adhesives: barnacles use secretions to glue calcareous base plates to rocks, mussels use a network of threads to attach their soft invertebrate body to hard surfaces, and both sandcastle worms and caddisfly larvae assemble a protective tubular shell by gluing together sand grains or stones.[1–3] It is well known that the adhesive abilities of the sandcastle worm and mussel both involve post-translational modifications of the adhesive proteins. Hydroxylated tyrosine, known as L-3,4-dihydroxyphenylalanine (DOPA), and phosphorylated serine are common adhesion promoters.[4–8] The importance and use of DOPA in synthetic mimics has been reviewed extensively in several excellent reviews.[9–12] Recently, it was emphasized by Waite that catechol moieties alone are insufficient to ensure proper underwater adhesion and that the performance is a complex interplay between DOPA and its local environment.[13] Therefore, attention is shifted to include other (noncovalent) interactions used in these natural glues, and much progress has been made in understanding both their performance and delivery process.[14]

In this review, we take the sandcastle worm and mussel as a basis for inspiration. We discuss (noncovalent) interactions found in these natural adhesive systems and extend our discussion to additional supramolecular moieties that can be used to control the adhesive and cohesive performance of synthetically designed adhesives. In Section 2, we examine the natural systems and identify the versatile supramolecular interactions used in such protein-based adhesives. These include electrostatic interactions, hydrogen bonding, hydrophobic forces, π–π interactions, metal coordination, cation–π complexation, and dynamic covalent linkages. The use of these interactions in synthetic adhesive systems is explored in the subsequent sections. Section 3 is devoted to the different interactions that catechols (the functional group of DOPA) display to bond to a submerged substrate or to provide cohesive properties to the adhesive. Despite the fact that catechols have already been the topic of many excellent reviews,[9,13,17] we believe that catechols play a pivotal role in both the sandcastle worm and the mussel adhesive systems and, therefore, should not be omitted from this review. In Section 4, we discuss the use of electrostatic interactions in protein-based and synthetic adhesive formulations for wet conditions. These interactions can be tailored to a wide distribution of bond strengths and thus can be tuned to change multiple mechanical properties, which is essential for design of an adhesive. Besides the effect on the adhesive and cohesive properties, we highlight work where electrostatic interactions cause liquid–liquid phase separation in aqueous polymer solutions. The resulting (complex) coacervate is a concentrated, liquid, yet water-insoluble phase of the adhesive material, which can act as a powerful delivery tool for underwater adhesives. Hydrogen bonding in adhesives is explored in Section 5. The use of hydrogen bonding to adjust the viscoelastic properties of adhesives has been identified decades, ago, and hydrogen bonding moieties are commonly used in pressure sensitive adhesives (PSAs). However, besides simple, single hydrogen bonding motifs, many interesting alternative

Dr. A. H. Hofman, I. A. van Hees, Dr. M. Kamperman
Physical Chemistry and Soft Matter
Wageningen University
Stippeneng 4, 6708 WE Wageningen, The Netherlands
E-mail: marleen.kamperman@wur.nl
Dr. J. Yang
Rolls-Royce@NTU Corporate Lab
Nanyang Technological University
65 Nanyang Drive, Singapore 637460, Singapore
The ORCID identification number(s) for the author(s) of this article can be found under https://doi.org/10.1002/adma.201704640.

DOI: 10.1002/adma.201704640

motifs have been developed by the supramolecular chemistry community; both will be covered in this section. Since hydrogen bonds have mainly been studied in dry applications, this section will also describe adhesion under dry conditions. In analogy to possible hydrophobic interactions in mussels, bonding by means of hydrophobic interactions through host–guest complexation will be the subject of Section 6. More specifically, we discuss cyclodextrins (CDs) and cucurbiturils (CBs) that both show the ability to strongly bind to hydrophobic guest molecules. For a more in-depth description of several of these systems, we refer the reader to another excellent review on hydrogen bonding and host–guest interactions for adhesive design by Heinzmann et al.[18] In Section 7, metal coordination and other interesting, yet less explored interactions, will be discussed.

2. Wet Adhesion in Nature

In the upcoming subsections, we will discuss the features and mechanisms of adhesion by sandcastle worms and mussels. Even though there are large differences between the organisms, the adhesive chemistries also show similarities. Therefore, at the end of this section, a concise overview of the important chemical interactions for both adhesion and cohesion is given.

2.1. Sandcastle Worms

Sandcastle worms, *Phragmatopoma californica* (**Figure 1**a), are marine organisms that live in colonies along the coast of North America. These worms build protective shells which are formed from minerals found in their surroundings. The mineral particles, such as sand grains or pieces of shell, are glued together underwater with a bioadhesive packaged in granules that are secreted from adhesive glands.[14] After an initial curing period of less than 30 s, the adhesive is strong enough to hold the particles in place. In the next hours, a second curing step follows which darkens the color. The resulting cement is a porous solid with the pores being filled with liquid (Figure 1b).[19]

2.1.1. Adhesive Composition

The main constituents of the sandcastle glue are six different types of adhesive proteins, sulfated polysaccharides, and magnesium ions. The proteins can roughly be divided into two groups: anionic proteins and cationic proteins (Figure 1c). The two anionic proteins are referred to as Pc3A and Pc3B, after *P. californica* (Pc). These proteins contain large quantities of phosphorylated serine, thereby introducing negative charges into the protein.[20] Pc1, Pc2, Pc4, and Pc5 are cationic proteins that are rich in the nonpolar amino acid glycine, with an exception of Pc5, which contains a mixture of several nonpolar amino acids. The positive charges on these proteins originate from quaternized histidine and lysine residues, which represent 5–18% of the total amino acid content.[16] In addition, all six proteins contain at least 10% aromatic amino acids.[16,20] These aromatic residues include tyrosine and DOPA. DOPA originates from the post-translational modification of tyrosine by tyrosinase[20] and is considered to be an important feature for underwater adhesion, because it forms interactions through a high variety of chemistries, as will be discussed in Section 2.2.2.[11,13]

Anton Hofman received both his M.Sc. (2012) and Ph.D. (2016) degrees in polymer science from the University of Groningen, The Netherlands, under supervision of Prof. Gerrit ten Brinke and Prof. Katja Loos. In 2017, he joined the Physical Chemistry and Soft Matter group at Wageningen University, The Netherlands, to work as a postdoctoral researcher on polyelectrolyte-containing block copolymers for enhanced underwater adhesives. His research interests include supramolecular chemistry, controlled/living polymerization techniques, and the synthesis and self-assembly of complex block-copolymer systems.

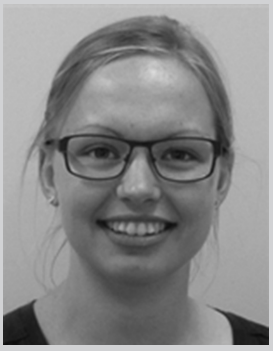

Ilse van Hees received her M.Sc. degree in molecular life sciences from Wageningen University, The Netherlands, in 2015. She is currently a Ph.D. candidate in the group of Physical Chemistry and Soft Matter, Wageningen University, under supervision of Dr. Marleen Kamperman and Prof. Jasper van der Gucht. Her research focuses on the development of synthetic polymers for bioinspired underwater adhesion.

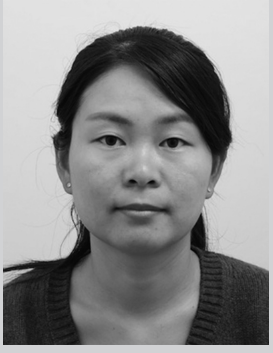

Juan Yang is currently a research fellow at the Rolls-Royce@NTU Corporate Lab at Nanyang Technological University, Singapore. She obtained her Ph.D. in polymer chemistry from Wageningen University in 2016 under supervision of Prof. Martien A. Cohen Stuart and Dr. Marleen Kamperman, where she worked on the development of mussel-inspired materials used as waterborne paints. Her current research focuses on the development of functional nanocomposites.

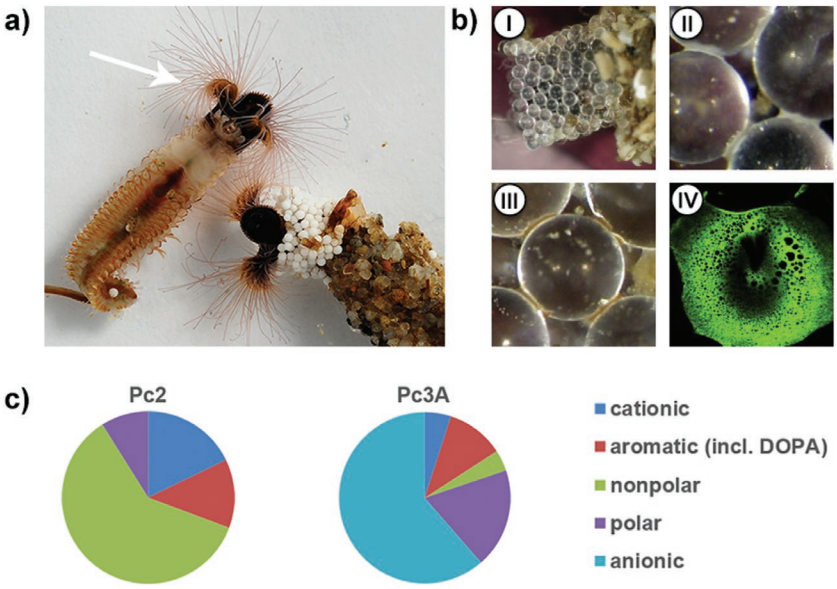

Figure 1. a) Image of sandcastle worms, *Phragmatopoma californica*; the worms are depicted inside and outside their protective shells. New particles are placed onto the shell by its ciliated tentacles (white arrow). The shells in the figure were partially built in a laboratory environment, explaining the different colors of the granules. Image was kindly provided by and used with permission from Russell J. Stewart. b) Glass beads can also be used by the worms for building shells (I). The adhesive was only applied around the contacts of the beads and spread over the surface, which suggests a low interfacial tension (II). After protein secretion, the initially white glue turned brownish in a few hours as a result of DOPA oxidation (III).The final adhesive has a porous, foam-like structure (IV). b) Reproduced with permission.[15] Copyright 2011, Elsevier. c) An overview of the chemical characteristics of the amino acids present in cationic Pc2 and anionic Pc3A. Pc2 is used as representative for all cationic Pc proteins. Data are derived from refs. [14] and [16].

2.1.2. Adhesive Storage

The adhesive proteins are stored in two different types of secretory granules inside the adhesive glands, i.e., the homogeneous and heterogeneous granules (**Figure 2**a). The homogeneous granules contain cationic Pc2 and Pc5 proteins together with sulfated polysaccharides.[21,23] The heterogeneous granules contain two separate domains each with a different content. The main domain encloses cationic Pc1 and Pc4,[23] whereas the subgranules contain anionic Pc3A and Pc3B proteins together with cationic magnesium ions.[24] The fluid, yet concentrated character of the adhesive before secretion, is likely explained by complex coacervation.[21]

Complex coacervation is the association of oppositely charged polyelectrolytes resulting in liquid–liquid phase separation (Figure 2b).[25] This process is often driven by electrostatic interactions, but may involve other types of interactions. The combination of oppositely charged compounds in both the homogeneous and the subgranules suggests that complex coacervates are formed in the granule. The use of coacervation is advantageous for storage and application because it enables surface wetting through low interfacial tension and it concentrates the materials, while maintaining fluid-like properties.[26] Besides electrostatic interactions, additional interactions, such as hydrophobic, cation–π, or π–π interactions, may take place.[27] These interactions have not been identified in the adhesive of sandcastle worms, but hydrophobic interactions may increase the driving force for coacervation, and cation–π interactions may relate to the cationic character of Pc1 and Pc4, which remains unexplained so far.[14,28]

2.1.3. Adhesive Application and Curing Mechanisms

The sandcastle worm applies its adhesive onto the mineral particle from pores in the surface of the building organ. These pores are close together, and it is suggested that each pore secretes a particular granule, i.e., a homogeneous or heterogeneous granule.[14] After granule rupture, the fluid-like contents fuse together into a single heterogeneous material without extensive mixing of the anionic and cationic proteins (Figure 2c).[23] Because it is not clear whether specific proteins are solely located at the adhesive interface,[4] it is also not clear which specific interactions are responsible for adhesion. However, based on similarities between the proteins of the sandcastle worm and mussel, it is expected that comparable mechanisms are involved. Both the sandcastle worm cement and the mussel plaque are rich in phosphate and catechol groups, i.e., DOPA, that are known adhesion promotors. Surface interactions of DOPA are discussed in Section 2.2.2, because in literature they are mainly associated with mussel adhesion.

Several toughening and curing mechanisms start to play a role after application. First there is a change from acidic pH in the gland to the slightly basic pH of seawater.[20] The increase in pH solidifies the Mg^{2+}/sulfated Pc3 complexes that are present in the heterogeneous subgranules.[15,20] Second, the metal ion content in the adhesive changes. While before secretion the granules solely contain Mg^{2+}, significant amounts of Ca^{2+} were detected in the cured adhesive, that were presumably extracted from the seawater.[4,14] Besides magnesium and calcium, also iron, manganese, and zinc were detected in the secreted adhesive material. These ions might cause complexation, by forming ionic bonds or coordinating to DOPA. As a result, they can contribute to the solidification process and act as physical crosslinks.[4,29,30]

At last, the adhesive changes color from off-white to reddish brown while curing (Figure 1b). This color change occurs over a time span of several hours to days and is caused by the oxidation of DOPA. The enzyme catechol oxidase is enclosed in both adhesive granules (Figure 2a) and oxidizes DOPA into DOPA-quinone (**Figure 3**), subsequently leading to the formation of covalent bonds that contribute to the cohesion of the adhesive.[21,31]

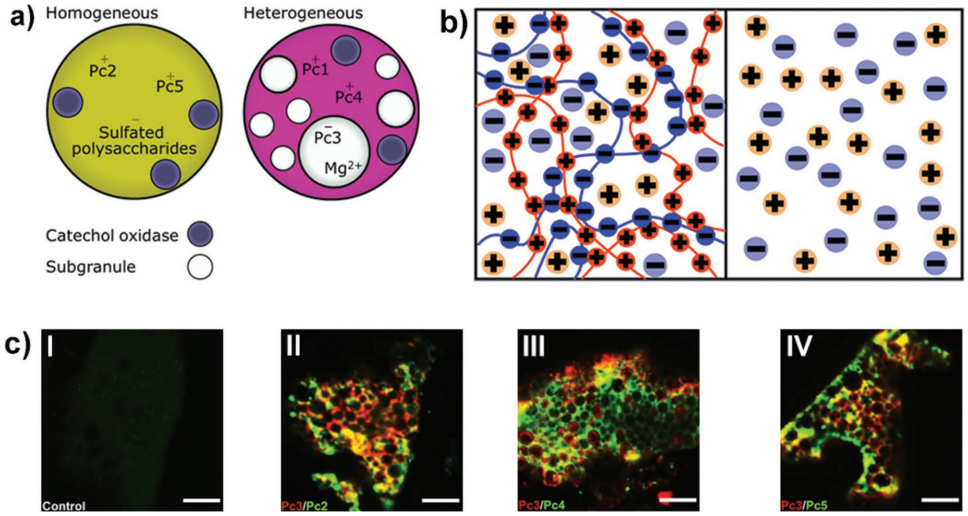

Figure 2. a) The adhesive proteins of the sandcastle worm are secreted from two types of granules (homogeneous and heterogeneous granules) that both contain catechol oxidase. Besides a main compartment, the heterogeneous granules also contain subgranules. Redrawn from ref. [21]. b) Complex coacervates are formed when oppositely charged polyelectrolytes complex and release their counterions. Two phases coexist; a concentrated coacervate phase (left) and a dilute phase (right). Reproduced with permission.[22] Copyright 2015, American Chemical Society. c) The different sandcastle-worm proteins were imaged by fluorescence microscopy after immunological labeling. The cationic proteins (Pc2, Pc4, and Pc5) were labeled green, and Pc3 was labeled red. Hardly any overlap (yellow) of the cationic and anionic proteins was visible. I) Negative control (without any labeling), II) Pc2 and Pc3, III) Pc4 and Pc3, and IV) Pc5 and Pc3 were labeled. Scale bars are 20 µm. Reproduced with permission.[23] Copyright 2012, The Company of Biologists Ltd.

2.1.4. Structural Characteristics of the Adhesive

The adhesive that is formed after curing has an open and foam-like structure, similar to mussel plaque (Figure 1b, IV).[19] Different hypotheses exist about the formation of these porous structures. As Pc3 proteins were solely found at the pore walls, it is hypothesized that the pores in sandcastle adhesives are caused by swelling of the subgranules and subsequent phase inversion. The other proteins from the heterogeneous granule form a matrix closely around the subgranules, which is expected to limit pore growth by providing a counter pressure. Also, this pressure balance on the pore walls might provide mechanical stability to the adhesive after curing.[14,23] Additionally, the sandcastle worm adhesive has a porosity gradient from small pores at the interface of the joint to larger pores inside the joint. Efficiently, high amounts of material are present at highly stressed spots, while only little material is located at spots with low stress.[3,19]

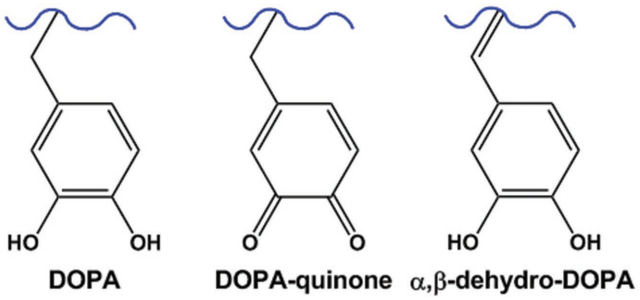

Figure 3. Chemical structures of DOPA, its oxidized form (DOPA-quinone), and the tautomerized form of DOPA-quinone (α,β-dehydro-DOPA).

2.2. Mussels

Mussels are extensively studied marine organisms that stick to surfaces using their byssal threads (**Figure 4**a). These threads consist of three parts: the adhesive plaque, the rigid distal thread, and the flexible proximal thread, which are all coated by cuticle (Figure 4c).[13,32,33] The byssal thread is formed by the mussel foot (Figure 4b), a flexible organ that is pressed against the surface that the mussel aims to adhere to. The byssal thread proteins are secreted in the ventral groove that is isolated from the environment. Three glands were found in the mussel foot: the phenol gland, the collagen gland, and the accessory gland, each secreting granules that contain proteins for different parts of the thread (Figure 4c). After all proteins have been secreted, the mussel retracts its foot, and the byssal thread can obtain its final properties through equilibration with the environment.[2,13,33–36]

2.2.1. Byssus Thread Proteins

So far, 25–30 different mussel foot proteins (mfps) have been identified, of which only 5 types are found in the plaque.[17] These five protein types can be roughly divided into two groups, i.e., the DOPA-rich mfp-3 and mfp-5 proteins at the surface, and the mfp-6, mfp-2, and mfp-4 proteins that are located higher in the plaque (Figure 4d).[17] Mfp-3 is a polymorphous polar protein, meaning that there are many variations of this

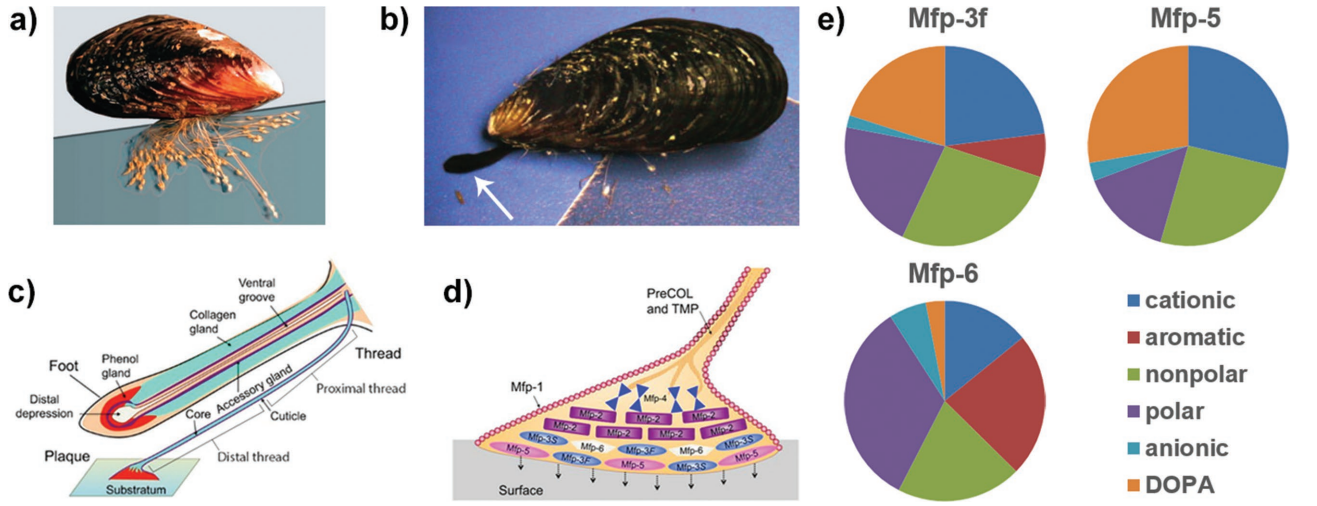

Figure 4. Image of an adult mussel, a) *Mytilus californianus*, that secreted multiple byssal threads b) from the mussel foot (white arrow). The foot is extended from the shell and attaches to the surface before protein secretion. c) Firm attachment to the surface takes place by lifting the ceiling of the distal depression; then, the byssus proteins are secreted into the ventral groove. The phenol gland (red) secretes the proteins that form the plaque (red). The proteins secreted from the collagen gland (green) form the core of the thread (green). The accessory gland (purple) secretes mfp-1 proteins for the cuticle (purple). d) After protein secretion, the mussel foot retracts, leaving the byssus behind in which the proteins are highly organized. The adhesive and DOPA-rich mfp-5 (pink) and mfp-3 (blue) are located at the bottom of the plaque. Above these, the cohesive mfp-6 (white), mfp-2 (purple) and mfp-4 are located. Mfp-4 facilitates the attachment of the plaque to the thread that is made from collagen (PreCOL) and thread matrix protein (tmp). Mfp-1 covers the byssus as a cuticle. a–d) Reproduced with permission.[13] Copyright 2017, The Company of Biologists Ltd. e) An overview of the chemical characteristics of the amino acids present in the mussel foot. Data derived from ref. [17].

type, originating from post-translational modifications,[17] for example, through conversion of tyrosine into DOPA and conversion of arginine into 4-hydroxyarginine.[37] The mfp-3 variants are subdivided into two groups, mfp-3 fast (mfp-3f) and mfp-3 slow (mfp-3s), based on their distinct elution in electrophoretic analysis. Both groups are rich in nonpolar glycine and polar asparagine, but differ substantially in their DOPA and cationic residue contents. Mfp-3f contains a significant amount of DOPA, while mfp-3s has only half of this amount in favor of other aromatic residues. Furthermore, the cationic residue content, mostly protonated 4-hydroxyarginine, is almost twice as high in mfp-3f as in mfp-3s.[38] Mfp-5 is very similar to mfp-3 but is larger (9 vs 6 kDa), and contains significant amounts of cationic lysine instead of arginine. Furthermore, the conversion of tyrosine into DOPA in mfp-5 is almost complete and also comparable between the mfp-5 proteins (Figure 4e). In addition to the post-translational conversions mentioned above, anionic groups are introduced in mfp-5 by phosphorylation of serine.[17,39]

Mfp-6 can be found further away from the surface. Similar to mfp-3 and mfp-5, mfp-6 is rich in glycine and aromatic residues, although a much lower amount of tyrosine is converted into DOPA, and also fewer cationic groups are present.[17,40] Above the mfp-5/mfp-3/mfp-6 layer, mfp-2 can be found which covers 25% of the total protein content in the plaque. The DOPA content in mfp-2 is low, and part of the cysteine residues is crosslinked by disulfide bonds as a result of oxidation.[17,33,41] At the very top, hydrophobic and cationic mfp-4 can be found that is rich in copper-binding histidine. In contrast to all other adhesive mussel proteins, mfp-4 is poor in aromatic amino acids as it only contains trace amounts of DOPA.[17,38]

Besides these five plaque proteins, thread and cuticle proteins are important in byssus formation as well. The thread is attached to the top of the plaque and contains both aligned collagen and thread matrix proteins. The structure of the collagen is as found in other animals $[GX_1X_2]_n$, i.e., a repeated amino acid sequence starting with glycine followed by two varied amino acids in the second and third positions. As a result of the repetitive amino acid sequence, protein domains with a semicrystalline structure of β-sheets are formed. The crystallinity, and thus the stiffness of the thread, is determined by the variation of the amino acids in the second and third positions and is therefore different in distal and proximal byssal regions (see Figure 4c). Final alignment of the semicrystalline domains is likely a result of contraction of the mussel foot during thread formation.[13,33] The thread matrix protein, tmp-1, is rich in hydrophobic glycine and tyrosine residues, but the conversion of tyrosine into DOPA is low in contrast to mfp-3f and mfp-5. Finally, mfp-1 is used to coat the mussel byssus thread with cuticle and thus resides at the water/byssus interface.[13] Mfp-1 has equal amounts of DOPA and cations, and contains many uncharged polar residues, while the amount of nonpolar residues is limited.[15,17,33]

2.2.2. Adhesion

Mfp-3 and mfp-5 are mainly responsible for adhesion of the plaque to the surface. More specifically, DOPA is thought to play a dominant role in both dehydration of and binding to the surface. A submerged hydrophilic surface is generally covered by a layer of ions, water, and several other compounds.[13] For

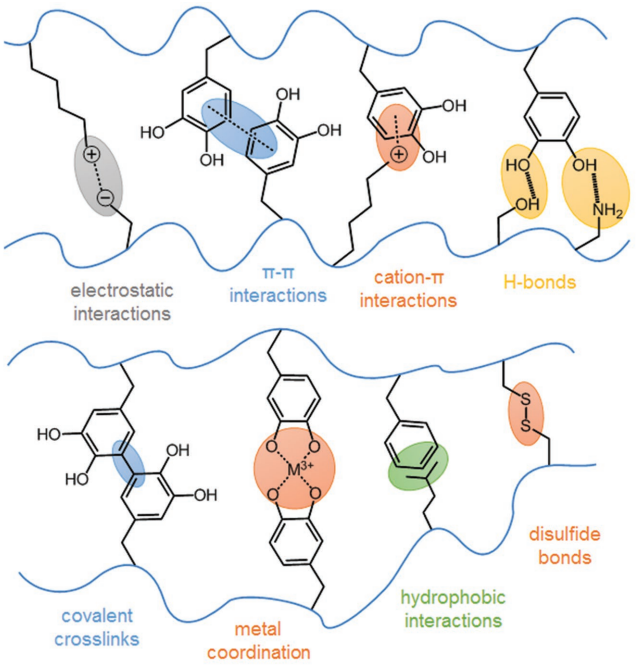

Figure 5. Overview of the different adhesive and cohesive interactions as found in or hypothesized for wet adhesion by sandcastle worms and mussels. Color codes used for each interaction correspond to the different sections of this review. Blue (Section 3: covalent bonding and π–π interactions), grey (Section 4: ionic bonding), yellow (Section 5: hydrogen bonding), green (Section 6: hydrophobic interactions), and orange (Section 7: metal coordination, cation–π interactions and dynamic covalent bonding).

proper adhesion, this layer has to be removed first. For several mimics, it was shown that DOPA efficiently dehydrated surfaces, while tyrosine was inefficient. These experiments also revealed that dehydration was enhanced when DOPA was in the proximity of cationic lysine or incorporated into a coacervate of polyampholytic peptides.[13,36,42,43] After dehydration, DOPA can adhere to a surface by using different mechanisms such as hydrogen bonding, metal oxide coordination, or cation–π interactions (**Figure 5**), as will be discussed more extensively in Section 3.[11,13,17,43] Other amino acids of mfp-3 and mfp-5 may contribute to adhesion by electrostatic or hydrophobic interactions.[13]

In seawater, DOPA is readily oxidized to DOPA-quinone, which can subsequently be converted to α,β-dehydro-DOPA through tautomerization (Figure 3). Both DOPA and α,β-dehydro-DOPA can form hydrogen bonds with the surface, but DOPA-quinone cannot.[34] For this reason, oxidation of DOPA has to be tuned carefully and therefore DOPA-quinone tautomerization seems an easy approach to maintain the adhesive abilities. Furthermore, in the mussel proteins, except for mfp-1, and also in the sandcastle worm proteins, the nonpolar amino acid glycine is mostly located next to DOPA.[16] From synthetic polymers, and from comparing hydrophilic mfp-3f and hydrophobic mfp-3s, it was shown that nonpolar groups inhibit oxidation of DOPA when located in close proximity, hypothetically, through hydrophobic or electrostatic shielding of the DOPA moiety.[44,45] Therefore, glycine likely controls the degree of DOPA oxidation in the adhesive proteins of sandcastle worms and mussels. Additionally, a special feature in the mussel plaque is the reducing ability of mfp-6 that is located in the proximity of mfp-3 and mfp-5. It was shown that both cysteine and DOPA residues in mfp-6 contribute to the reduction of a radical scavenger and are thus expected to reduce DOPA-quinone in the mussel plaque.[11,13,17,46,47] At neutral pH, however, thiols show high reactivity toward quinones and a cysteine–DOPA adduct is formed. This adduct has a slightly lowered oxidation potential compared to DOPA, but is still a strong reducing agent.[31,47] At last, DOPA oxidation can be controlled by careful tuning of the conditions in the ventral groove of the mussel foot. While seawater has a pH of 8.2, the pH in the groove is acidic which severely limits both auto-oxidation and enzymatic oxidation. Catechol oxidase is cosecreted with the mfps and has an optimal activity at pH 8. As a result, the activity of catechol oxidase is minimal in the ventral groove.[11,13]

2.2.3. Processing of the Adhesive

While complex coacervation is expected to concentrate the adhesive proteins of the sandcastle worm before secretion, complex coacervation in the mussel adhesive is unlikely because so far no oppositely charged molecules have been found to complex with the cationic mfps. Alternatively, concentration of the adhesive is hypothesized to take place through coacervation. Coacervation differs from complex coacervation because it involves a liquid–liquid phase separation in a system containing one type of macromolecules, instead of two. From the mfps, mfp-3s was shown to coacervate before full charge neutralization was obtained,[48] suggesting that ionic coacervation of mfp-3s is enhanced by additional interactions such as hydrophobic, cation–π, or π–π interactions.[11,13,48,49] Cation–π interactions were shown to induce a liquid–liquid phase separation of recombinant mfp-1 from solution.[28] At constant pH (7.2), phase separation was induced by increasing the salt concentration till 0.7 M, which is equal to the salt concentration in seawater. As mfp-1 lacks anionic amino acids, cation–π-induced coacervation is a plausible mechanism for concentrating mfps.

2.2.4. Toughening and Curing Mechanisms

The mfps are in a fluid state during secretion and therefore have to solidify and cure afterward, which can be induced by the addition of metal ions or by increasing the pH and ionic strength.[13,33,36] For example, DOPA is able to form metal coordination bonds, such as those occur between Fe^{3+} and mfp-1, and between Fe^{3+} and mfp-2. These metal ions change to a higher stoichiometry (i.e., the number of catechol groups per metal ion) with increasing pH, resulting in stronger binding. However, depending on the amino acids that surround DOPA, the pH at which this strengthening occurs varies.[11,13,33,36,41,50] In addition, pH increase leads to both auto- and enzyme-induced oxidation of DOPA, which is similar in the DOPA-containing proteins of sandcastle worms.[4,11,13]

Besides DOPA, additional functional groups were found to be responsible for solidification and hardening of the byssal thread. For example, proteinaceous phosphate groups, e.g., in

mfp-5, complex with calcium or magnesium ions that were added to the adhesive, post secretion. Upon pH increase, these ionic complexes insolubilize.[13,20,33] Similar insolubilization was identified in the collagen thread; at pH values >6, histidine's imidazolium side group is able to form coordination bonds with zinc and copper ions, resulting in additional toughening of the byssal thread.[13]

Exposure to seawater may also result in changes at the interface. For metal oxide surfaces, such as rock, hydrogen bonds between the surface and catechols are weakened by increasing the ionic strength, due to deprotonation of the hydroxyl groups. Upon sufficient increase of the pH, formation of stronger coordination bonds with the metal oxide groups compensates for this weakening, resulting in improved adhesion.[13,50]

2.2.5. Plaque Characteristics

After curing, the adhesive plaque has a porous structure that is similar to sandcastle glue. Priemel et al. revealed by Raman spectroscopy that the environment of the tyrosine moieties in the byssal thread proteins changes from hydrophobic to hydrophilic during thread formation. This observation suggests that the transition from a fluid to a foam-like structure of the plaque coexists with a conformational change of the proteins.[33] However, this technique did not reveal the mechanism for foam formation. Phase inversion might be an explanation for pore formation in both the mussel plaque and sandcastle worm cement (Section 2.1.4), since phase inversion of complex coacervates led to similar porous structures in synthetic systems.[13,36]

2.3. Adhesion and Cohesion of Adhesives from Sandcastle Worms and Mussels

Even though the sandcastle worm and the mussel adhesives have different characteristics, several strategies seem to be used by both organisms. Figure 5 summarizes all different interactions that have been identified in either the sandcastle worm or the mussel. The adhesive compounds of the sandcastle worms are rich in nonpolar and ionic groups.[16,20] Enhanced by nonpolar amino acids, complex coacervates and metal ion–polyelectrolyte complexes are formed from oppositely charged compounds.[14,21] As a result of complexation, which is a cohesive feature, the adhesive material is concentrated and insoluble in water.[13,14] In addition to the ionic groups, sandcastle worm glue contains moderate amounts of DOPA, which is abundantly present in mfps.[13,16,20] DOPA can interact noncovalently with both the surface and other moieties inside the glue through multiple mechanisms, i.e., H-bonds, metal(oxide) coordination bonds, cation–π interactions and π–π interactions.[11,13,51] Both organisms co-secrete catechol oxidase with their proteins, resulting in the conversion of DOPA into DOPA-quinone.[13,21] Consequently, covalent bonds are formed between DOPA-quinone groups or other amino acids that promote cohesion, such as cysteine or lysine.[11,13,17] This variety of interactions and possible chemical reactions have been used either separately or combined in the development of improved underwater adhesives, as will be described in the following sections.

3. Catechol-Based Materials Used as Underwater Adhesive

The most common method to design biomimetic underwater adhesives is to incorporate DOPA or another catechol functionality into the material. These materials have been reviewed extensively; comprehensive overviews of synthetically produced catechol-based materials are described by Faure et al.,[9] by Moulay,[10] and by Forooshani et al.[11] in addition to excellent summaries of specific subsets of this field including hydrogels based on catechol–metal ion coordination[12] and polydopamine (PDA).[52] Recent findings have indicated that catechol moieties alone are insufficient to ensure proper underwater adhesion and that the performance is also determined by other factors. Therefore, in this part, we will highlight the requirements that have to be considered for designing synthetic DOPA-functionalized adhesives (Section 3.1). In addition, we aim to avoid repetition of work that is already described in recent reviews and limit our discussion to the most recent and exciting work on synthetic catechol-based adhesives for biomedical applications (Section 3.2).

3.1. Tuning the Underwater Adhesion of Catechol-Containing Materials

As discussed in Section 2, among the different mfps, mfp-3 and mfp-5, that are both located at the interface between the plaque and the solid substrate[17] accommodate the highest amount of catechol-containing amino acid DOPA (20 and 28 mol%, respectively). This specific distribution of mfp-3 and mfp-5 has triggered two questions: (1) the presence of DOPA (or catechol) is apparently crucial for aqueous interfacial adhesion; and (2) why has the mussel selected the DOPA content to be around 30 mol% but not more? In the following sections, we will address several aspects that have to be taken into account for wet adhesion properties of catechol-containing materials.

3.1.1. Role of Water in Wet Adhesion

Under aqueous conditions, a thin hydration layer on the substrate prohibits intimate contact between the adhesive polymer (or proteins) and the surface, and thereby creates an obstacle for achieving satisfying wet adhesion.[4,53] Mussels may overcome this obstacle because of the presence of stoichiometric levels of cationic residues that are in close proximity to DOPA.[17] Lysine residues may seize this hydration layer, allowing the catechols to interact with the underlying surface. This hypothesis has been confirmed by using model peptide systems. Maier et al. determined the adhesion of catechol analogs between two mica surfaces at pH 3.3 (ionic strength = 200 mM). By using a surface force apparatus (SFA), they found that the peptide analogs containing both catechol and amines exhibited much stronger adhesion (adhesion strength of 15–18 mJ m^{-2}) than the material that only contained amines (2 mJ m^{-2}) or only catechols (negligible adhesion).[42] Therefore, catechol and lysine groups were proven to work synergistically to promote the mussel's adhesion to wet surfaces.

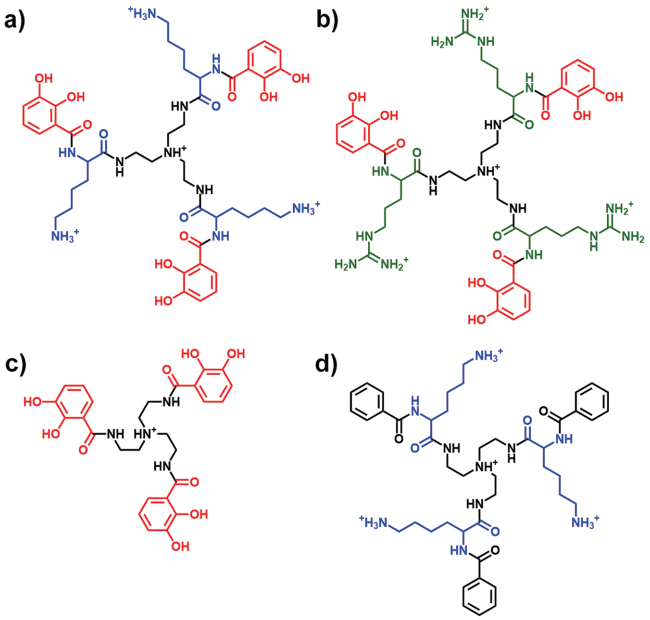

Figure 6. Chemical structures of catechol analogs that were used to investigate the influence of cations on the adhesive performance of catechol-containing tripeptides. a) Tren–lysine–catechol (TLC) and b) Tren–arginine–catechol (TAC) contain both catechols and cations. c) Tren–catechol (TC) only contains catechols, while d) Tren–lysine–Bam (TLB) only contains cations.[54]

Besides lysine, other cationic residues, such as arginine, may also promote wet adhesion by withdrawing the hydrated film from the surface.[54] Rapp et al. studied the adhesion of two synthetic tripeptides that were attached to a tris(2-aminoethyl) amine (Tren) scaffold, i.e., Tren–lysine–catechol (TLC, **Figure 6**a) and Tren–arginine–catechol (TAC, Figure 6b), respectively.[54] Whereas both molecules contained the same amount of catechol units, lysine was incorporated in TLC and arginine in TAC. They found that, in comparison to arginine, lysine's cation was more effective in promoting wet adhesion between mica surfaces in an acetate buffer solution (pH 3.3). This difference was attributed to the bulkier structure and delocalized charge of arginine,[55] which decreased the electrostatic interaction between the cation and the negatively charged sites on mica. In addition, it should be remarked that intramolecular proximity of catechols and cations is necessary to enhance adhesion. Mixing two separate molecules that only contained catechols or amines (Tren–catechol, TC, and Tren–lysine–Bam (benzyl with amine), TLB, respectively, Figures 6c,d), did not create the same adhesion as that of one molecule containing both functional groups. By varying the compositions of such mixtures (TC: 0.02–1 mM, and TLB: 0.2 mM), the adhesive force was identical to that measured in solutions of only TLB; enhanced adhesion was thus not detected.

Compared to hydrophilic surfaces, hydration layers are easier to remove from hydrophobic surfaces because the layer is less strongly attached to this type of surface. Akdogan et al. studied the diffusion dynamics of surface water, either on hydrophobic polystyrene (PS) or hydrophilic silica (SiO_2) surfaces, in the presence of various mfps, i.e., mfp-1, mfp-3s, and mfp-5.[56] By measuring the diffusion coefficient of the surface-bound water molecules, the ability of mfps to perturb the surface water dynamics was used as an indication of the intimacy between surfaces (PS or SiO_2) and mfps. They found that the hydration layer was weakly attached to PS. Mfp-3s exposed the hydrophobic part of the protein toward the PS surface, thereby expelling the weakly bound hydrated layer. In comparison, the SiO_2 surface was surrounded by a much stronger hydration barrier,[57,58] and the water layer was more difficult to remove. It was reported that mfp-1, mfp-3f, and mfp-5, as measured by SFA, can bind ten times stronger to hydrophobic surfaces than to hydrophilic surfaces.[59]

3.1.2. Catechol Surface Interactions

The ability of mussels and sandcastle worms to adhere to various substrates originates from the versatility of the interactions that catechol can undergo (see also Section 2). In other words, it depends on the surface chemistry of the substrate.[11,13,17,43,48,57,60,61] A summary of all the possible interactions between catechols and various surfaces has been described by Ye et al.[62]

By using an SFA, Lu et al. studied the interaction between mfp-1 and several substrates (mica, SiO_2, poly(methyl methacrylate) (PMMA), and PS) at pH 5.5. The wet adhesive strength between symmetric mica substrates bridged by mfp-1 was significantly higher than between PS, SiO_2, and PMMA substrates. Assuming that DOPA is residing at the interface, DOPA dominates the interfacial interaction between surfaces. Mica is hydrophilic, and under aqueous conditions its surface exposes silicate groups with minor replacement of Si by Al (**Figure 7**). Possible interactions between catechol and mica include (1) bidentate hydrogen bonding between the hydroxyl groups of catechol and the oxygen atoms of mica and (2) metal complexation to oxidized Al groups. For SiO_2 and PMMA, bonding was primarily via bidentate hydrogen bonding and hydrophobic interactions, respectively. For PS surfaces, a combination of hydrophobic, cation–π, and π–π stacking interactions was involved. Among

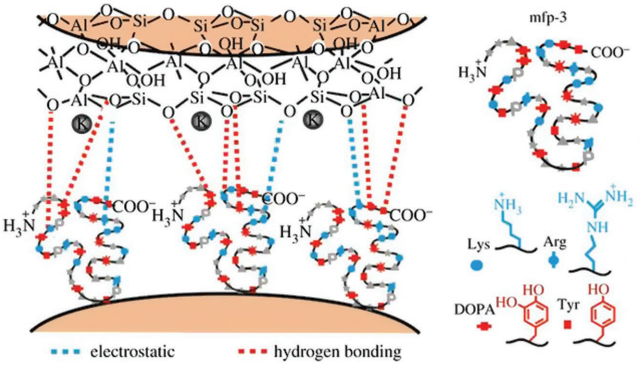

Figure 7. A mica substrate can interact through several mechanisms with mfp-3f proteins that are rich in DOPA and cationic amino acids. Hydrogen bonding can occur between the metal oxide groups of the mica surface and hydroxyl groups of DOPA in mfp-3f. In addition, the metal oxide groups interact electrostatically with cationic lysine and arginine moieties. Reproduced with permission.[57] Copyright 2013, The Royal Society.

these types of interactions, the strength of cation–π complexation is stronger than hydrogen bonding and π–π stacking in aqueous solution.[57,63,64] Compared to hydrogen bonding, the metal ion–catechol coordination bonds (Ti^{4+}, Fe^{3+}, and Al^{3+}) are considerably stronger.[65]

Anderson et al. investigated the adhesion of a mussel-inspired synthetic copolymer (2-hydroxyethyl)-L-glutamine and DOPA (18 mol% of DOPA) using SFA between symmetric titania (TiO_2) and mica surfaces.[66] They found that the adhesion of the copolymer to TiO_2 (0.5 mJ m^{-2}) was much stronger than to mica (0.05 mJ m^{-2}).

Yu et al. studied the interaction of mfp-1, mfp-3f, and mfp-5 on hydrophobic surfaces (CH_3-terminated self-assembled monolayers (SAM) on gold) and hydrophilic surfaces (OH–SAM) at pH 3 by using SFA. They found that all mfps bonded more strongly to hydrophobic CH_3–SAM surfaces (mfp-1, mfp-3f, and mfp-5 had adhesion energies of 3.5, 8.9, and 0.7 mJ m^{-2}, respectively), than to hydrophilic OH–SAM surfaces (mfp-1, mfp-3f, and mfp-5 had adhesion energies of 0.25, 0.37, and 0.31 mJ m^{-2}, respectively). They proposed that the strong adhesion to hydrophobic surfaces originated from the hydrophobic interactions between the alkyl surface and the aromatic moieties of catechol in mfps. The interaction between mfps and the OH–SAM surface is likely via hydrogen bonding between the hydroxyl groups of catechol and the modified surfaces.[59]

3.1.3. The Adhesion–Cohesion Balance under Wet Conditions

For obtaining good adhesive performance, the cohesive interactions within the bulk material are equally important as the adhesive interactions. The catechol functionality contributes to cohesion through a combination of various covalent and noncovalent interactions. Covalent interactions are based on quinone-mediated crosslinking,[5,67–69] in which the catechols are easily oxidized to reactive *o*-quinones that can undergo subsequent secondary reactions with nucleophiles (e.g., amines or thiols). By tuning certain parameters (e.g., pH, the type of oxidant, and the oxidant concentration), it is possible to adjust the crosslinking reactions, and consequently, the cohesion properties of the synthetic adhesive. A systematic description of the possible variables has been reported in a recent review by Yang et al.[31]

Besides covalent bonding, natural systems also employ cohesive noncovalent bonds involving DOPA to achieve superior properties, including coordination interactions with metal ions, hydrophobic interactions, cation–π interactions, and hydrogen bonding.[70–74] The most studied noncovalent interaction is the coordination complexation between catechols and metal ions, e.g., Fe^{3+}, Mg^{2+}, and Ca^{2+}. Since an extensive review on catechol–metal ion complexation was recently given by Krogsgaard et al.,[12] the details will not be repeated here. The use of coordination complexation with metal ions in synthetic systems will be discussed in-depth in Section 7.

The aforementioned dual role of catechols has brought up the importance of optimizing the catechol content to achieve a good adhesive–cohesive balance.[69,75] The optimization of the catechol content has been studied in synthetic polymer systems. For instance, North et al. synthesized a series of poly(catechol–styrene) copolymers with a catechol content varying between 0 and 40 mol%.[75] After having cured the material in artificial seawater for 72 h, they measured the lap shear strength using aluminum substrates. The maximum underwater adhesion was achieved with a polymer that contained 22 mol% catechol units (3 MPa). A further increase in catechol content resulted in a decrease of the adhesion strength to 1.8–2.4 MPa.

Li et al. synthesized three polyvinylpyrrolidone-based catechol-containing copolymers with catechol contents of 9, 16, and 23.5 mol%.[76] The copolymers were crosslinked by adding $FeCl_3$ (molar ratio of Fe^{3+}:catechol is 1:1) during the preparation of the lap shear specimen. Lap shear testing of the polymers between two glass substrates underwater showed that the adhesion peaked at 1.36 MPa for the polymer that contained 16 mol% catechol. The polymer containing 9 and 23.5 mol% of catechol exhibited lap shear strengths of 0.71 and 0.8 MPa, respectively. All copolymers demonstrated cohesive failure.

3.1.4. How to Prevent Catechol Oxidation to Maintain Adhesion?

For both natural adhesive proteins and synthetic catechol-containing materials, catechol oxidation is detrimental to its adhesive ability, since the formed *o*-quinones are nonadhesive. For instance, when the catechols in mfp-5 were oxidized at pH 5.5, mfp-5 had a threefold lower adhesion energy than at pH 2.6.[77] Adhesion of both mfp-3f and mfp-5 was negligible at pH > 7.5.[77,78]

Under basic conditions, it might be possible to lower the possibility of catechol oxidation by introducing hydrophobic groups into the material. Hydrophobic moieties can interact with the aromatics in catechol, and thereby reduce the sensitivity of catechols toward oxidation.[57] Zhong et al. designed a hybrid material by fusing the DOPA-based adhesive mfp-5 and amyloid-based protein CsgA (the major subunit of the adhesive fibers in *Escherichia coli*[79]) using synthetic biology techniques. After self-assembly of CsgA into nanofibers, the disordered mfp-5 was exposed to the exterior of the amyloid cores.[80] Using atomic force microscopy (AFM) with a colloidal probe technique, they found that the obtained protein mfp-5-CsgA maintained its adhesion strength under both acidic and neutral conditions (pH 2.5–7.0), showing an adhesion force of 50, 52, and 55 mN m^{-1} at pH 2.5, 5.0, and 7.0, respectively. At elevated pH (10.0), mfp-5-CsgA still exhibited considerable adhesion with an adhesion force of 40 mN m^{-1}. The improved tolerance of mfp-5-CsgA toward auto-oxidation was ascribed to hydrophobic interactions between the aromatic residues and the amyloid fibers. Similarly, by partial conversion of mfp-5-CsgA's tyrosine residues into DOPA (50–70%), the remaining hydrophobic tyrosine residues also inhibited oxidation of DOPA at neutral pH. The adhesion strength at acidic pH values of 2.5 and 5.0 was 130 and 136 mN m^{-1}, respectively, and only dropped slightly at neutral pH to 118 mN m^{-1}. The increase in adhesion as compared to the protein before tyrosine conversion is most likely related to the higher DOPA content.

It is also possible to limit catechol oxidation by introducing protection groups into the material. One promising functional group is borate that can form bidentate catechol–boronate complexes with DOPA. As reported by Kan et al., the presence of

borates at pH 7.5 can retard catechol oxidation. The adhesion between two symmetric mica surfaces bridged by mfp-5 was fully maintained as compared to that at pH 3.0.[81] Narkar et al. designed a copolymer containing catechol and borax functional groups, i.e., a copolymer composed of dopamine methacrylamide and 3-(acrylamido)phenylboronic acid. By performing contact mechanics tests on the hemispherical copolymer sample and the substrate, they measured the work of adhesion at acidic and basic conditions. At acidic pH (pH 3), the copolymer binds strongly to the substrate (work of adhesion 2 J m^{-2}), mainly because of hydrogen bonding between borosilicate surfaces and the catechol and phenylboronic groups. At basic pH (pH 9), adhesion decreased significantly (0.5 J m^{-2}). This diminished adhesion is due to the formation of catechol–boronate complexes, leaving a few free catechols or phenylboronic groups available to interact with the surface. Catechol oxidation, commonly taking place at elevated pH, was suppressed via this approach. Although the polymer showed limited adhesion at basic conditions, adhesion could be recovered by decreasing the pH to acidic conditions. Therefore, this protection strategy provides a route for designing pH-responsive adhesives that can switch between adhesive and nonadhesive behavior.[82]

3.2. Synthetic Catechol-Containing Adhesives

Because of the unique wet adhesion properties, one of the most promising and evident applications of natural adhesive proteins is their use as surgical tissue adhesives. Therefore, it is desirable to obtain adhesives directly from natural organisms. However, the limited quantities that can be obtained through extraction from mussels and sandcastle worms make it a rather demanding and costly task. Currently available commercial adhesives, such as cyanoacrylates, are not suitable for biomedical applications due to problems involving their slow degradation rate, toxicity, and poor adhesive performance in a humid environment.[83,84] Therefore, considerable efforts have been devoted to develop biomimetic adhesives via synthetic methods using, for instance, hybrid materials. Because of the vast amount of literature on catechol-containing synthetic materials,[85] in this part we will only highlight the most recent catechol-functionalized polymers that were used for biomedical applications.

The most straightforward method to obtain catechol-based adhesives is to incorporate the catechol moiety into materials that are already used for biomedical applications, such as chitosan, poly(ethylene glycol) (PEG), hyaluronic acid, and alginate.[86–89] Kim et al. synthesized a catechol–tethered chitosan polymer containing 20.5 mol% catechol. The mucoadhesion of the modified polymer exhibited a fourfold increase in performance compared to neat chitosan. At low pH, this catechol–tethered chitosan associated with negatively charged mucin by electrostatic interactions. Subsequently, on raising the pH to neutral conditions, covalent bonding occurred between oxidized catechols and thiols in mucin. By evaluation of the polymer through an oral administration to mice, the researchers found that the polymer had a retention time of up to 10 h, which was significantly longer than that for neat chitosan. Furthermore, the polymer did not exhibit any cytotoxicity.[88]

Kastrup et al. designed a catechol-conjugated alginate polymer, which formed a gel initiated by catechol oxidation. As determined by lap shear testing, the gel exhibited an adhesive shear strength two to three orders of magnitude higher than that generated by physiological blood flow. By injection of the gel solution into the carotid arteries of mice, the gel could crosslink and coat the blood vessel with long-term durability under blood flow (>30 d). The gel coating did not exhibit a prolonged chronic inflammatory response and is therefore promising for biomedical applications.[86]

Shin et al. designed a tissue adhesive by functionalizing hyaluronic acid with an adhesive catecholamine (HA–CA).[90] The obtained HA–CA hydrogel exhibited much stronger adhesion to liver tissue compared to the control sample hyaluronic acid–methacrylate (HA–ME). By encapsulating human hepatocyte cells in a HA–CA hydrogel, the cells showed improved viability compared to those in the HA–ME hydrogel.

Liu et al. designed a nanocomposite adhesive hydrogel composed of eight-armed PEG and nanosilicate Laponite (Laponite is a trademark of the company BYK Additives Ltd.), in which PEG was end-functionalized with dopamine.[92] By mixing PEG (15 wt%) and Laponite (5 wt%), hydrogels formed due to the interfacial interactions between PEG-bound dopamine and Laponite. The formed hydrogel was initially stretchable and could be remolded to different shapes. After a prolonged period (>24 h), the basic nature of Laponite induced auto-oxidation of catechols, thereby crosslinking the hydrogels and fixating the shape. The hydrogel exhibited excellent adhesion; by applying the hydrogel (incubated for 20 h) with a syringe around the contour of collagen tubing over the suture line, no leakage was observed when phosphate-buffered saline (PBS) was pumped through the tubing.

In another example, Han et al. developed an adhesive polydopamine–clay–polyacrylamide hydrogel in which the dopamine was intercalated into clay sheets (**Figure 8**).[91] The hydrogel could adhere to various hydrophobic and hydrophilic

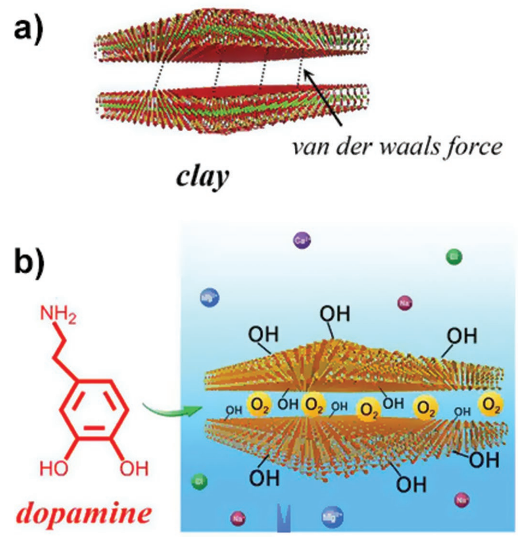

Figure 8. a) Clay has a layered structure that is held together by van der Waals interactions. b) Dopamine monomers intercalate into the space between the nanoclay layers. Reproduced with permission.[91] Copyright 2017, American Chemical Society.

surfaces, such as glass, titanium, polyethylene, and porcine skin. The hydrogel was cytocompatible and favored cell adhesion. By loading the gel with epidermal growth factor to repair in vivo skin defects, wounds closed almost completely after 21 d and had a healing ratio of 80%, which was much faster than the untreated wounds. Therefore, these types of material are promising for clinical applications.

4. Adhesives Based on Electrostatic Interactions

Several research groups have been inspired to develop adhesive materials based on electrostatic interactions, because these interactions play an important role in the adhesive processing and performance of sandcastle worms and mussels (Section 2). The strength of electrostatic interactions can be controlled by varying the ionic strength or pH and can thus be used to tune the mechanical properties. In this section, materials based on electrostatic interactions will be discussed, including (complex) coacervation (Figure 2b) and ion-based crosslinking, of either recombinant proteins or synthetic materials. We will also highlight work where (complex) coacervation is used as a delivery tool for underwater adhesives. **Tables 1** and **2** provide an overview of the adhesive strengths as measured by SFA and lap shear testing, respectively.

4.1. Protein-Based (Complex) Coacervate Adhesives

4.1.1. Natural Mussel Foot Proteins

The most obvious approach to obtain a functional underwater adhesive is to use the adhesive proteins from the marine animals themselves. To this end, Wei et al. isolated mfp-3s from the mussel plaque, which is so far the only natural mussel foot protein that has been shown to phase separate by coacervation at low salt concentrations.[45,48] Coacervation usually occurs when the proteins carry equal amounts of positive and negative charges, which is at pH > 7.5 for mfp-3s. Here, phase separation occurred at lower pH values (pH = 5.5), which suggested that additional interactions between the now net-charged proteins enhanced electrostatically driven coacervation. Adhesion was determined by both SFA and quartz crystal microbalance dissipation (QCM-D). Optimal adhesion to hydroxyapatite (from QCM-D) was obtained in a buffer at pH 5.5, which was the condition that resulted in the most fluid-like material. Wei et al.[48] speculated that the mfp-3s coacervate in optimal conditions is able to dissipate the energy of deformation which results in improved adhesion compared to mfp-3s coacervates at different pH.

4.1.2. Recombinant Mussel Foot Proteins

Unlike Wei et al., Choi et al. did not isolate proteins from the mussel glue but produced natural mfp-5 protein from recombinant *E. coli*.[95] However, since these bacteria are not able to convert tyrosine into DOPA, because they lack the tyrosinase enzyme of mussels, mushroom tyrosinase was added to the protein solution after purification. Adhesion of recombinant mfp-5 was investigated by lap shear tests. Adhesive strengths of 1.11 MPa to aluminum were measured after incubation with tyrosinase for 4 h at 37 °C (Table 2). Since complexation with a polyanion was shown to further improve adhesion of mussel foot proteins,[96] a complex coacervate (Figure 2b) was formed by mixing cationic mfp-5 with hyaluronic acid, an anionic polyelectrolyte commonly present in the human body.[6,96,97] After complexation, the shear strength increased to 1.73 MPa and could compete with values previously reported for recombinant mimics of mussel adhesive proteins that were also complexed into coacervates.[95,96,98]

Table 1. Overview of adhesion strengths of electrostatically based adhesives measured by SFA. Complex coacervates are depicted as polycation/polyanion. Unoxidized DOPA (u), oxidized DOPA (o), coacervated (c), and catechol (Cat).

System and conditions	Substrate	Wet/dry	Solvent conditions	Strength [mJ m^{-2}]	Ref.
mfp-3s					
u	Mica	Dry	N/A	3.7	[48]
Quaternized chitosan/catechol-functionalized poly(acrylic acid) (30 mol%)					
u	Glass	Wet	Water	2000	[93]
u, w/o catechol functionalization	Glass	Wet	Water	≈0	[93]
Random copolymer of 3-(3,4-dihydroxyphenyl)-2-hydroxypropyl acrylate (30 mol%), 2-(diethylamino)ethylacrylate (6 mol%), acrylic acid (4 mol%), hydroxyethyl acrylate (51 mol%), methyl acrylate (9 mol%)					
u	Mica	Wet	Water (pH 7)	32.9	[44]
Zwitterions					
Z-Cat-C10, u	Mica	Wet	Deionized water	10.1	[94]
Z-Cat-C10, o, dried	Silicon	Dry	N/A	175	[94]
Z-Cat-C4, u	Mica	Wet	Deionized water	19.2	[94]
Z-Cat-C8, u	Mica	Wet	Deionized water	2.5	[94]
Z-Ben-C8, u (benzene i/o cat)	Mica	Wet	Deionized water	0	[94]
Z-Cat-Cat, u (cat i/o alkyl)	Mica	Wet	Deionized water	8.1	[94]

Table 2. Overview of adhesion strengths of electrostatically based adhesives measured by lap shear tests. Complex coacervates are depicted as polycation/polyanion. Unoxidized DOPA (u), oxidized DOPA (o), coacervated (c), and hyaluronic acid (HA), double-network (DN), room temperature (RT).

System and conditions	Substrate	Wet/dry	Solvent conditions	Strength [MPa]	Ref.
mfp-5					
u	Aluminum	Dry	N/A	1.1	[95]
u, c HA	Aluminum	Dry	N/A	1.7	[95]
mfp-131					
u	Aluminum	Dry	N/A	1.87	[96]
u, c HA	Aluminum	Dry	N/A	4	[96]
mfp-151					
u	Aluminum	Dry	N/A	1.98	[96]
u, c HA	Aluminum	Dry	N/A	3.17	[96]
u, c HA	Aluminum	Wet	Deionized water	0.24	[96]
o, c HA	Aluminum oxide	Wet	Water	0.88	[6]
o, c HA, w/o DOPA	Aluminum oxide	Wet	Water	0.11	[6]
Poly(acrylamide-*co*-aminopropyl methacrylamide)/2-(methacryloyloxy) ethyl phosphate dopamine methacrylamide					
o	Bone	Wet	Phosphate buffer, 170 mM (pH 7.4)	0.06	[100]
o, Ca^{2+}	Bone	Wet	Phosphate buffer, 170 mM (pH 7.4)	0.1	[100]
Aminated collagen hydroxylate/poly(monoacryloxyethyl phosphate-*co*-dopamine methacrylamide)					
u, Ca^{2+}	Aluminum	Wet	Water (pH 7.4, 37 °C)	0.27	[101]
u, Mg^{2+}	Aluminum	Wet	Water (pH 7.4, 37 °C)	0.65	[101]
o, Ca^{2+}	Aluminum	Wet	Water (pH 7.4, 37 °C)	0.55	[101]
o, Mg^{2+}	Aluminum	Wet	Water (pH 7.4, 37 °C)	0.77	[101]
poly(acrylamide-*co*-aminopropyl methacrylamide)/2-(methacryloyloxy) ethyl phosphate dopamine methacrylamide					
o, Ca^{2+}	Aluminum	Wet	Water (RT)	0.512	[103]
o, Ca^{2+}, DN 17.7 wt%	Aluminum	Wet	Water (RT)	0.973	[103]

An example of a protein mimic is mfp-151, developed by Hwang et al.[98] Mfp-151 is composed of a mfp-5 protein sequence in the middle of the protein, flanked by six repeats of an mfp-1 sequence on both sides. The protein was post-translationally exposed to tyrosinase to obtain DOPA, and subsequently complexed to hyaluronic acid.[26] The adhesive showed immediate surface wetting because of the low interfacial tension with water that is typical for complex coacervates, and shear thinning enabled facile application through a syringe. In addition, for the coacervates high friction coefficients of 1.2–1.4 were obtained and were independent of the degree of coacervation, and therefore presumably caused by the presence of DOPA in mfp-151.

In subsequent work, Lim et al. tested the adhesion of hyaluronic acid complexed to mfp-151 and mfp-131 (mfp-3 flanked by six mfp-1 repeats), which were treated with tyrosinase to acquire DOPA.[96] This work demonstrated that complexed recombinant mfps may acquire stronger adhesion than complexed natural mfp-5 (Table 2).[95] In addition to adhesion, Lim et al. also investigated the formation of microcapsules from these recombinant mfp-based complex coacervates.[96] They found that red pepper seed oil was completely taken up by the coacervate droplets. This finding illustrates the opportunities for employing complex coacervates in medicine, for example, as drug carrier.

The water-insoluble mfp-151/hyaluronic acid complex was applied as medical adhesive for urinary fistula sealing and bone graft binding by Kim et al.[6,97] For urinary fistula sealing, the adhesive was covalently cured by oxidizing DOPA with sodium periodate (12 h, 37 °C) after application to the surface. Subsequently, the wet shear strength of the cured complex was investigated under physiological conditions and compared to conventional medical glues. On the one hand, adhesion of the material to metal oxide surfaces was only half as strong as adhesion of conventional cyanoacrylate, while on the other hand, wet adhesion to porcine skin appeared to be four times stronger. This difference in adhesion was attributed to the presence of surface-bound nucleophilic groups (e.g., hydroxyl groups) on the porcine skin that form covalent bonds with DOPA, but not with acrylates.[6] In the second application, an unmodified, so DOPA-free, mfp-151/hyaluronic acid complex enriched with deproteinized bovine bone minerals was applied as bone graft binder.[97] Complex coacervation was required to avoid dispersion of the protein by blood. Without curing, the bovine-enriched complex coacervate displayed improved resistance to uniaxial compression, and improved bone regeneration with 50%, at 8 weeks postsurgery.[97] These two examples indicate that complex coacervates of recombinant adhesive proteins are promising materials for medical applications, irrespective of the DOPA content.

4.2. Synthetic Adhesives with Opposite Charges

4.2.1. Polyelectrolytes

In contrast to the protein-based adhesives discussed in the previous section, Zhao et al. designed a fully synthetic underwater adhesive that was applied to a water immersed surface via solvent exchange.[93] The adhesive consisted of oppositely charged polymers: a random copolyanion containing anionic acrylic acid and catechol-functionalized acrylic acid (7:3), and a polycation composed of quaternized chitosan ion-paired with bis(trifluoromethane)sulfonamide (Tf_2N^-). The use of Tf_2N^- counterions allowed chitosan to dissolve in dimethylsulfoxide (DMSO). Without complex formation taking place, the polymers were combined in a single DMSO solution and subsequently applied onto a water-immersed glass slide. Miscibility of DMSO and water enabled solvent exchange, which resulted in deprotonation of acrylic acid by water, followed by complexation of acrylic acid and chitosan (**Figure 9**a). The material sedimented, spread over the glass surface, and initial setting occurred in 25 s. After a few more minutes, water blasting could be resisted and after immersing two glass slides in demineralized water for 1 h, an adhesive energy of 2 J m^{-2} was measured with a SFA. Such strong adhesion was attributed to the catechol units in the polyanion because adhesion weakened considerably when the catechol units were omitted or blocked for surface interaction by addition of Fe^{3+}. The catechol content also affected the structure of the material, as increasing the catechol content increased porosity. The polyelectrolyte complex adhesive attached to a wide variety of surfaces, ranging from glass to plastics and from metals to wood, making it a multifunctional underwater glue.[93]

Examples of synthetic coacervate-based adhesives where electrostatic interactions take place inter- and intramolecularly, i.e., polyampholytes, have also been reported. Seo et al. synthesized catechol-functionalized mimics of mfp-3s with varying amounts of nonpolar and ionic monomers to investigate the influence on catechol oxidation, adhesion and cohesion, by cyclic voltammetry and SFA, respectively.[44] Two polymers without or with a reduced number of nonpolar groups were analyzed. It was shown that nonpolar groups efficiently inhibited oxidation of catechol and provided cohesion to the adhesive material. However, very thin layers of polymer (1–6 nm) have been used for these SFA measurements. At such small length scales, the surface affects the conformation of the polymers throughout the whole film. Therefore, the observed cohesion does not reflect the cohesive properties of bulk material, but only that of the measured film. Furthermore, the pH dependence of adhesion was tested, showing a maximum at pH 4 (17.0 mJ m^{-2}) through optimal surface coverage because of the coacervate phase. However, both optimal adhesion and cohesion to mica were obtained by increasing the pH from 4 to 7 (Table 1), possibly because of optimal surface coverage combined with reduced repulsion between the polymers after pH increase.

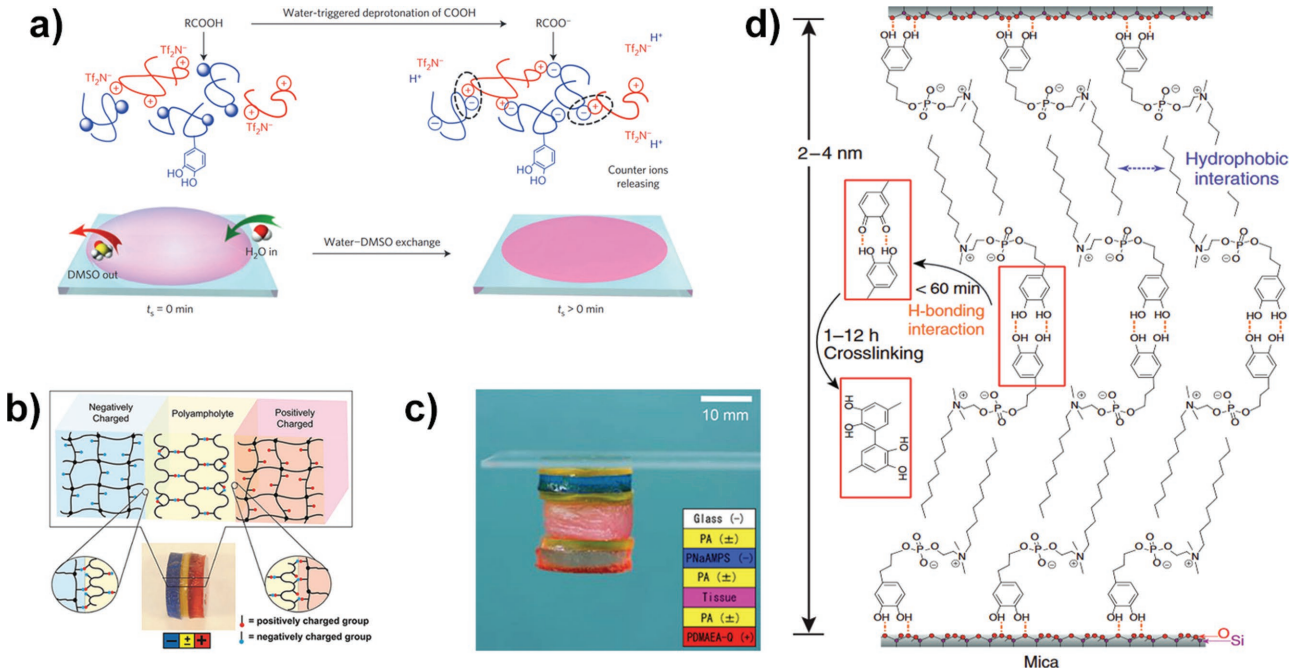

Figure 9. a) A complex coacervate, based on catechol-functionalized poly(acrylic acid) and chitosan, was used for the formation of a wet adhesive. Solvent exchange of the initial solvent DMSO and bulk water resulted in deprotonation of acrylic acid followed by complex coacervation. Reproduced with permission.[93] Copyright 2016, Macmillan Publishers Ltd. b) Polyampholyte gels (yellow), with equal amounts of positive and negative charges, adhered to both anionic (blue, left) and cationic (red, right) hydrogels. The blue and red dots in the scheme represent the anionic and cationic charges, respectively. Counterions were omitted from the scheme for clarity. c) The polyampholyte gel also adhered to glass and pork tissue that are both moderately charged. b,c) Reproduced with permission.[99] Copyright 2015, Wiley-VCH. d) A double bilayer was formed from amphiphilic zwitterions between the mica surfaces through H-bonding and hydrophobic interactions. Further strengthening of the adhesive was obtained by covalent crosslinking through DOPA oxidation. Reproduced under the terms of the Creative Commons Attribution 4.0 International License.[94] Copyright 2015, Macmillan Publishers Ltd.

4.2.2. Ionic Gels

Roy et al. developed a polyampholyte gel, i.e., a covalently crosslinked copolymer containing monomers of opposite charge (Figure 9b).[99] Covalent crosslinking was necessary to acquire sufficient strength. Despite the crosslinks, the gel was soft, viscoelastic, and contained about 52% water. In addition to the polyampholyte hydrogel, several anionic, cationic, and neutral gels were also prepared that functioned as substrate for adhesion. By tensile and lap shear tests, the researchers showed that the polyampholyte gel adhered to both cationic and anionic gels. For anionic substrates, a maximum adhesive shear energy of 30 J m^{-2} and a tensile bond strength of 236 kPa were observed. On the contrary, adhesion to neutral hydrogels was significantly weaker with only 0.3 J m^{-2} shear energy and 42 kPa bond strength. As a result, the researchers concluded that adhesion of the polyampholyte hydrogel was based on ionic interactions, regardless of the nature of the surface charge, as both cationic and anionic charges are present in the gel. Pork tissue, which is slightly charged, was used as a model system for adhesion in medical applications (Figure 9c). The anionic hydrogels did not adhere to liver tissue at all, and cationic hydrogels only adhered shortly, while the polyampholyte outperformed all other gels with a critical energy of 3 J m^{-2} and a bond strength of 24 kPa. For this reason, ampholytic gels may be promising adhesives for applications in life sciences.

4.2.3. Zwitterions

Ahn et al. developed low-molecular-weight zwitterions for preparing complexes as an alternative to polyampholytes (Figure 9d).[94] The zwitterions were functionalized with two short aliphatic carbon tails of which one contained a catechol unit at the end. In agreement with the findings of Seo et al., a longer carbon tail, thus higher hydrophobicity, led to a decreased solubility and increased resistance to catechol oxidation.[44] Adhesion was determined after adsorbing the zwitterions in thin films onto the mica surface of the SFA. As deduced from the interfacial energies, all films failed cohesively (Table 1). The thickness of the adhesive layer depended on the tail length (2–4 nm). Based on this observation, the authors suggest that the zwitterion coating consists of a double bilayer that is formed by attachment of the catechol groups to the surface through hydrogen bonding. A second layer of zwitterions then binds hydrophobically to the first layer. When this process takes place at two surfaces, the outer catechol groups on either bilayer can again form hydrogen bonds upon contact (Figure 9d). Adhesion by the zwitterions could be further improved via covalent crosslinking of the catechol groups through oxidation with sodium periodate. The combination of crosslinking and drying of the material resulted in optimal adhesion to silicon (175 mJ m^{-2}).

4.3. Ionic Crosslinking of Polyelectrolytes

4.3.1. Metal Ion-Enhanced Complex Coacervates

It is also possible to enhance or induce complexation by adding nonpolymeric ions to polyelectrolytes. The effect of metal ions in complex coacervate adhesives was explored by Shao et al. who complexed an anionic catechol-functionalized random copolymer that contained phosphate groups, with a cationic amine-functionalized random copolymer.[100] Adding a 4:1 mixture of Mg^{2+} and Ca^{2+} to the complex coacervate of these polymers enhanced complexation and increased the mass of the concentrated phase. Wet adhesion to bones was tested after curing with sodium periodate (pH 7.4, 24 h, 100% humidity), and was improved with an increasing amount of metal cations. It was hypothesized that singly charged amine groups of the polymer were replaced by the doubly charged metal ions, supposedly leading to a conformational change in the network and stronger adhesion. Despite the addition of the metal ions and sodium periodate for covalent crosslinking of catechol, limited bond strengths of only one-third of the natural sandcastle worm glue were measured.

Hereafter, Shao et al. further investigated the influence of adding divalent cations to complex coacervates using a slightly different system. This material was prepared from a cationic aminated collagen hydroxylate polymer, and an anionic copolymer of monoacryloxyethyl phosphate and dopamine methacrylamide.[101] The resulting complex coacervates were toughened with either Ca^{2+} or Mg^{2+}, resulting in solidification of the complex with increasing metal concentration and pH. Optimal bond strengths were obtained by covalent curing of the catechol moieties through oxidation by sodium periodate. Magnesium-containing complexes adhered with 0.77 MPa to aluminum, which was 40% higher compared to calcium-enhanced complexes (Table 2).[101]

Subsequent work presented a calcium-enhanced adhesive for craniofacial reconstruction,[102] a process where loose bone parts of the face or skull are repositioned and fixated for improved bone healing. The adhesive was tested in rats and it maintained alignment of the fixated bones, improved bone regeneration, and it was biodegradable. Blood did not dilute the adhesive nor did it flow in between the adhesive and bone interface, which is one of the key advantages of using complex coacervate based systems. Therefore, these metal-enhanced complex coacervate glues are interesting systems for application in humid environments.

The same material, enhanced by addition of calcium and covalent crosslinking of the catechols, was further strengthened by addition of a separate network of covalently crosslinked poly(ethylene glycol) diacrylate. Crosslinking took about 24 h for reaching a conversion of ≈40%, and doubled the lap shear strength to 973 kPa (Table 2). Moreover, inclusion of the second network induced shear thinning at high shear rates. As a result, the material could be easily dispersed from a syringe as shown in **Figure 10**a.[103] In addition, Mann et al. filled the adhesive with silica nanoparticles and investigated the potential use for sealing fetoscopic defects.[104] Fetoscopy is a procedure where the fetus is evaluated or treated during pregnancy by entering the uterus, which has to be sealed post-treatment. The adhesive was tested by adhering a patch onto model tissue. The glue spread nicely over the tissue/patch interface, thereby sealing the defect; exposure to a water solution did not result in leakage. Human cells did not reveal any cytotoxicity after exposure, which is promising for future research of this and similar adhesives.[105]

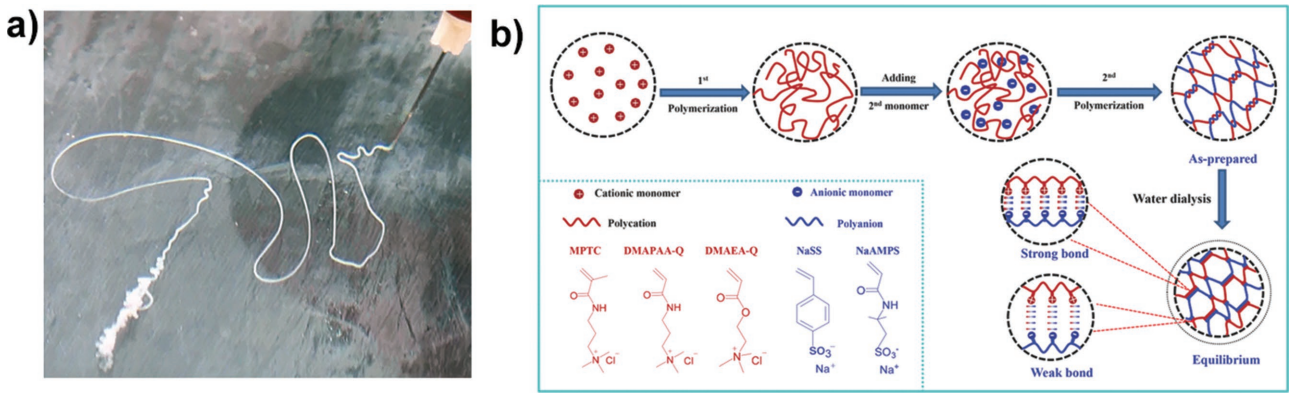

Figure 10. a) Kaur et al. developed an adhesive via a combination of complex coacervation and a separate covalently crosslinked network. The water-insoluble adhesive displayed shear thinning behavior, which enabled extrusion from a syringe. Reproduced with permission.[103] Copyright 2011, American Chemical Society. b) An alternative route for preparing double-network systems was applied by Luo et al. A cationic polymer was synthesized, followed by drying and grinding of the product. Subsequently, the ground polymer was dispersed in a solution of anionic monomer, followed by their polymerization. The double-network hydrogel was further strengthened by counterion removal. Reproduced with permission.[106] Copyright 2015, Wiley-VCH.

4.3.2. Ion-Crosslinked Polyelectrolytes

A simplification of ion-crosslinked systems was proposed by Lapitsky and co-workers who prepared a gel from cationic polyallylamine (120–200 kDa) combined with multivalent anionic pyrophosphate or tripolyphosphate.[107,108] Because of the high charge density on the polymer, high crosslinking densities enabled both anions to form stiff gels with storage moduli of about 400 kPa. Adhesion strengths comparable to natural wet adhesives (0.35–0.45 MPa) were observed for attachment to both hydrophilic and hydrophobic surfaces, using a universal testing machine. Interestingly, adhesion to the hydrophilic surface resulted in cohesive failure, while adhesion to the hydrophobic surface showed adhesive failure. This means that the interactions between the gel and hydrophilic surface were stronger than the bonds to the hydrophobic surface. Remarkable features of this adhesive were its ease of production and facile upscaling; the order of mixing did not make a difference, and bulk quantities of the precursors were inexpensive. Additionally, the pH and ionic strength could be used to adjust the storage modulus from 60 to 400 kPa, and to adjust the tensile strength from 0.05 to 0.45 MPa.[107,108]

4.4. Promising Ionic Materials for Use as Adhesive

4.4.1. Polyelectrolyte Complexation

Several additional systems based on electrostatic interactions have been reported in literature, but have not yet been investigated for their adhesive performance. Since some of these systems may be interesting for use in adhesives, a selection will be provided below.

Zhang et al. used ring-opening polymerization to synthesize two oppositely charged copolypeptides from randomly copolymerized *N*-carboxyanhydride monomers.[109] Using this method, the researchers tried to mimic the proteins of the sandcastle worm (aiming for similar chemical functionality and molecular weight), while reducing nature's complexity. Six different amino acids were used; aromatic DOPA and tyrosine, nonpolar glycine, cationic lysine, polar serine and anionic phosphoserine. At high salt concentrations, i.e., 4.0–4.7 M, the oppositely charged polymers formed complex coacervates. At lower salt concentrations, however, complexation was inhibited due to a net negative charge on the material. Because of oxidation of DOPA, complex coacervates darkened with time. Using an acidic buffer solution, oxidation could be prevented and surface tensions were reduced, i.e., 35 mN m^{-1} for nonbuffered and 15 mN m^{-1} for buffered coacervates. In rheology, exceptionally high shear thinning (four orders of magnitude) was observed for nonbuffered coacervates. In addition, the rheological data revealed long relaxation times showing long lifetimes of interchain connections and a relatively low storage modulus, representing a low crosslinking density. It would be interesting to study the adhesive performance of this material, because it exhibits features that are promising for underwater adhesion.[109]

For transcatether embolization, Jones et al. developed a polyelectrolyte complex from polycationic salmine sulfate and polyanionic phytic acid, enhanced with tantalum powder.[110] Transcatheter embolization is a method for blocking blood vessels by injecting a liquid embolic to stop bleeding or selectively disrupt blood supply to certain (e.g., cancer) tissues. Liquid embolics have to be injectable, but have to be insoluble in blood and stiff enough to block the blood vessel. A high salt concentration (1.2 M) resulted in a fluid-like material that, upon injection in the blood vessel, formed a gel at physiological conditions (0.15 M salt) while it shrank by only 3%. Tantalum powder was added to increase the viscosity that also resulted in shear thinning behavior that is advantageous for injection. The tantalum-enhanced polyelectrolyte complex was injectable, fully blocked the vessel till the deepest capillaries, and kept its position for the first 90 min after injection. Furthermore, nontoxic materials were used and thus no toxic response was observed. However, the individual components have very short life-times in blood and therefore long-term stability of the complex has to be investigated.

4.4.2. Double Networks

An innovative strategy to obtain ionic hydrogels was suggested by Luo et al. Instantaneous homogeneous materials were obtained by first polymerizing the cation, followed by drying and powdering. The ground polycation was subsequently immersed in a solution containing anionic monomers, followed by their polymerization (Figure 10b).[106,111] The resulting polyion complexes were elastic but soft (≈0.1 MPa stress at 16 mm mm^{-1} strain in tensile testing) due to an excess of counterions that remained in the hydrogel after polymerization. Equilibration of the hydrogels in deionized water resulted in shrinkage, but doubled the strength and toughness. Despite the low amount of unbound ions, bonds could break and reform, as was shown by the gradual disappearance of stress after deformation. In addition to not being cytotoxic, the hydrogels were stable at a pH ranging from 0 to 12, at salt concentrations up to physiological conditions (0.15 M salt) and till temperatures as high as 90 °C.[106] In subsequent research, Luo et al. showed that small changes in the monomer structure had a large impact on the properties of the gel. They showed that the introduction of methyl groups on the polymer backbone (i.e., acrylates were exchanged for methacrylates, and acrylamides for methacrylamides) stiffened the chain and strengthened the ionic bonds, which resulted in tougher hydrogels. The choice for an acrylamide- or acrylate-based monomer changed the morphology of the hydrogels as well, resulting in varying stiffnesses, extensibilities, and self-recovering properties. These examples demonstrate that the combination of polyelectrolyte complexation and optimization of the monomer structure can be an innovative approach for designing self-healing adhesive materials.

Besides sandcastle worms and mussels, plenty of other organisms are capable of strong underwater adhesion. This includes the larvae of the caddisfly, which were mimicked by Lane et al.[112] Caddisfly larvae live in water and use silk to form composite protective structures from objects out of their surroundings. This silk consists of a double network of proteins that lack DOPA and are mainly nonpolar, highly phosphorylated, and contain large amounts of Ca^{2+}. It is suggested that Ca^{2+} forms complexes with the silk proteins; however, the most interesting mechanical properties are likely caused by the double-network structure. Therefore, Lane et al. chose to synthesize a metal ion-enriched double-network gel from acrylamides and methacrylates that bear carboxylate, hydroxyl, and phosphate side chains. After hydrogel formation, divalent cations were introduced that enabled complexation with the phosphate and carboxylate groups. Tough hydrogels, with a maximum yield stress of 3.5 MPa (Zn^{2+}), were obtained by optimizing the phosphate content. For calcium-enhanced hydrogels, a high stiffness (10.3 MPa) was combined with self-healing properties (90% recovery of the initial length and modulus after being unloaded for 90 min). This behavior was attributed to the rupture and rebonding of the phosphate/Ca^{2+} salt bridges.[112] This material exhibits an interesting combination of a covalently crosslinked double network and reversible electrostatic crosslinks, which is essential for the design of an adhesive.

In this section, several materials were discussed of which adhesion was tested in different ways. Despite these differences, we compare the adhesive strength of the materials to find trends for obtaining optimal adhesive properties (Tables 1 and 2). At first, for strong adhesion, it is necessary to balance the cation and the anion content in the adhesive materials. When either one of the two charges was present in the adhesive material, such as in uncomplexed proteins, very low adhesive strengths were found, while adhesion improved after complex coacervation with a polycounterion.[48,95,96] In addition, only one unit of (each) charge per molecule was insufficient to obtain strong bonding, while multiple charged groups per molecule showed stronger adhesion. This can be deduced from the strong adhesion of the complex coacervate of quaternized chitosan/catechol functionalized poly(acrylic acid), compared to the zwitterions, and the low-molecular-weight copolymer of Seo et al., independent of the fact that these materials include catechol groups.[44,93,94] However, it seems that the addition of multiple catechol groups enhanced the adhesive strength, because the absence of catechol groups strongly reduced the adhesive strength in three systems.[6,93,94] An even higher adhesive performance, especially in wet conditions, could be obtained by oxidizing the catechol groups, which can lead to covalent crosslinking of the adhesive.[6,96,101] Finally, inclusion of metal ions or a second covalent network into the adhesive material further enhanced the adhesive strength of complex coacervate-based materials.[100,101,103]

5. Adhesives Based on Hydrogen Bonding

Hydrogen bonding is an important type of interaction that defines the strength of several natural adhesives. This interaction is, for instance, partially responsible for strong surface bonding via DOPA (Sections 2 and 3). Investigation of the impact of hydrogen bonding of DOPA's catechol group on the adhesive performance, however, remains rather complex as it can undergo various other interactions, including metal–ligand coordination and covalent bonding.

Since the reversible nature makes H-bonded materials particularly attractive to toughen adhesives, several research groups have studied more defined hydrogen bonding moieties to create synthetic adhesive materials.[18] By introducing such specific interactions, mechanical properties of existing polymer systems can be optimized, or polymer-like materials can be prepared by supramolecular polymerization of small molecules or oligomers.[113,114] Both approaches enable design of tough materials, as bond pairs can reform after deformation, a mechanism that is absent in conventional covalent adhesives. When using the second method, depolymerization can be triggered by external stimuli, resulting in a low-viscosity material and could therefore lead to better wetting of rough surfaces.

In contrast to the previous sections, adhesion of H-bonded systems, with the exception of a few, was exclusively studied in the dry state. This difference originates from the fact that the presence of water can disturb hydrogen bonding. Indeed, in certain examples that are covered in this contribution, adhesion was significantly affected with increasing humidity. However, since H-bonding remains an important factor in the adhesion of several marine organisms (see Section 2), it would be interesting to have a closer look at the performance of such synthetic glues in an aqueous environment. Multiple examples that will be reviewed in this section aimed at using

hydrogen bonding for preparing PSAs: materials that tightly bind to substrates under application of light pressures within a short amount of time.[115] Generally, these are rubber-like materials, i.e., materials that have a low glass transition and, above that, are viscoelastic. Because both adhesion and cohesion can be adjusted by incorporation of H-bonding groups, such supramolecular polymeric systems seem to be ideal candidates.

This section will start with a focus on relatively simple hydrogen-bonded adhesives, materials in which these interactions are rather random and undefined. In later sections, on the other hand, more sophisticated H-bonding moieties will be covered, including nucleobase chemistry, ureido-pyrimidinone-functionalized materials (2-ureido-4-pyrimidinone, UPy) and urea-functionalized materials.

5.1. Simple Hydrogen-Bonded Adhesives

For PSAs, the material should exhibit fluid-like properties on contact (good wetting of substrate), while it should have a high cohesive strength (solid-like) to resist debonding.[115] These demands conflict, and are therefore difficult to obtain when using a single type of material. Feldstein et al. solved this problem for a hydrophilic adhesive formulation by combining high-molecular-weight poly(*N*-vinylpyrrolidone) (PVP, $M_w \approx 10^6$ g mol^{-1}) and hydroxyl-terminated PEG oligomers ($M_w \approx 400$ g mol^{-1}), two polymers that neither show adhesive properties.[116] In such blends, PEG's hydroxyl end groups enabled formation of a supramolecular network by bridging PVP's carbonyl groups. Additionally, PEG acted as a spacer between PVP chains, thereby providing enhanced mobility to PVP. Blending thus resulted in both softening and enhanced cohesion of the material. However, since water could act as a plasticizing agent, the humidity played a crucial role as well. By studying the adhesion using various techniques, the optimum performance was found for systems that contained 36 wt% PEG and absorbed 6–12 wt% water. Peel strengths in the range of 550 N m^{-1} and debonding stresses of roughly 0.6 MPa (probe tack tests) were measured (**Table 3**).

In later work, PVP was replaced by poly(*N*-vinylcaprolactam) (PVCL), a more hydrophobic polymer that displays lower critical solution temperature (LCST) behavior around 35 °C.[117] Stronger complexation between PEG and PVCL tripled the degree of crosslinking, which resulted in considerably higher debonding stresses (1.1 MPa) and peel strengths (up to 2.3×10^3 N m^{-1}). Furthermore, whereas adhesion of the earlier described PVP blends declined rapidly with increasing moisture levels, still reasonable adhesion was maintained for the PVCL system at relatively high water contents. Above 30 wt% of water, however, the LCST behavior of PVCL started to play an important role. Collapse of the polymer chains above this transition caused a sharp and considerable drop of the peel strength (570 N m^{-1} to practically 0 N m^{-1}). Upon returning to room temperature, however, the opaque film transformed back into a transparent and tacky material with full recovery of the adhesion. Because such hydrophilic PSAs are expected to stick to wet surfaces and can be easily removed by adjusting the humidity or temperature, they could be ideal candidates for biomedical applications.

Table 3. Overview of the performance of a selection of synthetic adhesives based on hydrogen bonding. Experiments were performed using various test layouts and substrates.

System	Motif	Method	Substrate	Strength	Ref.
PEG/PVP blend	Hydroxyl/amide	Probe tack test	Glass/stainless steel	0.6 MPa	[116]
PEG/PVP blend	Hydroxyl/amide	Peel test	Polyethylene	550 N m^{-1}	[116]
PEG/PVCL blend	Hydroxyl/amide	Probe tack test	Glass/stainless steel	1.1 MPa	[117]
PEG/PVCL blend	Hydroxyl/amide	Peel test	PET	2.3×10^3 N m^{-1}	[117]
Oligo(bisphenol A) glass	Carboxylic acid/pyridine	Lap joints	Stainless steel	1.4 MPa	[118]
Polymer brushes	Phenol/pyridine	Lap joints	Silicon	0.84 MPa	[119]
Butylacrylate copolymers	AT nucleobases	Peel test	Stainless steel	790 N m^{-1}	[120]
PBA copolymers/small linker	AT nucleobases	Peel test	Glass	550 N m^{-1}	[121]
PBA copolymers/small linker	AT nucleobases	Lap joints	Stainless steel	0.1 MPa	[122]
Acrylamide hydrogel	AT nucleobases	Peel test	Aluminum	330 N m^{-1}	[123]
Acrylamide hydrogel	AT nucleobases	Peel test	PDMS	100 N m^{-1}	[123]
Hexyl methacrylate copolymers	UPy	Lap joints	Stainless steel	5.5 MPa	[124]
Supramolecular glass	UPy	Lap joints	Glass	1.2 MPa	[125]
Center-functionalized PIB	Bisurea	Probe tack test	Glass/stainless steel	55 J m^{-2} [a)]	[126]
Center-functionalized PIB	Bisurea	Probe tack test	Glass/PDMS	45 J m^{-2} [a)]	[126]
Center-functionalized PBA	Bisurea	Probe tack test	Glass/stainless steel	30 J m^{-2} [a)]	[127]
Center-functionalized PBA/glycidyl methacrylate (glycidyl MA) copolymer	Bisurea/epoxide	Probe tack test	Glass/stainless steel	90 J m^{-2} [a)]	[127]
Crosslinked PBA/glycidyl MA system	Bisurea/covalent	Probe tack test	Glass/stainless steel	104 J m^{-2} [a)]	[127]

[a)]According to Callies et al.,[127] an estimation of the peel force can be obtained through conversion of these adhesion energies (J m^{-2}) into peel strengths (N m^{-1}).

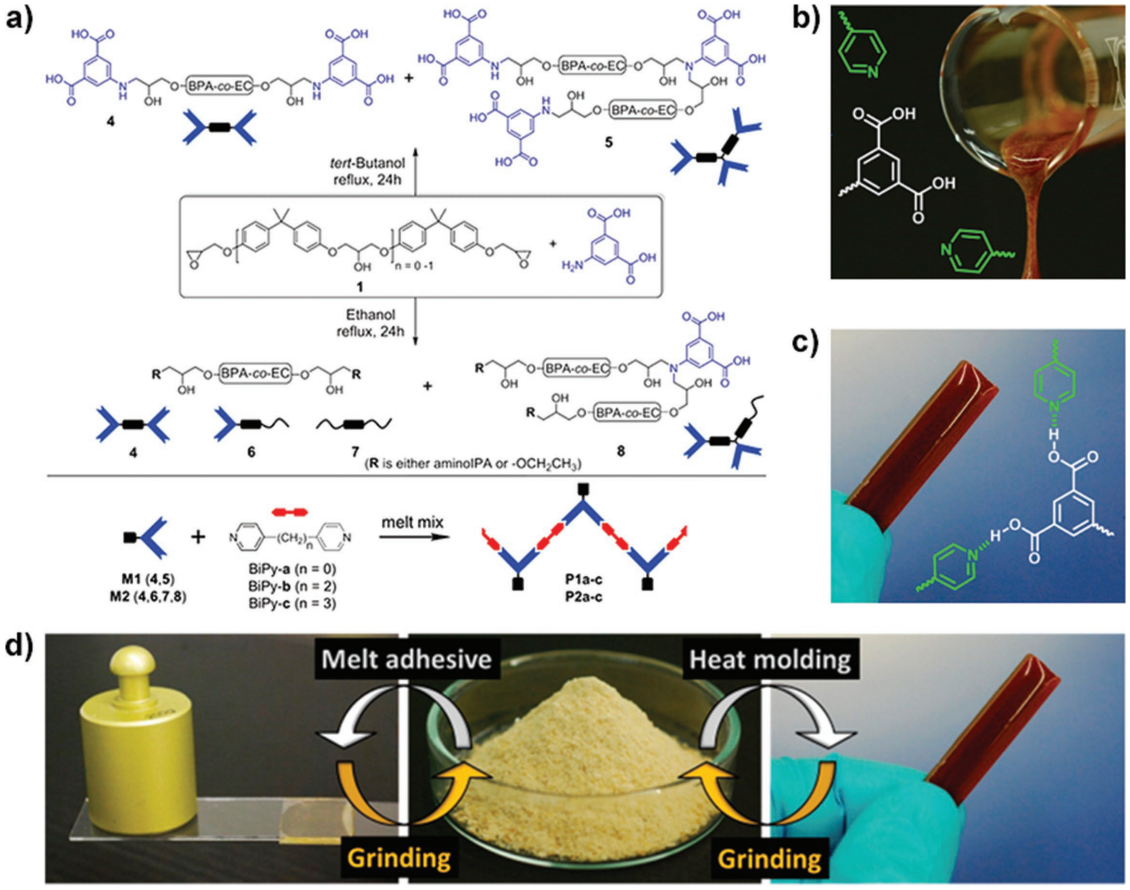

Figure 11. a) Chemical structures of the components of the H-bonded isophthalic acid/pyridine-based supramolecular glass synthesized by Balkenende et al. b) The material flows like a liquid at higher temperatures ($T_{flow} \approx 150$ °C), while c) an amorphous solid is formed on cooling because of the polydisperse nature of the building blocks ($T_g \approx 90$ °C). d) These properties and the reversibility make it suitable as a recyclable hot-melt adhesive. Reproduced with permission.[118] Copyright 2016, American Chemical Society.

An oligo(bisphenol A)-based supramolecular glass with low melt viscosity and excellent adhesion to both glass and steel was recently developed by Balkenende et al. (**Figure 11**a).[118] Such properties make this amorphous material ideal for application in hot-melt adhesives (Figure 11b,c). Its thermal properties could be tuned by modifying the chemistry of the bipyridine linker ($T_g \approx 75$–100 °C), whereas the polydisperse nature of the isophthalic acid-functionalized oligo(bisphenol A) derivative prevented crystallization. Lap shear strengths were found to be in the range of 1.4 MPa (Figure 11d), but premature failure was observed when the material was exposed to a humid environment. Furthermore, UV light enabled debonding within seconds, much faster than conventional styrene/butadiene triblock copolymers, a typical component of hot-melt adhesives.

Wang and Xie examined the interfacial interactions between two crosslinked epoxy polymers, containing hydroxyl and epoxy functional surface groups.[128] Pull-off strengths between both polymer samples were found to be comparable to superglue (4.5 vs ≈5.0 MPa). The high amount of crosslinks prevented interfacial chain entanglements and thereby chain scission on debonding, making bonding fully reversible. Up to 67% of the original strength could be recovered, while the performance could be further increased by grafting both surfaces with branched polyethyleneimine (up to 6.4 MPa). Wetting of both surfaces with methanol before contact was, however, crucial in order to disrupt intrasurface H-bonds; otherwise, a three times weaker interaction was measured. Residual solvent did not cause this enhanced adhesion, as heating the sample to 90 °C or subjecting it to vacuum did not affect the adhesive performance. Since this material cannot be used to join two different substrates, it should not be regarded as a true adhesive, although this surface modification-approach might still be useful for improving adhesion of epoxy resins to other hydrophilic surfaces.

Adhesion between proton donor (hydroxyethyl methacrylate, 4-hydroxystene) and acceptor (2- and 4-vinylpyridine) polymer brushes was investigated by Yoshioka et al.[119] Lap shear experiments revealed adhesion strengths of several hundred kPa, but successful bonding was only achieved when the brushes were wetted with an appropriate solvent. Methanol was applicable for all donor/acceptor combinations, while water was found to be unsuitable for most brushes, presumably caused by their low degree of swelling. For steric reasons and the strength of H-bonding, strongest adhesion was observed for the 4-vinylpyridine/hydroxystyrene combination

(843 kPa), while AFM and X-ray photoelectron spectroscopy (XPS) demonstrated both brushes to remain intact after debonding. In addition, debonding was also possible by simply immersing the sample in methanol. Both routes enabled repeatable usage.

5.2. Nucleobase-Containing Adhesives

Hydrogen bonding between complementary base pairs (adenine–thymine, cytosine–guanine, i.e., AT and CG) is one of the major reasons of the stability of the double helical structure of DNA. Since it is also possible to "melt" the structure (denaturing), multiple research groups have adopted this feature for designing reversible hydrogen-bonded supramolecular adhesives. As a result of its ability to form three hydrogen bonds (**Figure 12**a), the CG pair is the strongest of the two ($K_{assoc} \approx 10^5$ M^{-1} for CG in chloroform, while only 10^2 M^{-1} for AT).[129] However, most nucleobase-containing adhesives were based on the AT pair, for the simple reason that dimerization of G can significantly affect the adhesive performance ($K_{dim} = 10^4$ M^{-1} for GG).

One of the first examples demonstrating the concept of "smart" adhesives using nucleobase chemistry was given by Long and co-workers.[130] Hereby, PS was end-functionalized with T, while a silicon wafer was decorated with A recognition sites. XPS and contact angle measurements confirmed specific adhesion. PS–T did not adhere to a thiol-coated substrate, and PS–OH was not adsorbed by an A-coated substrate. The process was shown to be fully reversible; PS was completely removed by washing with an aprotic polar solvent, leading to disruption of H-bonds, but could be reattached afterward. Optimal adhesion was observed after modification of the substrate using a mixture of thiol and A, thereby minimizing competing self-association (AA conjugation) and steric hindrance between neighboring A groups.

The same research group incorporated A and T nucleobases in butylacrylate (PBA) copolymers.[120] Self-association of the adenine-containing copolymers resulted in the formation of needle-shaped aggregates. More homogeneous structures were obtained by blending this copolymer with a T-functionalized copolymer as evidenced by X-ray scattering and AFM. In addition, the blend showed a higher glass transition temperature and was established to have a tenfold higher storage modulus compared to the isolated components; an increased apparent molecular weight was achieved through hydrogen bonding. In a peel test, cohesive failure indicated strong adhesion to a stainless steel surface. Of all tested samples, the A/T copolymer blend displayed the highest adhesive performance (peel strength of 790 N m^{-1}).

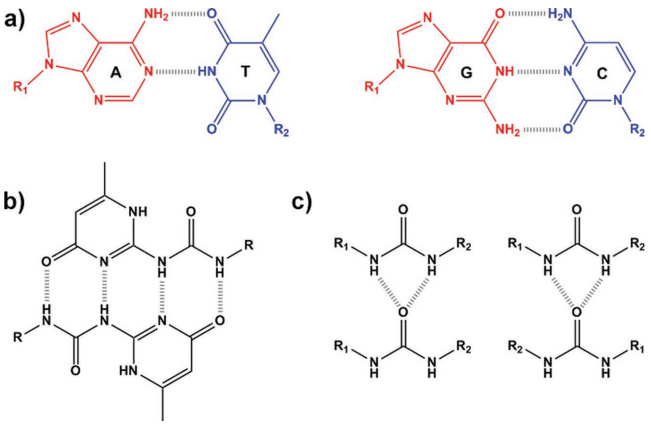

Figure 12. Chemical structures of most common hydrogen-bonding motifs. a) Nucleobase pairs adenine–thymine (AT) and guanine–cytosine (GC). b) 2-Ureido-4-pyrimidinone (UPy). c) Urea. R-groups can be used to introduce these functionalities into polymers, small molecules, or at surfaces. H-bonding in urea-containing compounds is less organized compared to UPy and nucleobase chemistry.

Instead of embedding both nucleobases in a polymer chain, Arimitsu and co-workers developed PSAs by combining a high-molecular-weight *n*-butylacrylate copolymer (containing 9 mol% T) and a small molecular crosslinking agent bearing two A groups (**Figure 13**a).[121] Compared to a fully polymeric system, both the reduced viscosity and plasticizing effect of such an approach facilitated mixing. Hydrogen bonds were broken by heat, while covalent crosslinking (photodimerization of T) could be accomplished by simultaneous heating and UV irradiation, leading to a thermally stable, crosslinked material. At room temperature the presence of the A linker only had little effect on the peel strength (≈550 N m^{-1}), while at high temperature it suppressed the decrease in strength compared to the pristine polymer. Irradiation of the PSA by UV light caused a slight increase of the peel strength (≈600 N m^{-1}), although the crosslinks were now irreversible. In a second publication the authors described significant improvement of the lap shear strength (up to 0.1 MPa) by increasing the molecular weight of the copolymer and by adding larger amounts of crosslinker (Figure 13b).[122] Additionally, a heat pretreatment greatly enhanced the mechanical properties, because of better wetting of the stainless steel substrate (Figure 13c).

A different approach was taken by Nakahata et al., who prepared DNA hydrogels by copolymerizing acrylamide, bisacrylamide, and a 16-mer acrylate (i.e., an acrylate bearing an oligonucleotide side group).[131] Macroscopic self-assembly of centimeter-sized pieces of complementary oligo-DNA gels was observed (rupture stress 1 kPa), while addition of free complementary oligonucleotides inhibited adhesion between the two different DNA gels. Furthermore, adhesion to a control gel that only contained T moieties was absent, thereby demonstrating the importance of the DNA sequence. In the same paper, toluene-swollen nucleobase-functionalized organogels were synthesized by replacing acrylamide, bisacrylamide and the 16-mer acrylate for styrene, divinylbenzene and a nucleobase-containing styrene monomer, respectively. The A-gel and T-gel were found to adhere selectively, with the strength increasing with concentration of nucleobase (up to 4 mol%, 3 kPa). Nevertheless, adhesion of the two gels was inhibited in the presence of solutions of linear A or T copolymer. The choice of solvent affected adhesion as well; the more polar the solvent, the weaker the interaction. Adhesion was, for instance, not observed when using dimethylformamide (DMF). Interestingly, C and G gels did not adhere to each other at all, despite the higher association constant of the CG pair. This observation confirms the impact of the self-association of G.

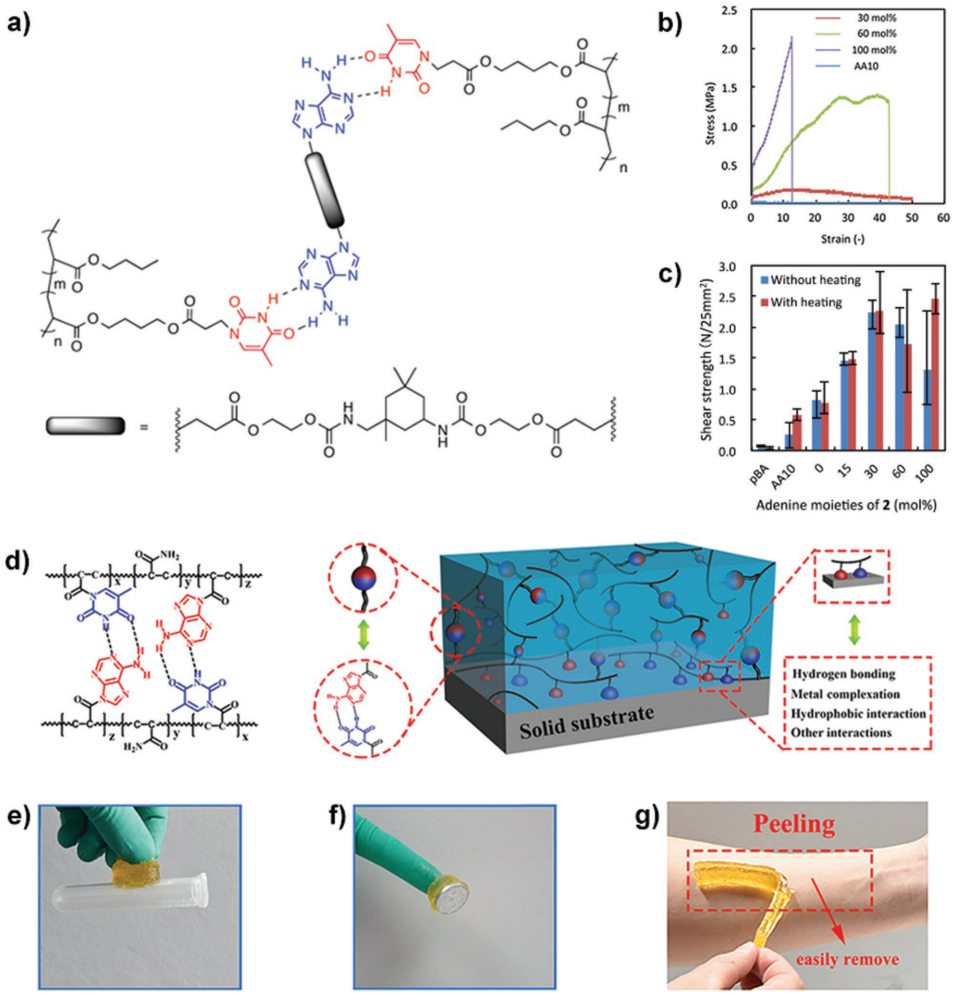

Figure 13. a) H-bonded supramolecular PSA based on nucleobase chemistry designed by Ishikawa et al. The T-modified acrylate copolymer was reversibly crosslinked by the addition of a small difunctional A-containing linker. b) Incorporation of these nucleobases resulted in a significantly stronger material compared to neat poly(butyl acrylate) (PBA) or an acrylic acid/butylacrylate copolymer (AA10). The tensile strength increased with the amount of linker added, while the elongation at break decreased. c) Further optimization of the lap shear strength was achieved by giving the PSA a heat pretreatment, due to better wetting of the substrate. The percentages in panels (b) and (c) indicate the relative amount of A compared to T. a–c) Reproduced with permission.[122] Copyright 2016, John Wiley & Sons, Inc. d–g) Liu et al. prepared a nucleobase-bearing, noncovalently crosslinked acrylamide hydrogel adhesive by including T- and A-modified monomers (d). It adhered successfully to both plastics (e) and metals (f) through various interactions. When glued to human skin, no residue remained after removal (g). Reproduced with permission.[123] Copyright 2017, American Chemical Society.

In contrast to Nakahata et al. who prepared separate nucleobase gels, Liu et al. included both A and T units in the same hydrogel.[123] Inside the acrylamide gel, the base pairs functioned as crosslinking agents, whereas free nucleobases at the surface enabled strong adhesion to various solids through a combination of H-bonding, metal coordination, and hydrophobic interactions (Figure 13d). Compatible materials included plastics, ceramics, metals, and wood (Figure 13e,f). Peel strengths ranged from 100 N m^{-1} (silicone rubber substrates) up to 330 N m^{-1} for aluminum substrates with the adhesion being fully reversible for at least ten cycles. Significantly higher peel strengths were measured compared to an unfunctionalized acrylamide hydrogel (aluminum, 70 N m^{-1}). Furthermore, the hydrogels could also bind to biological tissue, including human skin. Since no residue remained after rupture, such adhesive gels could be interesting for use in biomedical glues or wound dressings (Figure 13g). It should be noted that the single nucleotide-functionalized covalently crosslinked hydrogels investigated by Nakahata et al. could be promising for use in universal adhesives as well, because the surface of such A- or T-gels should be able to bind to other materials through identical interactions.[131] Unfortunately this property was not tested; this work only focused on the adhesion of dissimilar gels.

5.3. Ureido-Pyrimidinone-Containing Adhesives

In the late 90s, Meijer and co-workers developed the UPy motif, a functional group capable of forming H-bonds similar to the

nucleobases discussed in the previous paragraph. In contrast to nucleobase chemistry, complementary pairing is not required for UPy; it can selectively bind to another UPy moiety via four instead of only two (AT) or three (GC) hydrogen bonds (Figure 12b). UPy was demonstrated to be an effective agent for the preparation of viscosity enhancers, linear supramolecular polymers and reversible networks, when incorporated in small molecules, telechelic poly(dimethylsiloxane) (PDMS) oligomers and trifunctional star-shaped polymers, respectively.[132] Because of the strong dimerization constant ($K > 10^6$ M^{-1} in chloroform) and the low viscosity of such polymeric materials at high temperatures, several research groups were inspired by this work to design UPy-containing adhesive materials.

After studying the phase behavior and rheological properties of UPy-end-capped block copolymers,[133] Long and co-workers were the first to include UPy in PBA copolymers to investigate how this functional group affects the adhesion performance of PSAs.[134] At room temperature, the copolymers formed aggregates in nonpolar solvents, whereas the viscosity of the bulk material was found to be an order of magnitude higher than the viscosity of a PBA homopolymer of equal molecular weight. Above 80 °C or in polar solvents (like tetrahydrofuran (THF)), rupture of H-bonds caused the material to behave almost identical to unfunctionalized PBA. In a standard peel test, the peel strength of PBA/UPy copolymers increased with the amount of UPy and was significantly higher than pristine PBA, presumably caused by both intermolecular H-bonding and strong adhesion to the glass substrate.

Adhesive properties and contact mechanics of PBA–UPy copolymer thin films (thickness ≈ 0.1 µm) were later more extensively studied by Faghihnejad et al. by using an SFA that was coupled to an optical microscope.[135] They investigated the influence of the contact time, temperature and humidity. Although theoretical analysis pointed out that the UPy–UPy binding energy decreases with increasing water content,[136] a higher humidity unexpectedly led to stronger adhesion. Contact angle measurements demonstrated that surface migration of UPy groups was responsible for this. Stronger adhesion was also observed with increasing temperature, up to the H-bond dissociation temperature, because of enhanced chain mobility. The combination of temperature and humidity was found to be equally important, as both affect the bulk viscoelastic properties. Under moist conditions, severe plasticization was more prominent for PBA copolymers that contained a higher amount of UPy groups due to more facile diffusion of water into the bulk material, leading to weaker adhesion at higher temperatures. A longer contact time enabled the formation of more H-bonding pairs, which immediately had a positive effect on the adhesive strength. One of the major advantages of supramolecular adhesives was demonstrated in this work as well,[18] since after fracture, the reversibility of UPy H-bonding facilitated full recovery in 3 h, and remarkably, 40% of the original strength was restored in less than 100 s.

A similar study was performed by Heinzmann et al., but they exchanged butylacrylate for butyl or hexyl methacrylate.[124] Therefore, depending on the alkyl side group and the composition, UPy-copolymers showed a glass transition below or above room temperature, which directly altered the adhesive properties (shear strengths up to 5.5 MPa). High-T_g adhesives often showed brittle fracture and low adhesive strength, but this was improved when the glass transition was passed. Debonding on demand was tested as well, using heat or UV light. Lap joints failed when heated to 80 °C and exposed to low forces. UV absorbance of the polymer alone, that can cause local heating through radiationless decay, was found to be insufficient for light-induced debonding. This was overcome by blending the copolymer with a UV sensitizer (0.25 wt%); separation of the quartz slides occurred for most samples within a minute.

The same research group also investigated an optically responsive adhesive glass that was prepared via association of a trifunctional low-molecular-weight monomer (**Figure 14**a).[125] The presence of UPy caused this building block to form a dynamic, H-bonded supramolecular network. The high concentration of UPy groups prevented crystallization; an amorphous, i.e., glassy, solid (T_g ≈ 100 °C) was obtained on cooling from a slightly viscous melt (Figure 14b), while addition of a UPy-functionalized chain stopper allowed tuning of both the thermal and mechanical properties. In lap joint experiments,

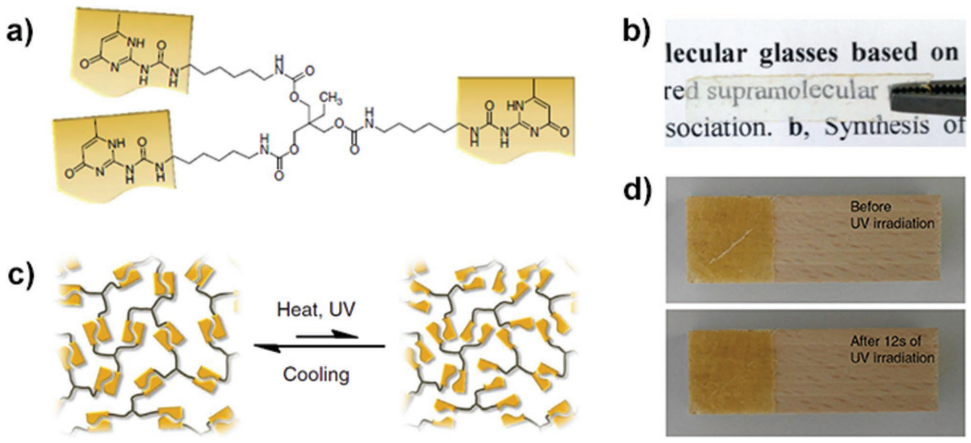

Figure 14. a,b) Balkenende et al. prepared a transparent supramolecular adhesive glass through H-bonding of a trifunctional low-molecular-weight UPy-containing monomer. c) The dynamic network enabled self-healing by exposing the material to heat or d) UV light; irradiation of the sample by UV light caused a scratch to disappear within 12 s. Reproduced under the terms of the Creative Commons Attribution 4.0 International License.[125] Copyright 2016, Nature Publishing Group.

the shear stress was found to be comparable to other supramolecular adhesives (1.2 MPa). Similar to the previous example, UV-induced debonding occurred within a minute, although incorporation of a sensitizer was not necessary. Adhesion was restored by exposing the fractured material to light or heat, with the properties being identical to the original samples. Healing times depended on the light intensity and the thermal conductivity of the substrate (Figure 14c,d).

Although not a true adhesive, the following example proves UPy to be a promising functional group for biomedical applications as well, particularly because of its nontoxic properties. Dankers et al. combined biodegradable telechelic UPy polycaprolactone oligomers with UPy-functionalized cell adhesion-promoting peptides.[137] Because of the supramolecular nature, the material could be easily processed into films, fibers, meshes, and grids. The presence of the UPy-modified peptides was crucial for obtaining strong and specific cell binding, both in vitro and in vivo. Although mixing polymers and peptides had been successful in tissue engineering before, supramolecular chemistry allowed facile tuning of the bioactivity by incorporating different biomolecules.

5.4. Urea-Containing Adhesives

Cordier et al. demonstrated the urea group to be a very versatile group for the development of supramolecular polymers as well (Figure 12c).[138] A fully biobased material was prepared by combining fatty acids with diethylene triamine that were subsequently treated with urea, resulting in an oligomeric mixture with multiple complementary hydrogen bonding groups, including diamido tetraethyl triurea and di(amino ethyl) urea groups. The mixture of different molecular architectures suppressed crystallization, and H-bonding between the oligomers enabled the formation of both linear chains and crosslinks. Mechanical properties of this supramolecular rubber could be tuned by addition of a plasticizing agent (dodecane). Since the material becomes a viscoelastic liquid at higher temperatures (160 °C), it is promising for use in hot-melt adhesives.

A similar strategy was employed by the group of Hayes.[139] Bisurethane supramolecular polymers were synthesized from relatively simple starting materials. Despite the low molecular weight of these di-end-functional urethane monomers (M_w < 1 kg mol^{-1}), the mechanical properties resembled that of linear polyurethanes with far higher molecular weights (M_w > 50 kg mol^{-1}). In addition, they could be tuned by changing the chemical structure of the H-bonding end groups (number of hydroxyl groups) or the linker between the urethanes (e.g., symmetric, aromatic or aliphatic). Unlike UPy, in which the H-bonding moieties are highly organized, the polymer-like behavior of these materials is a consequence of a large variety of H-bonds. Functionalization of a telechelic polyisobutylene (PIB) oligomer (5 kg mol^{-1}) with such bisurethane groups drastically changed the physical properties.[140] Whereas the unmodified PIB is a free-flowing liquid, H-bonding caused the modified oligomer to behave as a rubbery material, very similar to thermoplastic elastomers. Analogous to their previous work, optimization of the number of hydroxyls or switching from a urethane to a urea linker had an immediate effect on the thermal and rheological behavior.

Stronger phase separation between the linker and H-bonding groups was accomplished through exchange of PIB for a hydrogenated polybutadiene linker, and by including additional aromatic end groups (π–π stacking).[142] Enhanced network formation was indeed confirmed by X-ray scattering and resulted in a self-healing supramolecular material. After cutting the sample, the physical properties fully recovered by heating at 45 °C for only 15 min, and the damaged interface disappeared completely. This thermal transition was lowered to 37 °C by exchanging the benzyl for morpholine end groups, while maintaining the same number of urea moieties (**Figure 15**a).[141] Depending on the conditions (i.e., pretreated in distilled water, PBS buffer, at room or body temperature), yield strengths ranged from 0.5 to 0.7 MPa. Since urethanes are frequently used as adhesive, the polymer was tested to glue porcine skin. Preliminary tests showed cohesive failure, implying good contact between skin and the supramolecular material (Figure 15b). The lowered thermal transition allowed excellent healing capabilities at physiological conditions; at 37 °C, a pre-made cut disappeared completely within 2 h. Furthermore, the adhesive was found to be nontoxic, indicating that it could be promising for biomedical applications.

Instead of incorporating the urea functionality at the end of the polymer chain, Creton and co-workers designed supramolecular PSAs by inserting such bisurea units in the middle of the chain (Figure 15c).[126] Using probe tack experiments, adhesive performance of the bisurea center-functionalized PIB was closest related to 85 kg mol^{-1} unmodified PIB, while its molecular weight measured only 3.5 kg mol^{-1} (Figure 15d). Besides adhering very well to stainless steel (stress at debonding ≈0.9 MPa, debonding energy 55 J m^{-2}), adhesion of the bisurea copolymer to a crosslinked PDMS substrate was found to be almost identical (0.6 MPa, 45 J m^{-2}). A unique property, as silicones are normally used as release layer for labels. Also, no significant adhesion was observed between PDMS and linear PIB or acrylic polymers (<2 J m^{-2}). The internal structure of similar triurea center-functionalized butylacrylate polymers was later studied more extensively.[143] AFM and X-ray scattering showed these copolymers to be organized into hexagonally packed nanorods within an acrylate matrix. By increasing the molecular weight, the distance between the rods increased, although long-range order was lost for molecular weights above 20 kg mol^{-1}. Room temperature rheological data supported this observation, as high molecular weight polymers were found to be viscoelastic liquids.[144]

For commercial applications, however, clean removal of the PSA and high debonding energies are required. This means that strain-hardening should occur under large deformation. Inspired by classical epoxy resins, Callies et al. tried to solve this problem by synthesizing bisurea butylacrylate copolymers comprising additional glycidyl MA units that were subsequently covalently crosslinked by reaction with a diamine.[127] Competing H-bonding with glycidyl methacrylate led to formation of a supramolecular network with higher debonding energies (probe tack tests: 90 versus 30 J m^{-2} for the bisurea homopolymer), but still resulted in cohesive failure. Addition

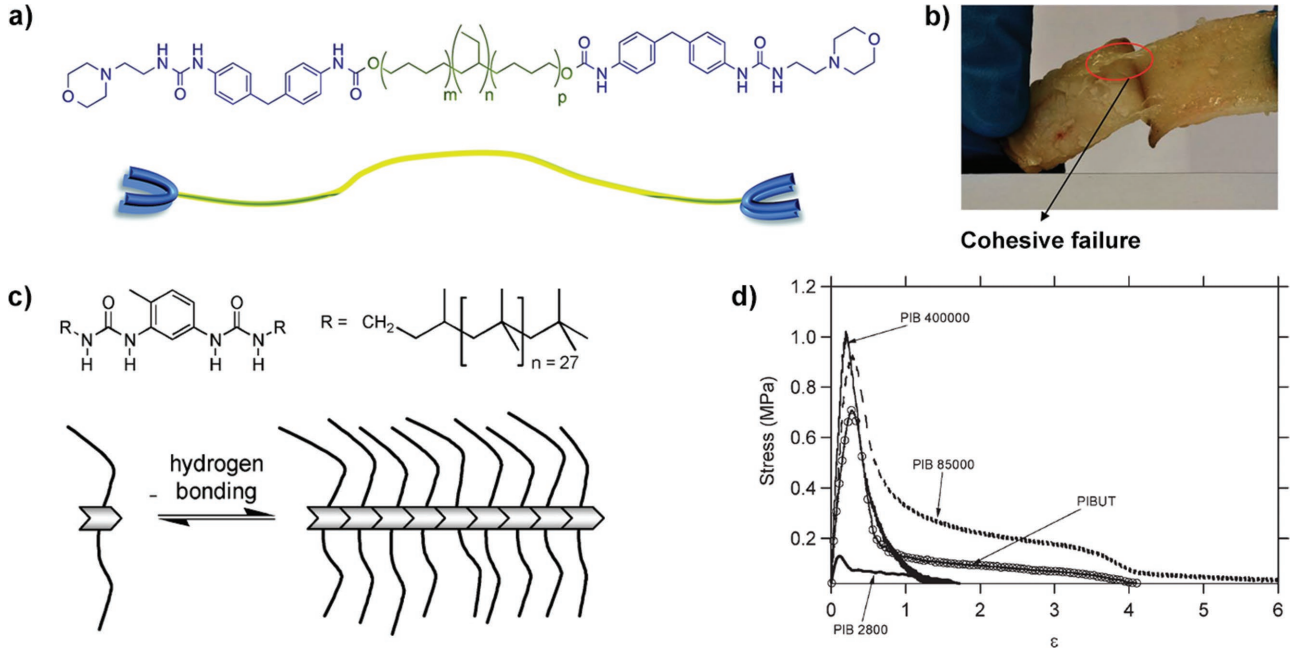

Figure 15. a) Self-healing supramolecular adhesive based on telechelic urea-functionalized low-molecular-weight hydrogenated polybutadiene ($M_n \approx 2.1$ kg mol^{-1}). b) Cohesive failure of this biocompatible adhesive was observed when glued to porcine skin. a,b) Reproduced with permission.[141] Copyright 2016, The Royal Society of Chemistry. c,d) From probe tack experiments, the adhesive performance of a bisurea center-functionalized polyisobutylene oligomer (PIBUT) (3.5 kg mol^{-1}) was found to be closest related to that of 85 kg mol^{-1} unmodified polyisobutylene (PIB). c,d) Reproduced with permission.[126] Copyright 2010, Wiley-VCH.

of the diamine gave a more gel-like behavior with even higher adhesion energies (up to 104 J m^{-2}), and in some cases the desired adhesive failure was observed. Low debonding energies due to increasing elasticity were obtained at higher crosslinking densities (<50 J m^{-2}). Although this work only showed preliminary results, further optimization of the adhesive performance is expected to be achieved by including for instance stronger H-bonding stickers (e.g., triureas).

6. Hydrophobic Interactions: Host–Guest-Mediated Adhesion

Hydrophobic interactions are an important driving force in marine adhesives. For instance, hydrophobicity is believed to promote complex coacervation of sandcastle glue (Section 2), while the hydrophobic groups of mfp-3s found in mussels protect DOPA against oxidation and reinforce the plaque by a combination of hydrophobic interactions and interresidual H-bonding (Sections 2 and 3).[45] Moreover, hydrophobic interactions become a more critical bonding strategy in case of less polar substrates.[59]

Despite being relatively weak compared to the previously discussed electrostatic interactions and H-bonding, hydrophobic interactions therefore have to be considered equally important for design of a proper underwater adhesive. Indeed, chemists have successfully prepared synthetic adhesives that were exclusively based on these driving forces, with host–guest chemistry being a particularly interesting example. Analogous to these natural adhesives, hydrophobicity is the key element that drives cyclodextrin- and cucurbituril-based host–guest complexation. In this specific class of host–guest chemistry, the hydrophilic entrance and exterior of the macrocyclic host enables solubility in polar solvents, while the relatively hydrophobic pocket facilitates accommodation of nonpolar guest molecules. The hydrophobic effect is one of the most important driving forces for interaction between host and guest species, as frustrated water is released from the host's cavity upon bonding, leading to an overall increase in entropy.[145] Since noncovalent interactions between host and guest thus rely on the difference in hydrophilicities of the guest, the interior of the host, and the surroundings, these features make host–guest chemistry particularly interesting for implementation in wet adhesives. By careful design of the host–guest system, the adhesive will be able to recognize specific molecules or surfaces, i.e., certain guest molecules will bind strongly to the host, while others will not.

Recent work on host–guest adhesives has mostly been limited to supramolecular complexes based on cyclodextrin and cucurbituril hosts, both having their advantages and disadvantages in terms of selectivity, binding strength and ease of functionalization. Examples of each system will be presented in the upcoming parts of this review.

6.1. Cyclodextrins

Cyclodextrins are cyclic cone-shaped oligosaccharides, and can consist of up to tens of glucose units linked together via 1,4-glycosidic bonds (**Figure 16**a,b). The size determines its selectivity, although in most cases it is limited to 6, 7 or 8 monomers (α-, β- or γ-CD, respectively).

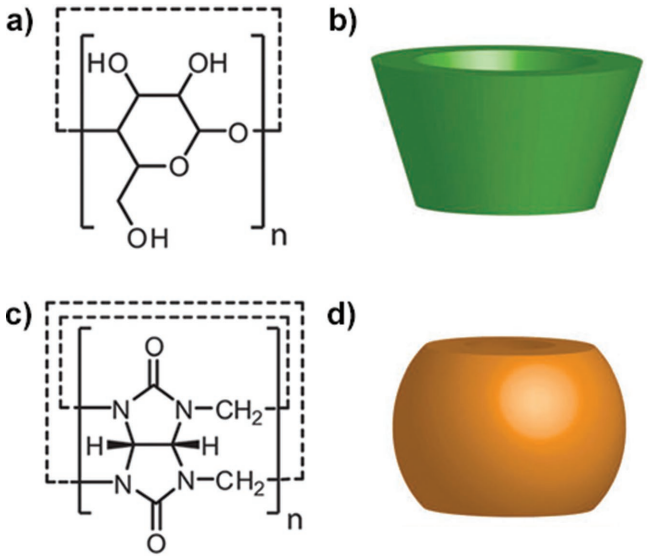

Figure 16. a–d) Chemical structures and schematic representations of a,b) the cone-shaped cyclodextrin and c,d) pumpkin-shaped cucurbituril hosts. Reproduced with permission.[147] Copyright 2012, The Royal Society of Chemistry.

Harada and co-workers were the first ones to incorporate CDs in a polymeric material.[146] Supramolecular host–guest crosslinked hydrogels were formed spontaneously when aqueous solutions of linear poly(acrylic acid) carrying α-CD or azobenzene moieties were mixed. Additionally, UV-induced *trans–cis* isomerization of the azobenzene unit changed the viscosity of the hydrogel, although it was found to be highly dependent on the polymer backbone-CD connection. When connected to the base (i.e., 3-position), UV irradiation caused the cis-isomer to be expelled from the host, leading to dissociation of the network and therefore a decreased viscosity (one order of magnitude). On the contrary, for the apex (i.e., 6-position) an interlocked complex was formed, giving a twofold increase of the viscosity. Irradiation by visible light reversed the mechanical properties of both systems. Nuclear Overhauser effect spectroscopy (NOESY) confirmed that the host–guest interactions were responsible for this behavior.

The same concept was used to design "smart" hydrogels, i.e., gels that can only adhere to specific surfaces.[148] Covalently crosslinked acrylamide hydrogels bearing different host and guest functionalities were prepared, including α-CD and β-CD hosts, and *n*-butyl and *tert*-butyl guests (**Figure 17**a). Upon simple shaking of dispersed centimeter-sized pieces of gel (Figure 17b), macroscopic self-assembly through molecular recognition was observed. Bulky *tert*-butyl gels adhered to the larger β-CD host gels, while the *n*-butyl gels preferably interacted with the smaller cavity of α-CD gel (Figure 17c). The gel complexes could be disrupted mechanically (in the range of 1 kPa) and adhesion could be inhibited by addition of competitive small, nonpolymeric guests (*n*-butanol or *tert*-butanol).

Following this work, the research group has extensively studied molecular recognition of hydrogels,[149] including the influence of the shape of the guest (linear vs cyclic),[150] the solvent polarity,[151] linkage between gel and guest (ester vs amide),[152] temperature responsiveness of benzyl gels,[153] pH responsiveness of fluorescent dansyl gels,[154] redox responsiveness of ferrocene gels,[155] photoswitchable azobenzene gels[156] and adhesion to glass surfaces.[157]

The previous examples show the high selectivity of host–guest chemistry, and the potential for use in wet adhesives, but the interactions between such hydrogels were in most cases rather weak (several kPa at most). However, by moving to the dry state (**Figure 18**a), the adhesive strength was increased by over three orders of magnitude (up to 5.1 MPa, **Table 4**).[158] Only a few microliters of water were needed to enhance the mobility of the surfaces of such dried hydrogels (xerogels), while without water no adhesion was observed between β-CD (host) and adamantane (guest) xerogels (Figure 18b). The inter-

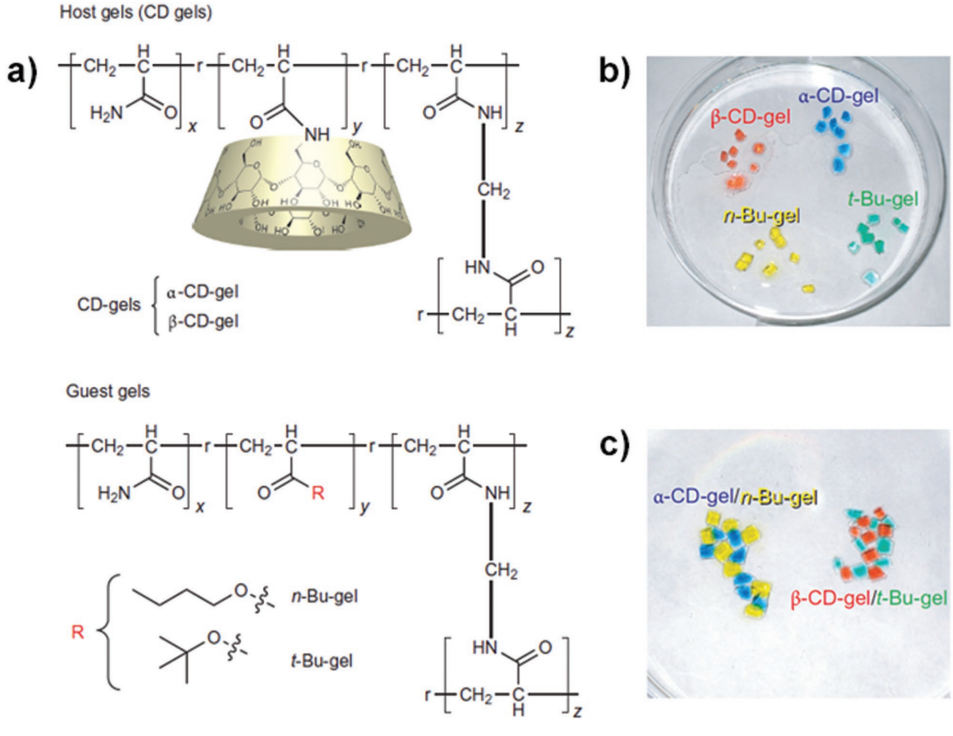

Figure 17. a) Chemical structures of host- (α-CD, β-CD) and guest-functionalized (*n*-butyl, *tert*-butyl) hydrogels. b) Upon shaking of dispersions of centimeter-sized pieces of the gels, the difference in size of the host and guest moieties caused c) selective adhesion of *n*-butyl to α-CD gel and *tert*-butyl to β-CD gel. Reproduced with permission.[148] Copyright 2011, Macmillan Publishers Ltd.

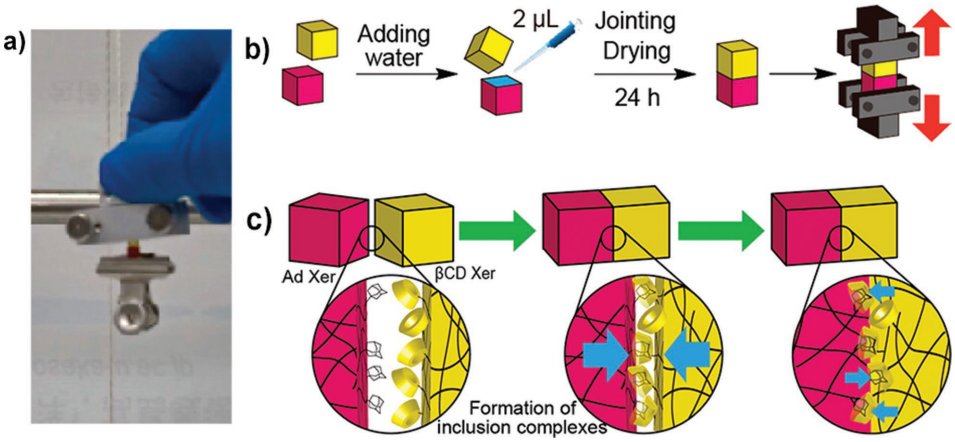

Figure 18. a) Image demonstrating adhesion of β-CD xerogel (yellow) to adamantane xerogel (red). b) Schematic representation of the procedure for preparing xerogel joints for tensile tests. c) Schematic illustration of the adhesion mechanism through host–guest chemistry. Reproduced with permission.[158] Copyright 2015, American Chemical Society.

action was also significantly weaker when one of the xerogel surfaces was wetted with an aqueous solution of competitive host or guest molecules, and pieces of the same kind (i.e., guest–guest and host–host) did not interact at all. Both host and guest xerogels showed adhesion to nonfunctionalized xerogels, but in that case only 10% of the original strength was obtained, again demonstrating the importance of host–guest complex formation. Microscopic imaging indeed revealed the gap between both surfaces to have disappeared within an hour, which was not observed for any other combination (Figure 18c). Furthermore, 80% recovery of the initial tensile strength was realized after healing the fractures by simple addition of water.

Guo et al. functionalized flexible and porous poly(ionic liquid) copolymers with β-CD or ferrocene (Fc).[159] Strong adhesion (80 kPa) between both polymeric strips was observed in air and in water after being subjected to a 400 g load for half an hour, independent of the pH. When the material was saturated with free host CD or free guest Fc, significantly lower shear strengths were measured (<20 kPa). This supramolecular Velcro debonded within minutes by addition of cucurbituril[7], a competitive host for the Fc-functionalized polymer. The polymeric strips could be reversibly unfastened mechanically, chemically and electrochemically, all up to at least five cycles, although only partial recovery of the initial shear strength was achieved. As evidenced by electron microscopy, this decrease in strength could be attributed to surface deformation and degradation. The ionic conductivity was essential for the reversible (electro)chemical nature, as it enabled efficient oxidation of Fc, and reduction of Fc^+ (a nonbonding guest).

Roling et al. used a slightly different strategy to develop a host–guest-based adhesive.[160] Instead of covalently linking CD to one of the surfaces, two identical glass surfaces bearing azobenzene copolymer brushes were glued together by addition of a commercially available β-CD host polymer (**Figure 19**). For a 2.24 cm^2 contact area, the adhesive could hold 1.9 kg (850 g cm^{-2}), and reversibility was tested for up to three cycles; 50% of the original strength was recovered after the third cycle. Control experiments demonstrated that no significant adhesion was obtained in the absence of either the brushes or β-CD polymer. While the azobenzene moieties are known to be light-responsive (*cis–trans* isomerization), irradiation with UV light did not lead to detachment of the glass slides. Incomplete conversion of the azobenzenes into the cis conformation was shown by UV/Vis spectroscopy, and thereby explained this unexpected behavior. The authors suggested that this might be the result of limited mobility of the copolymer brushes, since full isomerization was observed in both the free monomer and copolymer.

Thi et al. demonstrated that it is not necessary to covalently attach CD to a substrate or polymer backbone in order to achieve strong binding.[161] By simply mixing 5 wt% neat α-CD

Table 4. Overview of the performance of a selection of adhesives based on host–guest chemistry. Experiments were performed using various test layouts and substrates.

System	Motif	Method	Substrate	Strength	Ref.
Xerogels	β-CD/adamantane	Tensile testing	N/A	5.1 MPa	[158]
CD supramolecular Velcro	β-CD/ferrocene	Lap joints	N/A	80 kPa	[159]
Polymer brushes	β-CD/azobenzene	Lap joints	Glass	>83 kPa[a)]	[160]
Gelatin bioglue	α-CD	Lap joints	Porcine skin	27 kPa	[161]
Gelatin bioglue	γ-CD	Lap joints	Porcine skin	37 kPa	[161]
CB supramolecular Velcro	CB[7]/ferrocene	Lap joints	Silicon	1.1 MPa	[162]

[a)]For this example, the shear strength was at least 83 kPa (the sample did not break).

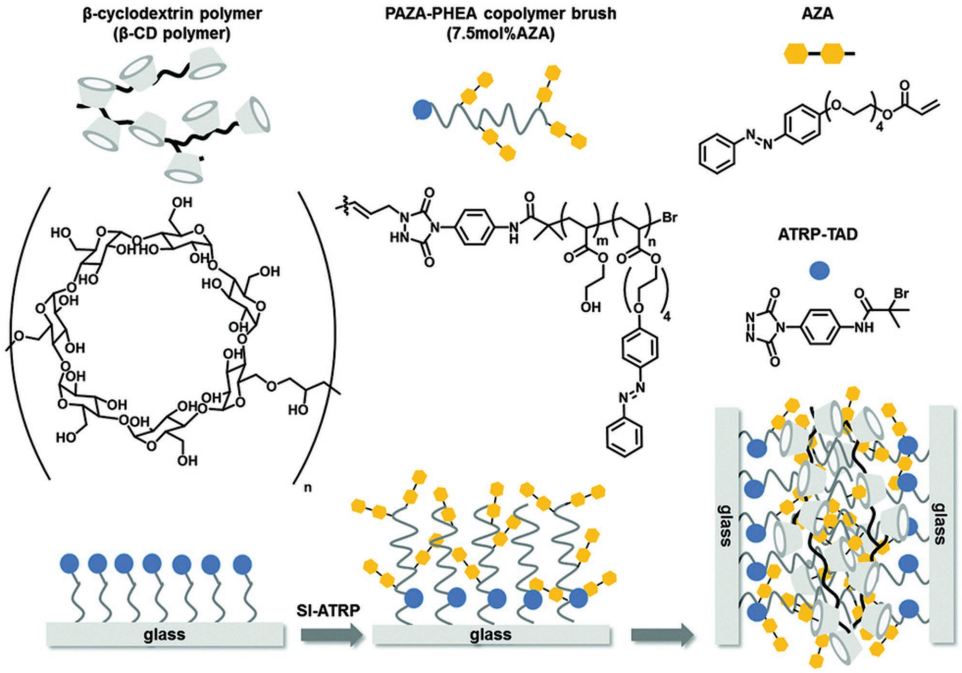

Figure 19. Schematic representation of β-CD-polymer-mediated adhesion of azobenzene-grafted (yellow) glass substrates. Azobenzene acrylate/hydroxyethyl acrylate (PAZA–PHEA) copolymer brushes were prepared by surface-initiated ATRP (SI-ATRP) using a custom-designed triazolinedione-tagged (TAD-tagged) initiator (blue). Reproduced with permission.[160] Copyright 2016, The Royal Society of Chemistry.

with a crosslinked hydroxyphenyl propionic acid-functionalized gelatine-based bioglue, the adhesion to skin was doubled compared to the pristine bioglue (lap shear strength 27 vs 11 kPa). Instead of using α-CD that can only accommodate a single guest, the ability of γ-CD to form multivalent complexes even further improved the adhesion (37 kPa). To understand this behavior, Au substrates were modified with fatty acids or phenolic compounds to mimic skin tissue. This study confirmed that inclusion of CD led to enhanced adhesion due to a combination of interactions. First, H-bonding occurred with the exterior of CD and second, host–guest complexation took place both inside the glue (inclusion of the bioglue's pendant hydroxyphenyl groups) and at the skin-glue interface (free phenols and fatty acids). Since this approach turned out (1) to be nontoxic, (2) to only require blending and (3) to function without additional chemical modifications, its use might not be limited to fundamental research, but may also find its way to true biomedical applications.

6.2. Cucurbiturils

Similar to cyclodextrins, cucurbiturils are cyclic polymers as well, and comprise *n* glycoluril units (Figure 16c). The name originates from their shape (Figure 16d), as instead of being cone-shaped, the shape of CB more closely resembles that of a pumpkin (which belongs to the cucurbitaceae family).[145] CBs can be obtained through a condensation reaction of glycoluril and formaldehyde under acidic conditions, resulting in a mixture of CB[*n*] macrocycles with *n* ranging from 5 to 10. The cavity sizes of CB[6], CB[7] and CB[8] are analogous to α-CD, β-CD, and γ-CD, respectively. Their host–guest behavior is remarkably different, though, which is caused by stronger polarization of the molecule. When looking at its electrostatic potential profile, both the inner cavity surface and portal region turn out to be negatively charged, while CDs are almost charge neutral.[163] Consequently, CD can bind to both positively and negatively charged guests, while CB hardly shows any affinity to negatively charged guests. Compared to β-CD, CB[7] is for example already able to bind a factor 10^6 stronger to a neutral ferrocene derivative, and upon introduction of a positively charged group, binding was increased by another factor 10^3.[163] K_a values of CDs are rarely higher than 10^6 M^{-1}, whereas up to 10^{17} M^{-1} has been reported for CB, making CBs highly attractive for use in adhesive materials.[164] Solubility issues and the difficulty of its functionalization initially limited applications of CBs, but as soon as these problems were tackled, the field started to develop.[163]

Scherman and co-workers have extensively studied the interesting mechanical properties of CB-based materials.[147,165,166] In the following examples, adhesive properties have unfortunately not been tested, but the reversibility of these materials could, however, still make them potentially useful for application in adhesives. Appel et al. fabricated hydrogels from a mixture of linear guest copolymers and CB[8], a host that can accommodate two guests simultaneously.[167] A cooperative, ternary complex with large association constant ($K \approx 10^{14}$ M^{-2}) was formed by inclusion of naphthyl and methyl viologen polymer side groups (**Figure 20**a). A color change indicated successful charge-transfer complex formation, while no gel was formed when CB[8] was omitted, or when CB[8] was exchanged for CB[7] (smaller cavity) (Figure 20b). The gels were found to be multiresponsive; reduction of methyl viologen or addition of a competitive guest, such as 2,6-dihydroxynaphthalene or an aromatic solvent, all disrupted the supramolecular network.

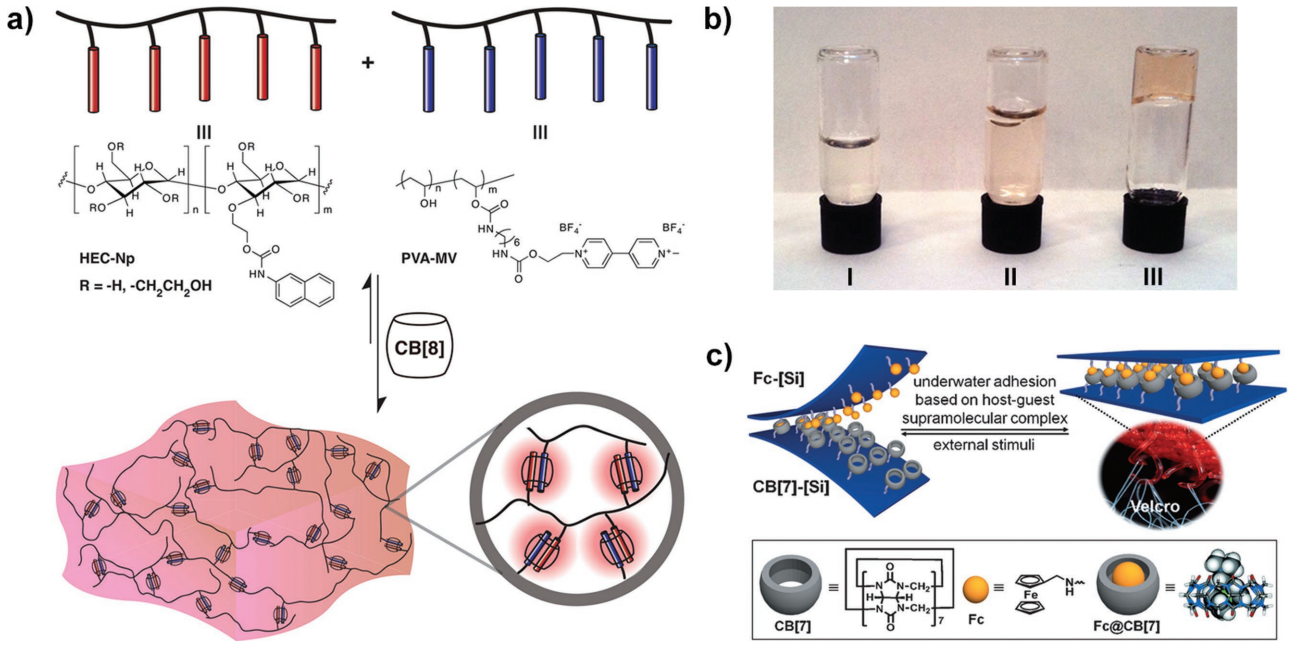

Figure 20. a) Illustration of ternary host–guest complex formation between naphthyl-functionalized polymer (HEC-Np), methyl-viologen-functionalized polymer (PVA-MV), and CB[8]. b) A hydrogel was not formed in the absence of CB[8] (I) or when CB[8] was exchanged for CB[7] (II); gelation was only observed for the ternary mixture (III). Reproduced with permission.[167] Copyright 2012, American Chemical Society. c) A supramolecular Velcro strategy employed by Ahn et al. enabled strong and selective adhesion between CB[7]- and ferrocene-modified silicon substrates. Reproduced with permission.[162] Copyright 2013, Wiley-VCH.

Investigation at the molecular level using single molecule spectroscopy led to the conclusion that two additional effects played a role in this exceptionally strong heteroternary complex. Besides host–guest chemistry, nonspecific hydrophobic interactions and interactions with the portal of CB[8] affected the strength as well.[168] In a later study, increased toughness of CB hydrogels was achieved by incorporating cerium phosphate ($CePO_4$) inorganic nanowires.[169] The high aspect ratio of such nanowires acts as a skeleton providing additional support, while the additional H-bonds at their surface reinforced the polymer network. The hybrid material demonstrated an up to 50% increase of the storage modulus.

In contrast to CD, only a few examples exist in literature in which CB was used to design adhesive materials, presumably caused by the challenging chemistry that was involved until recently. Despite the CD-based example that was discussed in the previous section,[159] Ahn et al. were the first to use the term "supramolecular Velcro," as the host–guest interaction mimics the "hook" and "loop" mechanism in macroscopic Velcro.[162] In an aqueous environment a water layer is usually present at the surface and prevents adhesion. Whereas nature tackled this obstacle by, for instance, incorporating cationic residues in mussel plaque (Section 3), the hydration layer can be a serious issue for synthetic adhesives. The presence of water is, however, required in host–guest chemistry, since expulsion of water from the cavity is the main driving force. In this work, silicon wafers were chemically modified with CB[7] and aminomethylferrocene (Figure 20c). The host–guest connection could withstand a 2 kg weight in water using only a 1 cm^2 contact area, while the strength further increased to 4 kg cm^{-2} after air drying. Lap shear strengths of over 1.1 MPa were measured, which is significantly stronger than common commercial adhesives. Compared to β-CD Velcro,[159] CB[7] Velcro was more than ten times stronger, well reflecting the difference in association constant (10^6 vs 10^{12} M^{-1}), although the functionalization density obviously also played a crucial role. Its performance was comparable to mussel-inspired biomimetic adhesive and none of the components of supramolecular Velcro turned out to be toxic. Furthermore, up to 70% of the original strength was recovered after mechanical unfastening. Similar to other ferrocene-involving studies, chemical oxidation enabled switchable adhesion as well, although the strength only recovered to about 40%. According to the authors, the reversibility might become more efficient when moving to electrochemical oxidation and reduction, because this route could avoid decomposition of ferrocene or adsorption of contaminants.

Neirynck et al. designed a nontoxic CB-based system for use in cell adhesion studies.[170] Since CB[7] forms a stable monolayer on gold spontaneously, ferrocene-labeled RGD proteins could be readily immobilized on this substrate. Adhesion of human umbilical vein endothelial cells (hUVECs) was induced by this RGD tripeptide, because it is a receptor for cell adhesion molecules. When using another tripeptide (Fc-cRAD), less spreading of the cells was observed. Only minor cell adhesion was obtained in other control experiments, i.e., using bare gold, only CB[7] or an CB[7]/ferrocenyl–PEG complex without peptide. Finally, a live–dead assay demonstrated that hUVECs remained viable, while a scratch–wound assay showed full recovery of the monolayer within a day.

This last example supports the broad range in which host–guest chemistry can be applied. While being highly selective, which might be preferential in certain fields, this is also immediately their disadvantage; host–guest adhesives cannot be used

as universal glue, because the adhesive performance primarily depends on the applied surface, not the glue itself.

7. Adhesion through Other, Less Explored Interactions

In Section 2, it was pointed out that multiple interactions contribute to the total strength of natural adhesives. Besides electrostatic interactions (Section 4) and H-bonding (Section 5), these, for instance, also include cation–π interactions and coordination bonding. Although the number of synthetic examples that are primarily focused on such forces is rather limited, these single-type examples could provide a better insight into their impact on the overall performance of natural adhesives secreted by marine organisms. For this reason, coordination-, cation–π- and dynamic covalent bonding-based adhesives are covered in the following sections. Materials that could be promising for use in such adhesives will be discussed as well.

7.1. Metal–Ligand Coordination

Because of their reversible polymerization and stimuli-responsive nature,[171,172] coordination-bonded metallo-supramolecular polymers[173] are highly attractive materials for use in adhesives. Although the materials that are reviewed in the first paragraphs of this section are primarily focused on their design and mechanical properties, they do provide a better insight into the role of coordination bonding in, for instance, biological adhesives. Indeed, coordination chemistry plays an important role in both the strength and reversibility of mussel adhesion as discussed extensively in the review by Krogsgaard et al. [12]

Inspired by mussels, Holten-Andersen et al. investigated hydrogels based on DOPA-functionalized star-shaped PEG.[174] Although DOPA is known to be able to form H-bonds, coordination bonds and cation–π interactions (Sections 2 and 3), this work was restricted to metal coordination. Supramolecular crosslinking of the PEG-chains was achieved by addition of $FeCl_3$, with the degree of coordination (mono, bis, and tris) being regulated by the pH as a result of deprotonation of the catechol moieties. This immediately had an effect on the mechanical properties: the material remained fluid-like at low pH (≈5, mono), while a sticky gel was obtained upon raising the pH (≈8, bis complex) and eventually became elastomeric at pH ≈ 12 (tris complex). Even though the redox activity of Fe^{3+} facilitates covalent crosslinking through oxidation of the catechol units, the gels could be fully dissolved by addition of a competing chelating agent, implying that the degree of covalent crosslinking was negligible within the time frame of these experiments. Therefore, the observed gelation was exclusively a result of coordination chemistry. Mechanical properties of the high-pH gels approached those of covalently crosslinked PEG–DOPA, but the latter lacked the self-healing ability of the supramolecular material. Furthermore, rheological characteristics could be finely tuned by choosing the appropriate metal ion (V^{3+}, Al^{3+}, or Fe^{3+}).[175]

Similar results were obtained by exchanging DOPA for histidine ligands.[177] As a result of the different dissociation rate constants, the mechanical properties of the gels could be adjusted by varying the metal ion (i.e., slow or fast crosslinks). Binary mixtures of Cu^{2+}, Ni^{2+}, and/or Zn^{2+}, on the other hand, enabled design of new hydrogels with any desired property, without having to substitute the polymer (**Figure 21**a).[176] Inclusion of such structural hierarchy was a universal approach, as it was applied successfully in two other hydrogel systems: (1) one

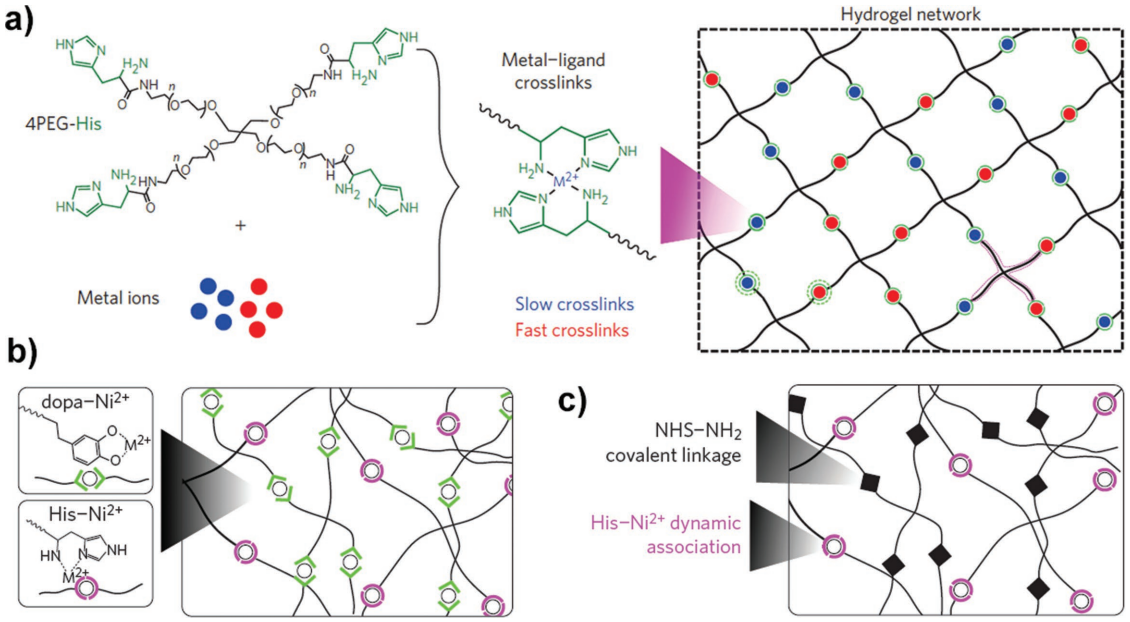

Figure 21. Structural hierarchy was used as a universal tool to modify the mechanical properties of metal-coordinated poly(ethylene glycol) hydrogels, without the need to synthesize a new polymer. This was achieved by metal–ligand coordination using a) a combination of different metal ions, b) using a single type of metal ion and two different ligands, or c) a combination of covalent and pH-responsive coordination bonding. Reproduced with permission.[176] Copyright 2015, Macmillan Publishers Ltd.

Table 5. Overview of the performance of a selection of adhesives based on coordination chemistry, cation–π complexation, and dynamic covalent bonding. Experiments were performed using various test layouts and substrates.

System	Motif	Method	Substrate	Strength	Ref.
Catechol coacervate	Zn^{2+} coordination	Lap joints	Aluminum	6.2 MPa	[181]
Catechol coacervate	Zn^{2+} coordination	Lap joints	Stainless steel	3.4 MPa	[181]
Rmfp-1 hydrogel	Fe^{3+} coordination	Lap joints	Porcine skin	0.13 MPa	[182]
Mebip-functionalized oligomer	Zn^{2+} coordination	Lap joints	Quartz	2.5 MPa	[183]
Aromatic epoxy resin	Cation–π complexation	Tensile testing	N/A	7.2 MPa	[184]
Poly(trityl methacrylate)	CH–π complexation	Lap joints	PTCD	1.0 MPa	[185]
Dynamic disulfide adhesive	Disulfide bonds	Lap joints	Glass	5.3 MPa	[186]
Phenylborate hydrogels	Phenylborate bonds	Lap joints	Glass	4.1 kPa	[187]
Phenylborate hydrogels	Phenylborate bonds	Lap joints	Porcine skin	5.2 kPa	[187]
Organogel/hydrogel hybrid	Acylhydrazone bonds	Tensile testing	N/A	64 kPa	[188]
Dynamic PDMS elastomer	Imine bonds	Lap joints	Glass	2.1 kPa	[189]
Methacrylate copolymers	Diels–Alder chemistry	Lap joints	Wood	36 MPa	[190]

metal ion and two ligands (DOPA and histidine) (Figure 21b), and (2) through a combination of covalent bonding and pH-responsive coordination bonding (Figure 21c). This route enabled tuning of the mechanical properties of a bulk material as well, by combining an imidazole-containing butylacrylate copolymer and a mixture of two different metals. Viscoelastic properties of the hydrogel networks could be further adapted by incorporation of a water-soluble radical photoinitiator.[178] Irradiation of the gels by UV light triggered metal ion redox chemistry, thereby changing the character of the coordination sites. This resulted in either softening or hardening of the network, depending on the initial metal species.

Self-healing hydrogels that could be promising for use in wet adhesion were recently developed by Krogsgaard et al., starting from DOPA-functionalized polyallylamine (grafting density of around 9.5%) and $FeCl_3$.[179] Compared to the previously discussed charge-neutral polymer-based materials, this system more closely resembles that of the lysine-rich mfps due to the cationic nature of polyallylamine. Analogous to the work of Holten-Anderson et al., the degree of complexation, and thus the gelation, could be adjusted by changing the pH. Whereas catechol complexation increased with pH and caused strengthening of the gel, when passing the isoelectric point of polyallylamine (pH ≈ 10), inhomogeneous collapse resulted in severe weakening of the material. Such multiresponsive behavior makes these materials attractive for use in applications in which stability is only desired in a specific pH range, e.g., in drug delivery. In later work the authors demonstrated this range to be tunable depending on the choice of the polyelectrolyte.[180] When polyallylamine was exchanged for chitosan, the pH at which the hydrogel's strength peaked shifted toward physiological conditions, i.e., pH = 8 instead of pH = 9.5.

Wang et al. prepared a coordination chemistry-based adhesive derived from zinc chloride and DOPA-functionalized poly(acrylic acid) (≈30 mol% catechol units).[181] As a result of catechol chelation and electrostatic interactions, a coacervate was formed spontaneously when both components were mixed under acidic conditions (pH = 4), whereas in the absence of either DOPA or acrylic acid no viscous solution was obtained. After curing at 40 °C, lap shear mechanical analysis demonstrated excellent adhesive performance to various metals (aluminum 6.2 MPa, stainless steel 3.4 MPa, **Table 5**), and in all experiments stronger adhesion was measured as compared to commercial cyanoacrylate-based adhesives (DOPA:Zn^{2+} = 1:4). Above that, wet-cured samples performed remarkably well, while the commercial adhesive completely lost its mechanical properties when cured underwater.

Kim et al. studied the role of metal coordination in DOPA-containing recombinant mfp-1 mussel adhesive proteins. Gelation of the material was accomplished through oxidation of DOPA (covalent crosslinking) or addition of $FeCl_3$ and subsequent increase of the pH (metal–ligand complexation).[182] Aiming for biomedical applications, lap shear tests were carried out using porcine skin tissue surfaces. Depending on the curing time, the covalent DOPA adhesive was slightly stronger (up to 200 kPa) than the Fe^{3+}-coordinated adhesive (130 kPa). Cohesive failure was identified for both materials; the reversible nature of metal–ligand bonding, however, enabled the coordination adhesive to retain its strength for at least six cycles, while the covalent adhesive lost its adhesion ability after four cycles.

Mebip (2,6-bis(1′-methylbenzimidazolyl)-pyridine) ligands for coordination bonding were studied by Heinzmann and colleagues.[183] A low-molecular-weight telechelic poly(ethylene-*co*-butylene) copolymer (3.1 kg mol^{-1}) was end-functionalized with these groups and blended with Zn^{2+} ions (**Figure 22**a). The as-formed metallo-supramolecular polymer demonstrated excellent adhesion between quartz slides (Figure 22b). Lap joint experiments displayed shear strengths exceeding 2.5 MPa, and the joints could be debonded on demand by exposure to heat or UV irradiation. In contrast to UPy-functionalized poly(ethylene-*co*-butylene), inclusion of a UV sensitizer was not needed, and adhesion was found to be twice as strong. Furthermore, bonding was reversible and full recovery of the initial strength was obtained after fracture (Figure 22c).

Inspired by proteins like hemoglobin, Harada and coworkers synthesized acrylamide hydrogels modified with Fe^{2+}-porphyrin groups or L-histidine groups.[191] Coordination chemistry caused the gels to self-assemble macroscopically,

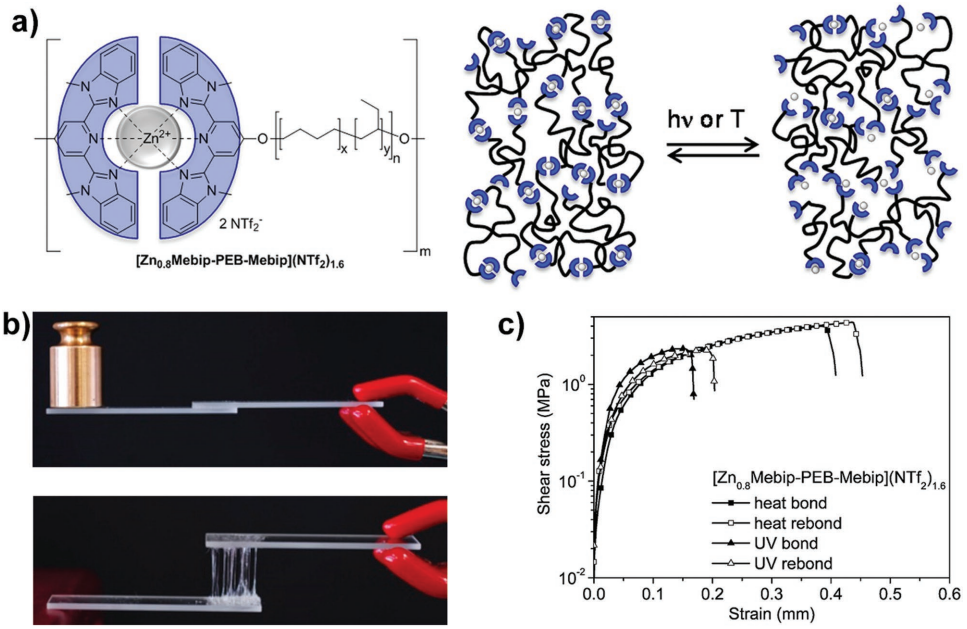

Figure 22. a) Schematic representation of a Mebip-functionalized poly(ethylene-*co*-butylene) metallo-supramolecular adhesive. Heat or UV light shifts the equilibrium toward the noncoordinated state, leading to softening of the material and thus severely weaker adhesion. b) Images of quartz-glass lap joints before and after fracture. c) As demonstrated by lap-joint experiments, full recovery of the adhesive properties was obtained through a heat or UV treatment. In contrast to a similar UPy-based adhesive, strong UV absorption of the Mebip groups did not require incorporation of a UV sensitizer. Reproduced with permission.[183] Copyright 2014, American Chemical Society.

similar to the host–guest gels discussed in Section 6. Depending on the composition of the hydrogels, rupture stresses of adhered gels reached values of up to 5 kPa. Addition of an aqueous solution of free L-histidine led to dissociation of the gels, but the process was fully reversible by washing the gels with fresh buffer. No adhesion between the Fe^{2+}-porphyrin and L-histidine gels was observed (1) in the absence of iron, (2) at low pH (due to protonation of the L-histidine moiety) or (3) to a Zn^{2+}-porphyrin gel. In another example, coordination chemistry was used to control the adhesion in host–guest gels.[192] Since both bipyridine and *tert*-butyl groups are able to bind to β-CD, competition between the two guests prevented specific adhesion of the β-CD/bipyridine-gel to the *tert*-butyl gel. However, because metal-coordinated bipyridine is too large to fit in β-CD's pocket, β-CD became available for binding *tert*-butyl through addition of copper(II) chloride. Adhesion between the two gels increased with increasing concentration of $CuCl_2$ and reached a maximum strength of about 1 kPa.

7.2. Cation–π Complexation

Cation–π interactions are essential for the secondary structure of proteins. While being hydrophobic, aromatic amino acids (like phenylalanine, tryptophan, and tyrosine) are overrepresented in binding sites at the cost of aliphatic residues.[193] Stabilization of their structure by interactions between aromatic and cationic amino acids (lysine or arginine) is quite common. Interestingly, calculations established that every protein of significant size has at least one cation–π interaction. The cation–π interaction is, for instance, crucial in $\alpha_4\beta_7$, a protein that promotes white blood cell adhesion. In the absence of Phe185 in the β_7 subunit, loss of the metal-ion binding site (that was connected to this complex through a cation–π interaction) led to a severe reduction of cell adhesion.[194] Metal ions also bind stronger to benzene than water (or other polar molecules, i.e., polar–π interactions), which originates from the higher electron density at the center of benzene's aromatic ring. Cations therefore interact with the π orbitals perpendicularly to the ring. In aqueous solution cation–π complexation was found to be stronger than hydrogen bonding and possibly even stronger than charge-charge interactions.[63,64] Therefore, the significant role of cation–π interactions in chemistry, materials science, and biology should not be underestimated.[195]

The impact of both cationic and aromatic groups on the nanomechanical behavior in aqueous media was investigated by Lu et al. using an SFA.[196] In this work, one surface was covered with cationic poly(L-lysine), while the other surface was spin-coated with different polyaromatics, i.e., polytryptophan (PTrp), polytyrosine (PTyr) or PS. Significantly enhanced adhesion to quaternized poly(L-lysine) was observed when moving from anionic poly(L-glutamic acid) to PTrp, pointing out that cation–π interactions can indeed be stronger than purely electrostatic interactions. Adhesion strengths of the aromatics to poly(L-lysine) followed the order PTrp > PS > PTyr, in line with interaction strengths found in previous gas phase experiments. Addition of $LiNO_3$ or $NaNO_3$ hardly affected the interaction, while KNO_3 and NH_4Ac both led to significantly reduced adhesion. The difference in hydration radius of these cations turned out to be responsible for this behavior.

Using the same technique (SFA), Kim et al. confirmed that cation–π interactions are part of the toughening mechanism

in recombinant DOPA-deficient mussel adhesive protein (Rmfp-1).[197] Interaction forces between protein-coated mica surfaces were studied at a pH below which lysine is protonated (pH < 9). Despite both surfaces being positively charged under these conditions, the surfaces adhered almost instantaneously. Screening of interprotein cation–π complexation by addition of KNO_3 resulted in significant weakening of the interaction strength. A combination of computer simulations and control experiments demonstrated minor contribution of other interactions to the adhesion mechanism in the symmetric case (H-bonding, van der Waals, and π–π interactions). The authors therefore concluded that cation–π complex formation is the dominant factor of Rmfp-1 cohesion. Similar results were obtained by Hwang et al. who studied underwater adhesion of pvfp-1, a foot protein of the Asian green mussel that lacks DOPA. Strong adhesion between symmetric protein films was observed. After having studied the influence of the ionic strength, pH, redox chemistry, metal complexation and temperature, cation–π complexation between aromatic and quaternized amino acids was thought to be the best explanation for the substantial cohesion.[198]

Inspired by mussel foot protein mfp-5, Gebbie et al. designed and compared wet adhesion of aromatic-rich proteins (composed of 36 amino acids) by systematic variation of the aromatic residue (Phe, Tyr, or DOPA) (**Figure 23**a).[51]

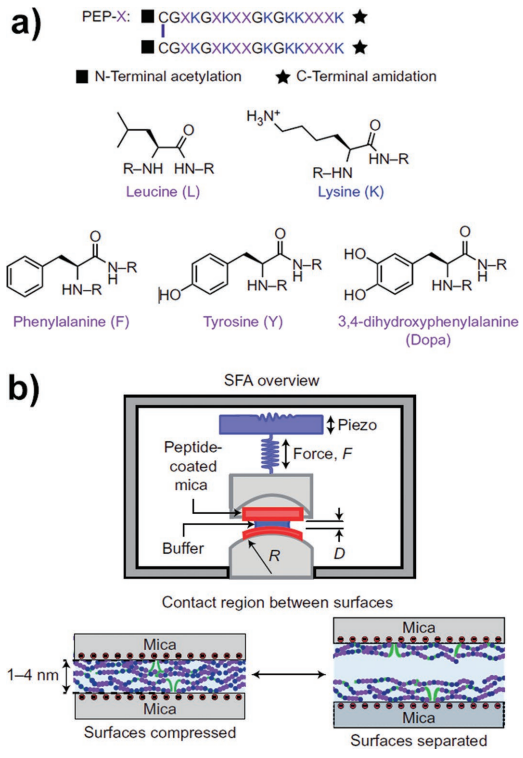

Figure 23. a) Sequence and structure of mfp-5-inspired peptides. X indicates the position of the aromatic amino acid, of which the type was varied systematically (phenylalanine, tyrosine, or dopamine), while nonaromatic leucine served as a control experiment. b) Their adhesion through cation–π complexation was investigated in an aqueous environment using a SFA. The adhesive strength increased significantly when an aromatic peptide film was included. Reproduced with permission.[51] Copyright 2017, Macmillan Publishers Ltd.

Cohesive failure was observed in all cases (Figure 23b), meaning that the measured strength was proportional to the protein interaction. Inclusion of an aromatic peptide film always resulted in significantly enhanced adhesion compared to the neat mica substrates or nonaromatic Leu control experiment. However, as pointed out in Section 4.2, one should be careful with interpretation of the term "cohesive" in experiments where extremely thin films (1–4 nm in this work) are studied by SFA, as the results do not represent the cohesive properties of the bulk material. 2D solid-state NMR confirmed the close proximity of Lys and Tyr, as the alkyl ^{13}Cs of Lys correlated with the aromatic protons of Tyr. In addition, ring currents caused the resonance of the quaternary ammonium to shift by almost 0.6 ppm compared to the Leu control experiment. Surprisingly, the deposition salinity appeared to be a critical parameter. For example, when deposited without background electrolyte (i.e., 0 mM KNO_3) followed by adjustment to the "high salt" concentration (250 mM KNO_3), worse adhesion was achieved as compared to deposition at high salt concentration. The authors claim that this was caused by morphological changes in the peptide thin film, although detailed evidence was not given.

Adhesion of two fully synthetic polymer systems by means of cation–π bonding was investigated by Wang and Xie.[184] While the interaction between polymer substrates often encompasses interfacial chain diffusion (entanglement formation), in this work it was avoided by using a tightly crosslinked aromatic-rich epoxy resin. Adhesion between this substrate and several other polymeric systems was tested and compared: polypropylene, crosslinked PS, surface sulfonated PS and surface sodium sulfonated PS. The presence of OH–π interactions strengthened adhesion between epoxy and PS ten times (3.8 MPa) compared to polypropylene (0.4 MPa), while a further doubling of the adhesive strength was found for sulfonated PS (electrostatic and H-bonding; 6.5 MPa) and sodium sulfonated PS (cation–π; 7.2 MPa). Inspection of the detached samples by XPS showed that failure of the latter two polymers was cohesive, so the measured values mainly reflected the properties of the bulk material (PS). Furthermore, since sodium sulfonated PS could not form H-bonds or salt bridges through protonation of the epoxy resin (unlike sulfonated PS), its strong adhesion was an immediate result of the interaction between the Na^+ ions and the aromatic rings on the epoxy surface. Raman spectroscopy confirmed the formation of this Na^+/π complex, by examination of a mixture of sodium methanesulfonate and the epoxy precursor.

Yamate et al. went a step further and studied how π-interactions could be used to bind polyolefins, because adhesion to such materials is very challenging and usually requires chemical modification of the surface.[185] CH–π bonding of polytetracyclododecene, an amorphous polyolefin (PTCD) to several aromatic polymethacrylates was investigated systematically. Although the CH–π bond is considered to be a rather weak interaction, lap shear strengths increased rapidly with increasing number of π-electrons. For instance, a layer of poly(methyl methacrylate) could be peeled off manually, while poly(trityl methacrylate) displayed very strong adhesion (1.02 MPa). Moreover, control experiments in which aliphatic polymers were directly compared to their aromatic analogs

(i.e., cyclohexyl vs benzyl, dicyclohexyl vs diphenyl), indeed demonstrated strong contribution of the π-electrons. Using a standard tape test, the concept appeared to be practically interesting as well, as the adhesive performance of aromatic polymers could be classified in the highest rank. When the PTCD substrate was replaced for crystalline, but more common polymeric materials, such as polyethylene and polypropylene, tape tests still indicated excellent adhesion of the aromatic poly(trityl methacrylate).

7.3. Dynamic Covalent Linkages

The use of covalent bonds has several advantages over supramolecular chemistry, since such bonds are stronger, more stable under humid conditions, and give a lower risk of chemical leakage, which is particularly important for biomedical applications. It is therefore also not surprising to see that both sandcastle and mussel adhesives are partially covalently crosslinked by oxidation of DOPA or cysteine residues (Section 2). The static character of covalent bonds unfortunately results in permanent joints like superglue, and therefore does not have the attractive reversible property of supramolecular adhesives. By moving to dynamic covalent bonds, such as disulfide bridges, imines and Diels–Alder chemistry, this drawback can be overcome. Furthermore, an external stimulus can trigger debonding, similar to supramolecular adhesives.[199]

Inspired by the disulfide linkages present in proteins, Michal et al. prepared a synthetic adhesive based on semicrystalline, thiol-capped telechelic thioether oligomers and a tetrathiol crosslinker (**Figure 24**a).[186] Heating of the material first caused melting of the crystalline domains (70 °C), while an additional, but significant drop of the viscosity was observed above 150 °C due to dissociation of the disulfide bridges. The same result was obtained by irradiation of the sample with UV light, and thus enabled rapid wetting of surfaces (Figure 24b). When applied above the melting point, shear stresses required to break glass lap joints were as high as several MPa, whereas application of the adhesive above the second phase transition led to doubled values of the shear strength, up to 5.3 MPa (Figure 24c). In addition, similar adhesion to a steel substrate was observed and the glue could be used multiple times without any loss in adhesive performance for at least three cycles. Finally, the mechanical properties could be adjusted by changing the chemistry of the oligomer or by incorporating cellulose nanocrystals.

Using the pH-sensitive character of phenylborate esters (see also Section 3), Wu and co-workers synthesized dynamic PEG hydrogels that were formed spontaneously by mixing aqueous solutions of four-armed PEG-dopamine and four-armed PEG–boronic acid under alkaline conditions.[187] At neutral pH the gels were relatively stable ($t_{1/2} \approx 8$ h), but degraded rapidly in an acidic environment ($t_{1/2} \approx 1$ h). Lap shear tests demonstrated solid bonding to both glass slides (4.1 kPa) and porcine tissue (5.2 kPa), and the dynamic character of the phenylborate-catechol bonds enabled reversible adhesion well. Because of their excellent cytocompatibility, the authors claim that the gels are potentially useful as bioadhesive for tissue engineering purposes or as drug delivery system.

Instead of using phenylborate esters, Deng et al. prepared both dynamically crosslinked PEG-hydrogels and PEG-organogels based on acylhydrazone bonds (**Figure 25**a).[188] Fast adhesion between the dynamic organogel and hydrogel was observed, and with an ultimate strength of 64 kPa, this is one of the strongest examples of adhesion between different gels discussed in this review. Adhesion was nonexistent when using a dynamic acylhydrazone hydrogel and a static urethane PEG–organogel, pointing out the relevance of the acylhydrazone linkages. Furthermore, the choice of the organic medium turned out be equally important, as adhesion was slowed down significantly (tens of hours vs minutes) when using nitroethane, DMF or DMSO instead of anisole or chloroform. A turbid emulsion interlayer was observed for the successful combinations, which presumably provided an increased contact area

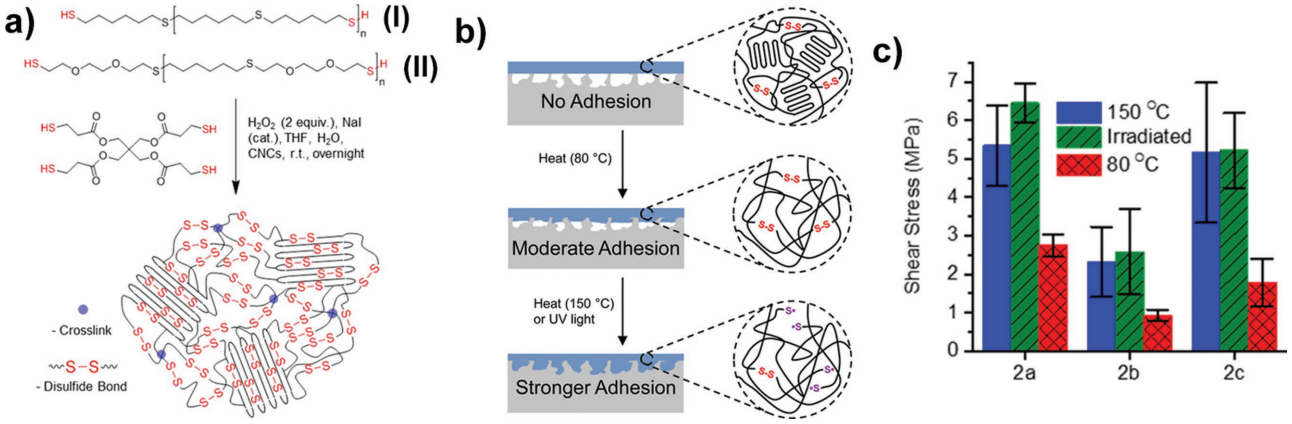

Figure 24. a) Michal et al. prepared a semicrystalline dynamic covalent adhesive based on disulfide linkages, through reaction of thiol-capped oligomers and a tetrathiol crosslinker. b) Heating above the melting point (80 °C) resulted in moderate adhesion, while dissociation of the disulfide bridges (via heat (150 °C) or UV light) reduced the viscosity of the material significantly. On cooling to room temperature, this led to better wetting and improved adhesion to the glass slides used for lap-joint experiments. c) Samples 2a–c indicate different compositions of the dynamic covalent network (2a: from (I); 2b: from 3 equivalents (I) and 1 equivalent (II); 2c: from (I) mixed with 10% cellulose nanocrystals). Reproduced with permission.[186] Copyright 2016, American Chemical Society.

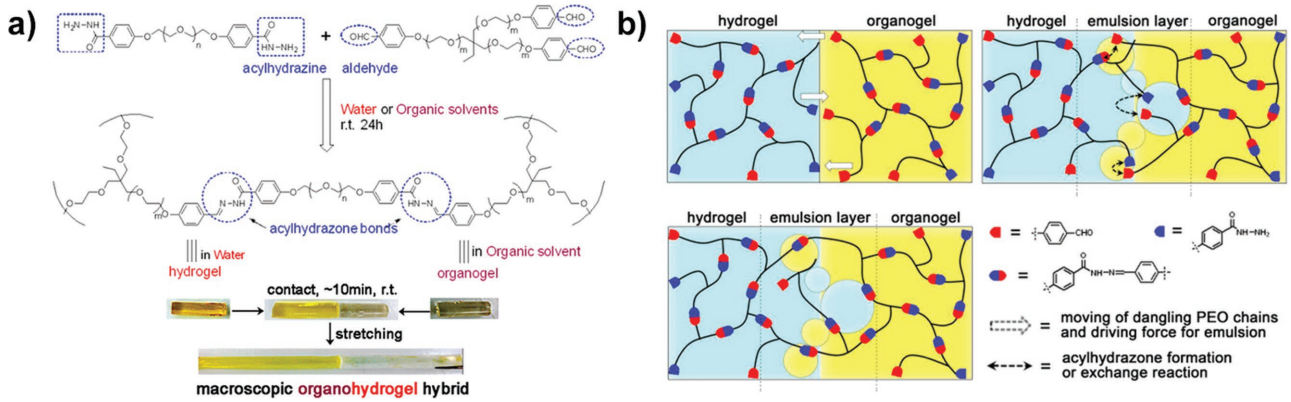

Figure 25. a) Formation of a dynamic covalent acylhydrazone network by reaction of linear and star-shaped PEG caused gelation of both aqueous and organic solutions. The hydrogel adhered to the organogel (anisole) within 10 min. b) The presence of an emulsion interlayer turned out to be a crucial factor for obtaining strong adhesion, as this increased the effective contact area and could therefore accelerate bond exchange. Reproduced with permission.[188] Copyright 2015, American Chemical Society.

between both surfaces and could therefore accelerate bond exchange (Figure 25b). Unfortunately, this does not explain the retardation observed for water-miscible organic solvents. The concept is very interesting though, as this approach would enable adhesion of hydrophobic to hydrophilic surfaces, with the presence of water at the interface no longer being an issue.

Zhang et al. designed a reversible silicone-based elastomer by starting from telechelic amine-terminated polydimethylsiloxane and triformylbenzene.[189] Dynamic imine bonds caused excellent self-healing properties of the highly stretchable material; full recovery of the mechanical properties was achieved within 10 h at room temperature. Self-healing even occurred at sub-zero conditions (24 h at –20 °C) and the healing time was reduced to only 30 min by simply heating the sample to 70 °C. Because of its insensitiveness to moisture, the elastomer was demonstrated to be a promising candidate for use in anticorrosion and antifouling coatings. Preliminary lap joint adhesion tests were performed as well. Depending on the drying conditions, glass slides with a contact area of 6.25 cm^2 could withstand a weight of up to 135 g. Although this material is not among the strongest adhesives discussed in this review (22 g cm^{-2} ≈ 2.1 kPa), full recovery of adhesion only required gently pressing of the glass slides for 5 min at room temperature.

Methacrylate copolymers of relatively low molecular weight (10 kg mol^{-1}) bearing furfuryl groups for Diels–Alder chemistry were synthesized by Kavitha and Singha.[190] An insoluble network was formed when the copolymer was mixed with a bismaleimide linker at room temperature, while as a result of retro-Diels–Alder chemistry, heating caused the product to become soluble again. Adhesion between wooden joints was significantly stronger in the presence of crosslinking agent (36 vs 18 MPa). Due to the thermo-reversible nature of the bridges, at higher temperatures the performance dropped to values characteristic for the pristine, uncrosslinked material. Furthermore, in the absence of the linker, heating did not affect the adhesive strength at all, thereby demonstrating the influence of the dynamic bonds.

Although based on static covalent bonding, the following example enables a direct comparison of supramolecular and covalent chemistry, and thus gives a good impression of the strength of both bond types. Instead of using reversible noncovalent motifs in their previous studies, Harada and co-workers later also investigated static bonding between hydrogels.[200] In this work, iodophenyl- and phenylboronic acid-functionalized acrylamide hydrogels were connected by means of Pd-catalyzed Suzuki–Miyaura coupling. Simple submersion into an aqueous $Pd(OAc)_2$-containing solution led to strong bond formation in 5 h, whereas bonding was not observed in the absence of catalyst, even after several days. Ultimate strengths of over 100 kPa were measured, which is significantly higher than the adhesion of H-bonded (1 kPa)[131] or host–guest gels (up to 10 kPa) [156]; see Sections 5 and 6, respectively. Slightly weaker adhesion was observed when gluing the iodophenyl or phenylboronic acid gels to complementary modified glass substrates (10 kPa). The approach is not very practical, though, as it requires the presence of a suitable catalyst and appropriate surface functionalization. Nevertheless, it is a versatile method, since adhesion through a different reaction mechanism, such as Cu(I)-catalyzed azide-alkyne cycloaddition (CuAAC), could be achieved by simply replacing the reactive groups and catalyst.[201]

Martínez-Triana avoided the use of an external Cu catalyst by simply using CuAAC to glue copper-rich surfaces.[202] Copper nail heads irreversibly adhered to glass surfaces by including a mixture of multivalent alkyne and azide crosslinkers. While the metal surface supplied the catalyst, bonding occurred via metal–ligand coordination (triazole group) and H-bonding to the glass surface. Using a custom-made peel-type instrument, adhesive strengths outperformed that of a commercial adhesive (55 vs 29 N) and were further improved by heating the sample to 70 °C (81 N). Gluing Cu-based alloys, such as brass, or metals that contain Cu impurities (e.g., iron) was successful as well, whereas adhesion to Cu-poor materials (e.g., steel) was promoted by addition of Cu(I) salts. On the other hand, the native oxide layer of aluminum hindered proper binding. Additionally, CuAAC-induced adhesion was also achieved under water without significant loss of the strength, but its performance reduced by about 50% over a period of several months if kept under moist conditions. Nevertheless, the commercial adhesive failed completely in both scenarios, i.e., both wet gluing and

storage. Alkyne/azide-based adhesives could therefore become interesting for applications in which an insulating glass coating is desired, such as in electronics.

8. Perspectives

8.1. Combinations of Supramolecular Moieties

The underwater adhesives secreted by mussels and sandcastle worms have inspired a very active research direction over the last decades: the investigation of what is required for attachment to wet surfaces, and how this knowledge can be turned into new strategies to join wet surfaces.

Early on, the presence of DOPA has been implicated to be the key component that governs adhesion and cohesion of the adhesives. More recently, other functional groups in the proteins were identified to be (equally) important.

In this review, we explored the versatile supramolecular interactions used in the protein-based adhesives secreted by sandcastle worms and mussels, and subsequently reviewed synthetically designed adhesives based on electrostatic interactions, hydrogen bonding, hydrophobic forces, metal coordination interactions, cation–π complexation, dynamic covalent linkages, and combinations of these.

The developments reviewed here evidence the potential of using the supramolecular toolbox for underwater adhesion. A picture is emerging that combinations of (noncovalent) interactions are highly important to ensure good underwater adhesive performance. In other words, "designer" adhesive systems may be developed by selecting multiple supramolecular moieties, in which a combination of different types of interactions is critical: (1) to promote adhesion, (2) to adjust cohesion, and (3) to facilitate processing.

(1) *Adhesion*: to adhere to changeable or different types of substrates, the adhesive must exhibit several bonding strategies by means of versatile and different functional groups. Interesting work in this direction is highlighted in this review. Catechols have a versatile character; they are able to interact to substrates via hydrogen bonding, metal–catechol coordination or cation–π complexation.[11,13] Moreover, both natural and synthetic polymer chains (containing amphiphilic or ionic features) can be self-adjustable.[56,99] That means that depending on the target surface, different parts of the adhesive are exposed to the surface ensuring strong adhesive bonding. For example, mfp-3s was shown to expose hydrophobic moieties toward a hydrophobic surface and hydrophilic moieties toward a hydrophilic surface.[56] Synthetic polyampholyte gels were shown to adhere strongly to both cationic and anionic surfaces, suggesting a self-adjustable ion-bond formation mechanism.[99]

(2) *Cohesion*: different types of interactions can result in a wide variety of bond strengths. Strong supramolecular bonds (such as iron(III)-catechol coordination bonds or host–guest interactions) can act as permanent crosslinks, imparting elasticity, whereas weak bonds (such as single hydrogen bonds) can reversibly break and reform, thereby dissipating energy. In recent years, it has been shown that materials that combine strong and weak bonds (e.g., physical polyampholyte hydrogels developed by Gong and co-workers) can be extremely strong, tough, and self-healing, even without covalent bonds.[203]

(3) *Processing*: sandcastle worm adhesives are (partially) secreted as complex coacervates. These concentrated liquids are water-insoluble and exhibit a low surface tension, features that make complex coacervates particularly suitable to deliver underwater adhesives. In addition to electrostatic interactions, as shown for mfp-3s,[48] (complex) coacervation may be driven by cation–π complexation[28] and can be enhanced by additional interactions. Thus, also for the delivery of the adhesives, a combination of supramolecular interactions can be critical.

Another important aspect in adhesive processing is the solidification after delivery. In natural adhesives this occurs upon an environmental trigger (for example, a change in pH). Analogously, the strength of supramolecular interactions in synthetic materials can be tuned by external triggers to transform the material from a liquid to a solid. For example, low-viscosity complex coacervates were obtained at high ionic strengths. After equilibration toward physiological ionic strength (i.e., after injection into the human body), the reduced ionic strength resulted in much stronger electrostatic interactions and solidified the material.[110]

8.2. Structural Design

In addition to chemical interactions, the performance of underwater adhesives is also determined by other factors. More specifically, the structural design of the adhesive (such as the hierarchical organization) is of great importance to the performance.[33,204,205]

For example, many of the developed underwater adhesives are a type of gel and contain water, which will strongly affect the performance. At low water concentrations, water can be a good plasticizer and can enhance the adhesive toughness. With an increase of the amount of water the cohesive strength may diminish. The optimum performance may be achieved by tailoring the water content, e.g., by the amount of hydrophobic moieties in the material.

With respect to the structural design, there is still a lot to learn from the natural systems. Despite substantial progress made in our understanding of mussel and sandcastle worm adhesion, several questions remain. For example, both sandcastle worm and mussel glue are porous solids, but the formation mechanism and the effect on the mechanical properties are not fully understood. The synthesis and processing of the adhesive proteins is regulated by enzymes (as discussed in Section 2) of which some remain active in the fully cured material. However, which roles the enzymes play and how this may be translated into synthetic adhesives remain largely open questions. The processing of mussel adhesive is thought to be facilitated by coacervation, but which mussel proteins are involved and whether this process occurs before or after secretion, or before or after foot lift-off has not been clarified. We expect that the design of biomimetic adhesives will benefit significantly from answering these questions. Connecting the chemical interactions, the structure and the

resulting material properties is essential in deploying bioinspired strategies when developing improved adhesives.

Acknowledgements

Prof. Russell J. Stewart (University of Utah) is acknowledged for helpful discussions and for providing a high-resolution picture of the sandcastle worm (Figure 1a). A.H., I.H. and M.K. thank the Netherlands Organization for Scientific Research (NWO) for financial support via a Vidi innovational research grant.

Note: Typographical errors on page 8 and 20 and in the caption of Figure 17 were corrected on May 7, 2018, after initial publication online. The footnote positions in Table 3, the author list of ref. 92, and the sentence "The increase in pH solidifies the Mg^{2+}/sulfated Pc3 complexes that are present in the heterogeneous subgranules" on page 3 were also corrected.

Conflict of Interest

The authors declare no conflict of interest.

Keywords

adhesion, bioinspired materials, mussels, sandcastle worms, supramolecular chemistry

Received: August 15, 2017
Revised: October 2, 2017
Published online: January 22, 2018

[1] G. Walker, *Mar. Biol.* **1970**, *7*, 239.
[2] J. H. Waite, N. H. Andersen, S. Jewhurst, C. Sun, *J. Adhes.* **2005**, *81*, 297.
[3] R. J. Stewart, J. C. Weaver, D. E. Morse, J. H. Waite, *J. Exp. Biol.* **2004**, *207*, 4727.
[4] R. J. Stewart, T. C. Ransom, V. Hlady, *J. Polym. Sci., Part B: Polym. Phys.* **2011**, *49*, 757.
[5] M. E. Yu, J. Y. Hwang, T. J. Deming, *J. Am. Chem. Soc.* **1999**, *121*, 5825.
[6] H. J. Kim, B. H. Hwang, S. Lim, B.-H. Choi, S. H. Kang, H. J. Cha, *Biomaterials* **2015**, *72*, 104.
[7] H. Lee, B. P. Lee, P. B. Messersmith, *Nature* **2007**, *448*, 338.
[8] H. Lee, N. F. Scherer, P. B. Messersmith, *Proc. Natl. Acad. Sci. USA* **2006**, *103*, 12999.
[9] E. Faure, C. Falentin-Daudré, C. Jérôme, J. Lysakawa, D. Fournier, P. Woisel, C. Detrembleur, *Prog. Polym. Sci.* **2013**, *38*, 236.
[10] S. Moulay, *Polym. Rev.* **2014**, *54*, 436.
[11] P. K. Forooshani, B. P. Lee, *J. Polym. Sci., Part A: Polym. Chem.* **2017**, *55*, 9.
[12] M. Krogsgaard, V. Nue, H. Birkedal, *Chem. Eur. J.* **2016**, *22*, 844.
[13] J. H. Waite, *J. Exp. Biol.* **2017**, *220*, 517.
[14] R. J. Stewart, C. S. Wang, I. T. Song, J. P. Jones, *Adv. Colloid Interface Sci.* **2017**, *239*, 88.
[15] R. J. Stewart, C. S. Wang, H. Shao, *Adv. Colloid Interface Sci.* **2011**, *167*, 85.
[16] B. J. Endrizzi, R. J. Stewart, *J. Adhes.* **2009**, *85*, 546.
[17] B. P. Lee, P. B. Messersmith, J. N. Israelachvili, J. H. Waite, *Annu. Rev. Mater. Res.* **2011**, *41*, 99.
[18] C. Heinzmann, C. Weder, L. Montero de Espinosa, *Chem. Soc. Rev.* **2016**, *45*, 342.
[19] M. J. Stevens, R. E. Steren, V. Hlady, R. J. Stewart, *Langmuir* **2007**, *23*, 5045.
[20] H. Zhao, C. Sun, R. J. Stewart, J. H. Waite, *J. Biol. Chem.* **2005**, *280*, 42938.
[21] C. S. Wang, R. J. Stewart, *Biomacromolecules* **2013**, *14*, 1607.
[22] S. L. Perry, C. E. Sing, *Macromolecules* **2015**, *48*, 5040.
[23] C. S. Wang, R. J. Stewart, *J. Exp. Biol.* **2012**, *215*, 351.
[24] C. S. Wang, K. K. Svendsen, R. J. Stewart, *Biological Adhesive Systems; From Nature to Technical and Medical Application*, 1st ed., Springer, Vienna, Austria **2010**.
[25] E. Spruijt, *Ph.D. Thesis*, Wageningen University **2012**.
[26] D. S. Hwang, H. Zeng, A. Srivastava, D. V. Krogstad, M. Tirrell, J. N. Israelachvili, J. H. Waite, *Soft Matter* **2010**, *6*, 3232.
[27] S. Kim, J. Huang, Y. Lee, S. Dutta, H. Y. Yoo, Y. M. Jung, Y. S. Jho, H. Zeng, D. S. Hwang, *Proc. Natl. Acad. Sci. USA* **2016**, *5*, 3191.
[28] S. Kim, H. Y. Yoo, J. Huang, Y. Lee, S. Park, Y. Park, S. Jin, Y. M. Jung, H. Zeng, D. S. Hwang, Y. Jho, *ACS Nano* **2017**, *11*, 6764.
[29] H. Zeng, D. S. Hwang, J. N. Israelachvili, J. H. Waite, *Proc. Natl. Acad. Sci. USA* **2010**, *107*, 12850.
[30] C. J. Sun, G. E. Fantner, J. Adams, P. K. Hansma, J. H. Waite, *J. Exp. Biol.* **2007**, *210*, 1481.
[31] J. Yang, M. A. Cohen Stuart, M. Kamperman, *Chem. Soc. Rev.* **2014**, *43*, 8271.
[32] H. G. Silverman, F. F. Roberto, *Mar. Biotechnol.* **2007**, *9*, 661.
[33] T. Priemel, E. Degtyar, M. N. Dean, M. J. Harrington, *Nat. Commun.* **2017**, *8*, 14539.
[34] R. Mirshafian, W. Wei, J. N. Israelachvili, J. H. Waite, *Biochemistry* **2016**, *55*, 743.
[35] L. Petrone, A. Kumar, C. N. Sutanto, N. J. Patil, S. Kannan, A. Palaniappan, S. Amini, B. Zappone, C. Verma, A. Miserez, *Nat. Commun.* **2015**, *6*, 8737.
[36] B. K. Ahn, *J. Am. Chem. Soc.* **2017**, *139*, 10166.
[37] V. V. Papov, T. V. Diamond, K. Biemann, J. H. Waite, *J. Biol. Chem.* **1995**, *270*, 20183.
[38] H. Zhao, N. B. Robertson, S. A. Jewhurst, J. H. Waite, *J. Biol. Chem.* **2006**, *281*, 11090.
[39] J. H. Waite, X. Qin, *Biochemistry* **2001**, *40*, 2887.
[40] H. Zhao, J. H. Waite, *J. Biol. Chem.* **2006**, *281*, 26150.
[41] D. S. Hwang, H. Zeng, A. Masic, M. J. Harrington, J. N. Israelachvili, J. H. Waite, *J. Biol. Chem.* **2010**, *285*, 25850.
[42] G. P. Maier, M. V. Rapp, J. H. Waite, J. N. Israelachvili, A. Butler, *Science* **2015**, *349*, 628.
[43] W. Wei, L. Petrone, Y. Tan, H. Cai, J. N. Israelachvili, A. Miserez, J. H. Waite, *Adv. Funct. Mater.* **2016**, *26*, 3496.
[44] S. Seo, S. Das, P. J. Zalicki, R. Mirshafian, C. D. Eisenbach, J. N. Israelachvili, J. H. Waite, A. K. Ahn, *J. Am. Chem. Soc.* **2015**, *137*, 9214.
[45] W. Wei, J. Yu, C. Broomell, J. N. Israelachvili, J. H. Waite, *J. Am. Chem. Soc.* **2013**, *135*, 377.
[46] J. Yu, W. Wei, E. Danner, R. K. Ashley, J. N. Israelachvili, W. J. H, *Nat. Chem. Biol.* **2012**, *7*, 588.
[47] S. C. T. Nicklisch, J. E. Spahn, H. Zhou, C. M. Gruian, J. H. Waite, *Biochemistry* **2016**, *55*, 2022.
[48] W. Wei, Y. Tan, N. R. Martinez Rodriguez, J. Yu, J. N. Israelachvili, J. H. Waite, *Acta Biomater.* **2014**, *10*, 1663.
[49] Q. Lu, D. S. Hwang, Y. Liu, H. Zeng, *Biomaterials* **2012**, *33*, 1903.
[50] L. Li, H. Zeng, *Biotribology* **2016**, *5*, 44.
[51] M. A. Gebbie, W. Wei, A. M. Schrader, T. R. Cristiani, H. A. Dobbs, M. Idso, B. F. Chmelka, J. H. Waite, J. N. Israelachvili, *Nat. Chem.* **2017**, *9*, 473.
[52] Y. L. Liu, K. L. Ai, L. H. Lu, *Chem. Rev.* **2014**, *114*, 5057.
[53] J. Israelachvili, H. Wennerström, *Nature* **1996**, *379*, 219.
[54] M. V. Rapp, G. P. Maier, H. A. Dobbs, N. J. Higdon, J. H. Waite, A. Butler, J. N. Israelachvili, *J. Am. Chem. Soc.* **2016**, *138*, 9013.
[55] P. E. Mason, G. W. Neilson, C. E. Dempsey, A. C. Barnes, J. M. Cruickshank, *Proc. Natl. Acad. Sci. USA* **2003**, *100*, 4557.

[56] Y. Akdogan, W. Wei, K. Y. Huang, Y. Kageyama, E. W. Danner, D. R. Miller, N. R. Martinez Rodriguez, J. H. Waite, S. Han, *Angew. Chem., Int. Ed.* **2014**, *53*, 11253.
[57] Q. Lu, E. Danner, J. H. Waite, J. N. Israelachvili, H. Zeng, D. S. Hwang, *J. R. Soc., Interface* **2013**, *10*, 20120759.
[58] B. P. Frank, G. Belfort, *Biotechnol. Prog.* **2002**, *18*, 580.
[59] J. Yu, Y. Kan, M. Rapp, E. Danner, W. Wei, S. Das, D. R. Miller, Y. Chen, J. H. Waite, J. N. Israelachvili, *Proc. Natl. Acad. Sci. USA* **2013**, *110*, 15680.
[60] N. D. Catron, H. Lee, P. B. Messersmith, *Biointerphases* **2006**, *1*, 134.
[61] M. J. Sever, J. J. Wilker, *Dalton Trans.* **2006**, *6*, 813.
[62] Q. Ye, F. Zhou, W. Liu, *Chem. Soc. Rev.* **2011**, *40*, 4244.
[63] J. P. Gallivan, D. A. Dougherty, *J. Am. Chem. Soc.* **2000**, *122*, 870.
[64] D. A. Dougherty, *Acc. Chem. Res.* **2013**, *46*, 885.
[65] S. T. Martin, J. M. Kesselman, D. S. Park, N. S. Lewis, M. R. Hoffmann, *Environ. Sci. Technol.* **1996**, *30*, 2535.
[66] T. H. Anderson, J. Yu, A. Estrada, M. U. Hammer, J. H. Waite, J. N. Israelachvili, *Adv. Funct. Mater.* **2010**, *20*, 4196.
[67] B. Liu, T. Burdine, T. Kodadek, *J. Am. Chem. Soc.* **2006**, *128*, 15228.
[68] C. R. Matos-Perez, J. D. White, J. J. Wilker, *J. Am. Chem. Soc.* **2012**, *134*, 9498.
[69] J. Yang, J. Keijsers, M. van Heek, A. Stuiver, M. A. Cohen Stuart, M. Kamperman, *Polym. Chem.* **2015**, *6*, 3121.
[70] P. C. Kearney, L. S. Mizoue, R. A. Kumpf, J. E. Forman, A. Mccurdy, D. A. Dougherty, *J. Am. Chem. Soc.* **1993**, *115*, 9907.
[71] S. H. Donaldson, S. Das, M. A. Gebbie, M. Rapp, L. C. Jones, Y. Roiter, P. H. Koenig, Y. Gizaw, J. N. Israelachvili, *ACS Nano* **2013**, *7*, 10094.
[72] S. Das, D. R. Miller, Y. Kaufman, N. R. Martinez Rodriguez, A. Pallaoro, M. J. Harrington, M. Gylys, J. N. Israelachvili, J. H. Waite, *Biomacromolecules* **2015**, *16*, 1002.
[73] M. J. Harrington, A. Masic, N. Holten-Andersen, J. H. Waite, P. Fratzl, *Science* **2010**, *328*, 216.
[74] B. K. Ahn, D. W. Lee, J. N. Israelachvili, J. H. Waite, *Nat. Mater.* **2014**, *13*, 867.
[75] M. A. North, C. A. Del Grosso, J. J. Wilker, *ACS Appl. Mater. Interfaces* **2017**, *9*, 7866.
[76] A. L. Li, Y. B. Mu, W. Jiang, X. B. Wan, *Chem. Commun.* **2015**, *51*, 9117.
[77] E. W. Danner, Y. J. Kan, M. U. Hammer, J. N. Israelachvili, J. H. Waite, *Biochemistry* **2012**, *51*, 6511.
[78] W. Wei, J. Yu, C. Broomell, J. N. Israelachvili, J. H. Waite, *J. Am. Chem. Soc.* **2012**, *135*, 377.
[79] M. R. Chapman, L. S. Robinson, J. S. Pinkner, R. Roth, J. Heuser, M. Hammar, S. Normark, S. J. Hultgren, *Science* **2002**, *295*, 851.
[80] C. Zhong, T. Gurry, A. A. Cheng, J. Downey, Z. T. Deng, C. M. Stultz, T. K. Lu, *Nat. Nanotechnol.* **2014**, *9*, 858.
[81] Y. J. Kan, E. W. Danner, J. N. Israelachvili, Y. F. Chen, J. H. Waite, *PLoS One* **2014**, *9*, e108869.
[82] A. R. Narkar, B. Barker, M. Clisch, J. F. Jiang, B. P. Lee, *Chem. Mater.* **2016**, *28*, 5432.
[83] W. R. Fortelny, A. Petter-Puchner, N. Walder, R. Mittermayr, W. Ohlinger, A. Heinze, H. Redl, *Surg. Endosc.* **2007**, *21*, 1781.
[84] P. Klimo, A. Khalil, J. R. Slotkin, E. R. Smith, R. Scott, L. C. Goumnerova, *Neurosurgery* **2007**, *60*, 305.
[85] L. Li, W. Smitthipong, H. Zeng, *Polym. Chem.* **2015**, *6*, 353.
[86] C. J. Kastrup, M. Nahrendorf, J. L. Figueiredo, H. Lee, S. Kambhampati, T. Lee, S. Cho, R. Gorbatov, Y. Iwamoto, T. T. Dang, P. Dutta, J. H. Yeon, H. Cheng, C. D. Pritchard, A. J. Vegas, C. D. Siegel, S. MacDougall, M. Okonkwo, A. Thai, J. R. Stone, A. J. Coury, R. Weissleder, R. Langer, D. G. Anderson, *Proc. Natl. Acad. Sci. USA* **2012**, *109*, 21444.
[87] Y. Liu, H. Meng, S. Konst, R. Sarmiento, R. Rajachar, B. P. Lee, *ACS Appl. Mater. Interfaces* **2014**, *6*, 16982.
[88] K. Kim, K. Kim, J. H. Ryu, H. Lee, *Biomaterials* **2015**, *52*, 161.
[89] M. Mehdizadeh, H. Weng, D. Gyawali, L. P. Tang, J. Yang, *Biomaterials* **2012**, *33*, 7972.
[90] J. Shin, J. S. Lee, C. Lee, H. J. Park, K. Yang, Y. Jin, J. H. Ryu, K. S. Hong, S. H. Moon, H. M. Chung, H. S. Yang, S. H. Um, J. W. Oh, D. I. Kim, H. Lee, S. W. Cho, *Adv. Funct. Mater.* **2015**, *25*, 3814.
[91] L. Han, X. Lu, K. Z. Liu, K. F. Wang, L. M. Fang, L. T. Weng, H. P. Zhang, Y. H. Tang, F. Z. Ren, C. C. Zhao, G. X. Sun, R. Liang, Z. J. Li, *ACS Nano* **2017**, *11*, 2561.
[92] Y. Liu, H. Meng, Z. Qian, N. Fan, W. Choi, F. Zhao, B. P. Lee, *Angew. Chem., Int. Ed.* **2017**, *56*, 4224.
[93] Q. Zhao, D. W. Lee, B. K. Ahn, S. Seo, Y. Kaufman, J. N. Israelachvili, J. H. Waite, *Nat. Mater.* **2016**, *15*, 407.
[94] B. K. Ahn, S. Das, R. Linstadt, Y. Kaufman, N. R. Martinez-Rodriguez, R. Mirshafian, E. Kesselman, Y. Talmon, B. H. Lipshutz, J. N. Israelachvili, J. H. Waite, *Nat. Commun.* **2015**, *6*, 8663.
[95] Y. S. Choi, D. G. Kang, S. Lim, Y. J. Yang, C. S. Kim, H. J. Cha, *Biofouling* **2011**, *27*, 729.
[96] S. Lim, D. G. Choi, Y. S. Kang, Y. H. Song, H. J. Cha, *Biomaterials* **2010**, *31*, 3715.
[97] H. J. Kim, B.-H. Choi, S. H. Jun, H. J. Cha, *Adv. Healthcare Mater.* **2016**, *113*, E847.
[98] D. S. Hwang, Y. Gim, H. J. Yoo, H. J. Cha, *Biomaterials* **2007**, *28*, 3560.
[99] C. K. Roy, H. L. Guo, T. L. Sun, A. Bin Ihsan, T. Kurokawa, M. Takahata, T. Nonoyama, T. Nakajima, J. P. Gong, *Adv. Mater.* **2015**, *27*, 7344.
[100] H. Shao, K. N. Bachus, R. J. Stewart, *Macromol. Biosci.* **2009**, *9*, 464.
[101] H. Shao, R. J. Stewart, *Adv. Mater.* **2010**, *22*, 729.
[102] B. D. Winslow, H. Shao, R. J. Stewart, P. A. Tresco, *Biomaterials* **2010**, *31*, 9373.
[103] S. Kaur, G. M. Weerasekare, R. J. Stewart, *ACS Appl. Mater. Interfaces* **2011**, *3*, 941.
[104] L. K. Mann, R. Papanna, K. J. Moise, R. H. Byrd, E. J. Popek, S. Kaur, S. C. G. Tseng, R. J. Stewart, *Acta Biomater.* **2012**, *8*, 2160.
[105] R. Papanna, L. K. Mann, S. C. G. Tseng, R. J. Stewart, S. S. Kaur, M. M. Swindle, T. R. Kyriakides, N. Tatevian, K. J. Moise Jr., *Placenta* **2015**, *36*, 888.
[106] F. Luo, T. L. Sun, T. Nakajima, T. Kurokawa, Y. Zhao, K. Sato, A. Bin Ihsan, X. Li, H. Guo, J. P. Gong, *Adv. Mater.* **2015**, *27*, 2722.
[107] Y. Huang, P. G. Lawrence, Y. Lapitsky, *Langmuir* **2014**, *30*, 7771.
[108] P. G. Lawrence, Y. Lapitsky, *Langmuir* **2015**, *31*, 1564.
[109] L. Zhang, V. Lipik, A. Miserez, *J. Mater. Chem. B* **2016**, *4*, 1544.
[110] J. P. Jones, M. Sima, R. G. O'Hara, R. J. Stewart, *Adv. Healthcare Mater.* **2016**, *5*, 795.
[111] F. Luo, T. L. Sun, T. Nakajima, T. Kurokawa, X. Li, H. Guo, Y. Huang, H. Zhang, J. P. Gong, *Polymer* **2017**, *116*, 487.
[112] D. D. Lane, S. Kaur, G. M. Weerasakare, R. J. Stewart, *Soft Matter* **2015**, *11*, 6981.
[113] L. Brunsveld, B. J. B. Folmer, E. W. Meijer, R. P. Sijbesma, *Chem. Rev.* **2001**, *101*, 4071.
[114] T. F. A. de Greef, M. M. J. Smulders, M. Wolffs, A. P. H. J. Schenning, R. P. Sijbesma, E. W. Meijer, *Chem. Rev.* **2009**, *109*, 5687.
[115] M. M. Feldstein, E. E. Dormidontova, A. R. Khokhlov, *Prog. Polym. Sci.* **2015**, *42*, 79.
[116] M. M. Feldstein, E. V. Bermesheva, Y. C. Jean, G. P. Misra, R. A. Siegel, *J. Appl. Polym. Sci.* **2011**, *119*, 2408.
[117] M. M. Feldstein, K. A. Bovaldinova, E. V. Bermesheva, A. P. Moscalets, E. E. Dormidontova, V. Y. Grinberg, A. R. Khokhlov, *Macromolecules* **2014**, *47*, 5759.
[118] D. W. R. Balkenende, R. A. Olson, S. Balog, C. Weder, L. Montero de Espinosa, *Macromolecules* **2016**, *49*, 7877.

[119] H. Yoshioka, C. Izumi, M. Shida, K. Yamaguchi, M. Kobayashi, *Polymer* **2017**, *119*, 167.
[120] S. Cheng, M. Zhang, N. Dixit, R. B. Moore, T. E. Long, *Macromolecules* **2012**, *45*, 805.
[121] N. Ishikawa, M. Furutani, K. Arimitsu, *ACS Macro Lett.* **2015**, *4*, 741.
[122] N. Ishikawa, M. Furutani, K. Arimitsu, *J. Polym. Sci., Part A: Polym. Chem.* **2016**, *54*, 1332.
[123] X. Liu, Q. Zhang, Z. Gao, R. Hou, G. Gao, *ACS Appl. Mater. Interfaces* **2017**, *9*, 17645.
[124] C. Heinzmann, U. Salz, N. Moszner, G. L. Fiore, C. Weder, *ACS Appl. Mater. Interfaces* **2015**, *7*, 13395.
[125] D. W. R. Balkenende, C. A. Monnier, G. L. Fiore, C. Weder, *Nat. Commun.* **2016**, *7*, 10995.
[126] J. Courtois, I. Baroudi, N. Nouvel, E. Degrandi, S. Pensec, G. Ducouret, C. Chanéac, L. Bouteiller, C. Creton, *Adv. Funct. Mater.* **2010**, *20*, 1803.
[127] X. Callies, O. Herscher, C. Fonteneau, A. Robert, S. Pensec, L. Bouteiller, G. Ducouret, C. Creton, *ACS Appl. Mater. Interfaces* **2016**, *8*, 33307.
[128] R. Wang, T. Xie, *Langmuir* **2010**, *26*, 2999.
[129] M. Fathalla, C. M. Lawrence, N. Zhang, J. L. Sessler, J. Jayawickramarajah, *Chem. Soc. Rev.* **2009**, *38*, 1608.
[130] K. Viswanathan, H. Ozhalici, C. L. Elkins, C. Heisey, T. C. Ward, T. E. Long, *Langmuir* **2006**, *22*, 1099.
[131] M. Nakahata, Y. Takashima, A. Hashidzume, A. Harada, *Chem. Eur. J.* **2015**, *21*, 2770.
[132] R. P. Sijbesma, F. H. Beijer, L. Brunsveld, B. J. B. Folmer, J. H. K. K. Hirschberg, R. F. M. Lange, J. K. L. Lowe, E. W. Meijer, *Science* **1997**, *278*, 1601.
[133] K. Yamauchi, J. R. Lizotte, D. M. Hercules, M. J. Vergne, T. E. Long, *J. Am. Chem. Soc.* **2002**, *124*, 8599.
[134] K. Yamauchi, J. R. Lizotte, T. E. Long, *Macromolecules* **2003**, *36*, 1083.
[135] A. Faghihnejad, K. E. Feldman, J. Yu, M. V. Tirrell, J. N. Israelachvili, C. J. Hawker, E. J. Kramer, H. Zeng, *Adv. Funct. Mater.* **2014**, *24*, 2322.
[136] H. Sun, H. H. Lee, I. Blakey, B. Dargaville, T. V. Chirila, A. K. Whittaker, S. C. Smith, *J. Phys. Chem. B* **2011**, *115*, 11053.
[137] P. Y. W. Dankers, M. C. Harmsen, L. A. Brouwer, M. J. A. Van Luyn, E. W. Meijer, *Nat. Mater.* **2005**, *4*, 568.
[138] P. Cordier, F. Tournilhac, C. Soulié-Ziakovic, L. Leibler, *Nature* **2008**, *451*, 977.
[139] P. Woodward, A. Clarke, B. W. Greenland, D. Hermida Merino, L. Yates, A. T. Slark, J. F. Miravet, W. Hayes, *Soft Matter* **2009**, *5*, 2000.
[140] P. Woodward, D. Hermida Merino, I. W. Hamley, A. T. Slark, W. Hayes, *Aust. J. Chem.* **2009**, *62*, 790.
[141] A. Feula, X. Tang, I. Giannokopoulos, A. M. Chippindale, I. W. Hamley, F. Greco, C. P. Buckley, C. R. Siviour, W. Hayes, *Chem. Sci.* **2016**, *7*, 4291.
[142] A. Feula, A. Pethybridge, I. Giannakopoulos, X. Tang, A. Chippindale, C. R. Siviour, C. P. Buckley, I. W. Hamley, W. Hayes, *Macromolecules* **2015**, *48*, 6132.
[143] C. Véchambre, X. Callies, C. Fonteneau, G. Ducouret, S. Pensec, L. Bouteiller, C. Creton, J. Chenal, L. Chazeau, *Macromolecules* **2015**, *48*, 8232.
[144] X. Callies, C. Véchambre, C. Fonteneau, S. Pensec, J. M. Chenal, L. Chazeau, L. Bouteiller, G. Ducouret, C. Creton, *Macromolecules* **2015**, *48*, 7320.
[145] S. J. Barrow, S. Kasera, M. J. Rowland, J. del Barrio, O. A. Scherman, *Chem. Rev.* **2015**, *115*, 12320.
[146] I. Tomatsu, A. Hashidzume, A. Harada, *J. Am. Chem. Soc.* **2006**, *128*, 2226.
[147] E. A. Appel, J. del Barrio, X. J. Loh, O. A. Scherman, *Chem. Soc. Rev.* **2012**, *41*, 6195.
[148] A. Harada, R. Kobayashi, Y. Takashima, A. Hashidzume, H. Yamaguchi, *Nat. Chem.* **2011**, *3*, 34.
[149] A. Harada, Y. Takashima, M. Nakahata, *Acc. Chem. Res.* **2014**, *47*, 2128.
[150] H. Yamaguchi, R. Kobayashi, Y. Takashima, A. Hashidzume, A. Harada, *Macromolecules* **2011**, *44*, 2395.
[151] Y. Zheng, A. Hashidzume, Y. Takashima, H. Yamaguchi, A. Harada, *Nat. Commun.* **2012**, *3*, 831.
[152] A. Hashidzume, Y. Zheng, Y. Takashima, H. Yamaguchi, A. Harada, *Macromolecules* **2013**, *46*, 1939.
[153] Y. Zheng, A. Hashidzume, Y. Takashima, H. Yamaguchi, A. Harada, *ACS Macro Lett.* **2012**, *1*, 1083.
[154] Y. Zheng, A. Hashidzume, A. Harada, *Macromol. Rapid Commun.* **2013**, *34*, 1062.
[155] M. Nakahata, Y. Takashima, A. Harada, *Angew. Chem., Int. Ed.* **2014**, *53*, 3617.
[156] H. Yamaguchi, Y. Kobayashi, R. Kobayashi, Y. Takashima, A. Hashidzume, A. Harada, *Nat. Commun.* **2012**, *3*, 603.
[157] Y. Takashima, T. Sahara, T. Sekine, T. Kakuta, M. Nakahata, M. Otsubo, Y. Kobayashi, A. Harada, *Macromol. Rapid Commun.* **2014**, *35*, 1646.
[158] T. Kakuta, Y. Takashima, T. Sano, T. Nakamura, Y. Kobayashi, H. Yamaguchi, A. Harada, *Macromolecules* **2015**, *48*, 732.
[159] J. Guo, C. Yuan, M. Guo, L. Wang, F. Yan, *Chem. Sci.* **2014**, *5*, 3261.
[160] O. Roling, L. Stricker, J. Voskuhl, S. Lamping, B. J. Ravoo, *Chem. Commun.* **2016**, *52*, 1964.
[161] T. T. H. Thi, J. S. Lee, Y. Lee, H. B. Park, K. M. Park, K. D. Park, *ACS Macro Lett.* **2017**, *6*, 83.
[162] Y. Ahn, Y. Jang, N. Selvapalam, G. Yun, K. Kim, *Angew. Chem., Int. Ed.* **2013**, *52*, 3140.
[163] K. Kim, N. Selvapalam, Y. H. Ko, K. M. Park, D. Kim, J. Kim, *Chem. Soc. Rev.* **2007**, *36*, 267.
[164] D. Shetty, J. K. Khedkar, K. M. Park, K. Kim, *Chem. Soc. Rev.* **2015**, *44*, 8747.
[165] J. Liu, C. S. Y. Tan, Z. Yu, Y. Lan, C. Abell, O. A. Scherman, *Adv. Mater.* **2017**, *29*, 1604951.
[166] J. Liu, C. S. Y. Tan, Z. Yu, N. Li, C. Abell, O. A. Scherman, *Adv. Mater.* **2017**, *29*, 1605325.
[167] E. A. Appel, X. J. Loh, S. T. Jones, F. Biedermann, C. A. Dreiss, O. A. Scherman, *J. Am. Chem. Soc.* **2012**, *134*, 11767.
[168] Z. Walsh-Korb, Y. Yu, E. R. Janeček, Y. Lan, J. del Barrio, P. E. Williams, X. Zhang, O. A. Scherman, *Langmuir* **2017**, *33*, 1343.
[169] C. Liu, G. Xiang, Y. Wu, S. J. Barrow, M. J. Rowland, D. E. Clarke, G. Wu, O. A. Scherman, *Polym. Chem.* **2016**, *7*, 6485.
[170] P. Neirynck, J. Brinkmann, Q. An, D. W. J. van der Schaft, L. Milroy, P. Jonkheijm, L. Brunsveld, *Chem. Commun.* **2013**, *49*, 3679.
[171] M. Burnworth, L. Tang, J. R. Kumpfer, A. J. Duncan, F. L. Beyer, G. L. Fiore, S. J. Rowan, C. Weder, *Nature* **2011**, *472*, 334.
[172] A. K. Miller, Z. Li, K. A. Streletzky, A. M. Jamieson, S. J. Rowan, *Polym. Chem.* **2012**, *3*, 3132.
[173] A. Winter, U. S. Schubert, *Chem. Soc. Rev.* **2016**, *45*, 5311.
[174] N. Holten-Andersen, M. J. Harrington, H. Birkedal, B. P. Lee, P. B. Messersmith, K. Y. C. Lee, J. H. Waite, *Proc. Natl. Acad. Sci. USA* **2011**, *108*, 2651.
[175] N. Holten-Andersen, A. Jaishankar, M. J. Harrington, D. E. Fullenkamp, G. DiMarco, L. He, G. H. McKinley, P. B. Messersmith, K. Y. C. Lee, *J. Mater. Chem. B* **2014**, *2*, 2467.
[176] S. C. Grindy, R. Learsch, D. Mozhdehi, J. Cheng, D. G. Barrett, Z. Guan, P. B. Messersmith, N. Holten-Andersen, *Nat. Mater.* **2015**, *14*, 1210.
[177] D. E. Fullenkamp, L. He, D. G. Barrett, W. R. Burghardt, P. B. Messersmith, *Macromolecules* **2013**, *46*, 1167.
[178] S. C. Grindy, N. Holten-Andersen, *Soft Matter* **2017**, *13*, 4057.

[179] M. Krogsgaard, M. A. Behrens, J. S. Pedersen, H. Birkedal, *Biomacromolecules* **2013**, *14*, 297.
[180] M. Krogsgaard, M. R. Hansen, H. Birkedal, *J. Mater. Chem. B* **2014**, *2*, 8292.
[181] W. Wang, Y. Xu, A. Li, T. Li, M. Liu, R. von Klitzing, C. K. Ober, A. B. Kayitmazer, L. Li, X. Guo, *RSC Adv.* **2015**, *5*, 66871.
[182] B. J. Kim, D. X. Oh, S. Kim, J. H. Seo, D. S. Hwang, A. Masic, D. K. Han, H. J. Cha, *Biomacromolecules* **2014**, *15*, 1579.
[183] C. Heinzmann, S. Coulibaly, A. Roulin, G. L. Fiore, C. Weder, *ACS Appl. Mater. Interfaces* **2014**, *6*, 4713.
[184] R. Wang, T. Xie, *Chem. Commun.* **2010**, *46*, 1341.
[185] T. Yamate, K. Kumazawa, H. Suzuki, M. Akazome, *ACS Macro Lett.* **2016**, *5*, 858.
[186] B. T. Michal, E. J. Spencer, S. J. Rowan, *ACS Appl. Mater. Interfaces* **2016**, *8*, 11041.
[187] M. Shan, C. Gong, B. Li, G. Wu, *Polym. Chem.* **2017**, *8*, 2997.
[188] G. Deng, Q. Ma, H. Yu, Y. Zhang, Z. Yan, F. Liu, C. Liu, H. Jiang, Y. Chen, *ACS Macro Lett.* **2015**, *4*, 467.
[189] B. Zhang, P. Zhang, H. Zhang, C. Yan, Z. Zheng, B. Wu, Y. Yu, *Macromol. Rapid Commun.* **2017**, *38*, 1700110.
[190] A. A. Kavitha, N. K. Singha, *ACS Appl. Mater. Interfaces* **2009**, *1*, 1427.
[191] Y. Kobayashi, Y. Takashima, A. Hashidzume, H. Yamaguchi, A. Harada, *Sci. Rep.* **2013**, *3*, 1243.
[192] T. Nakamura, Y. Takashima, A. Hashidzume, H. Yamaguchi, A. Harada, *Nat. Commun.* **2014**, *5*, 4622.
[193] D. A. Dougherty, *J. Nutr.* **2007**, *137*, 1504S.
[194] Y. Pan, K. Zhang, J. Qi, J. Yue, T. A. Springer, J. Chen, *Proc. Natl. Acad. Sci. USA* **2010**, *107*, 21388.
[195] A. S. Mahadevi, G. N. Sastry, *Chem. Rev.* **2013**, *113*, 2100.
[196] Q. Lu, D. X. Oh, Y. Lee, Y. Jho, D. S. Hwang, H. Zeng, *Angew. Chem., Int. Ed.* **2013**, *52*, 3944.
[197] S. Kim, A. Faghihnejad, Y. Lee, Y. Jho, H. Zeng, D. S. Hwang, *J. Mater. Chem. B* **2015**, *3*, 738.
[198] D. S. Hwang, H. Zeng, Q. Lu, J. Israelachvili, J. H. Waite, *Soft Matter* **2012**, *8*, 5640.
[199] F. García, M. M. J. Smulders, *J. Polym. Sci., Part A: Polym. Chem.* **2016**, *54*, 3551.
[200] T. Sekine, T. Kakuta, T. Nakamura, Y. Kobayashi, Y. Takashima, A. Harada, *Sci. Rep.* **2014**, *4*, 6348.
[201] T. Sekine, Y. Takashima, A. Harada, *RSC Adv.* **2015**, *5*, 56130.
[202] Y. M. Martínez-Triana, R. Whelan, M. G. Finn, D. D. Díaz, *Macromol. Chem. Phys.* **2017**, *218*, 1600579.
[203] T. L. Sun, T. Kurokawa, S. Kuroda, A. Bin Ihsan, T. Akasaki, K. Sato, M. A. Haque, T. Nakajima, J. P. Gong, *Nat. Mater.* **2013**, *12*, 932.
[204] E. Filippidi, D. G. DeMartini, P. Malo de Molina, E. W. Danner, J. Kim, M. E. Helgeson, J. H. Waite, M. T. Valentine, *J. R. Soc., Interface* **2015**, *12*, 0150827.
[205] K. W. Desmod, N. A. Zacchia, J. H. Waite, M. T. Valentine, *Soft Matter* **2015**, *11*, 6832.